Preparation of Microporous Cell-engineering Scaffolds from Liquid Crystalline Polysaccharide

SARANYOO SORNKAMNERD
Japan Advanced Institute of Science and Technology

Doctoral Dissertation

Preparation of Microporous Cell-engineering Scaffolds from Liquid Crystalline Polysaccharide

by

SARANYOO SORNKAMNERD

Supervisor: Professor Tatsuo Kaneko

School of Material Science

Japan Advanced Institute of Science and Technology

March 2018

Referee-in-chief:

Professor Dr. Tatsuo Kaneko

Japan Advanced Institute of Science and Technology

Referees:

Professor Dr. Noriyoshi Matsumi

Japan Advanced Institute of Science and Technology

Associate Professor Dr. Kazuaki Matsumura

Japan Advanced Institute of Science and Technology

Associate Professor Dr. Takumi Yamaguchi

Japan Advanced Institute of Science and Technology

Professor Dr. Hidetoshi Arima

Graduate School of Pharmaceutical Sciences Pharmacy, Kumamoto University, Kumamoto

Preparation of Microporous Cell-engineering Scaffolds from Liquid Crystalline Polysaccharide

Kaneko Laboratory, s1540009, Saranyoo Sornkamnerd

Background

Scaffold is a significant material of cell-engineering treatment. It possesses important functions of cells supporting materials that allowed for cells growth and new tissue formation. In order to become a cells supporting material, the scaffold need basic requirements such as biocompatibility, biodegradability, high porosity, and shape orientation. The microporous materials are the general formation of scaffolds. It has high water adsorption capacity and abundant interconnecting pore. The high water content that resembles the native tissue allowed for cells attachment and penetration. Sacran (Figure 1), polysaccharide, is extracted from Aphanothece sacrum cyanobacteria. The polymer contains various kinds of sugar residues such as Glc, Gal, Man, Xyl, Rha, Fuc, Ara, GalN, and Mur. It also consists of many functional groups such

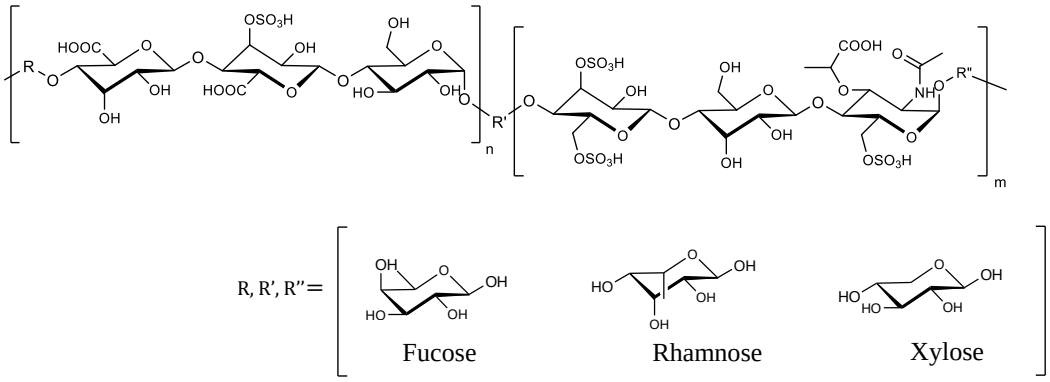

Figure 1. Chemical structure of sacran, a LC polysaccharide.

as hydroxyl, carboxylic, sulfate and amide. The amide sugar, acting like glycosaminoglycan, is the main content found in the extra cellular matrix. By this reason, sacran was selected for scaffold preparation. Moreover, liquid crystal behavior (LC) was observed in sacran solution. In the field of polymer orientation study, experiment conducted on LC has been considered to be a challenging

practice. Thus, sacran is one of the most suitable materials for making scaffolds with orientation controllability. Here a new microporous scaffold using LC polysaccharide with controlled orientation is presented. This scaffold was prepared by simple methods of solvent casting and freeze-drying. The characteristic in pore size, porosity, water adsorption capacity and mechanical properties were clarified. Moreover, the cell orientation capacity was confirmed.

Aim:

- **(i)** To prepare microporous materials scaffolds using sacran polymer.
- **(ii)** To study the biocompatibility of the scaffolds.
- **(iii)** To prepare sacran hydrogels with micro-patterned on the surface.
- **(iv)** To study the orientation property of sacran anisotropic porous and micro-patterned hydrogels.
- **(v)** To evaluate the orientation of cell on sacran materials.

Results and Discussions:

Chapter II, the surface selective microporous hydrogels with porous structure on side surface and flat on the top (Figure 2) were prepared by a combination of solvent casting and freeze drying techniques. Sacran water solution was casted at 60 °C to produce in-plane orientation thin films. The thin films were physical cross-linked at temperature 60, 80, 100, 120 and 140 °C without cross-linking agent. Then swollen hydrogels with in-plane orientation were created by water immersion of that cross-linked films. Finally, the swollen hydrogels were subjected to freeze dry

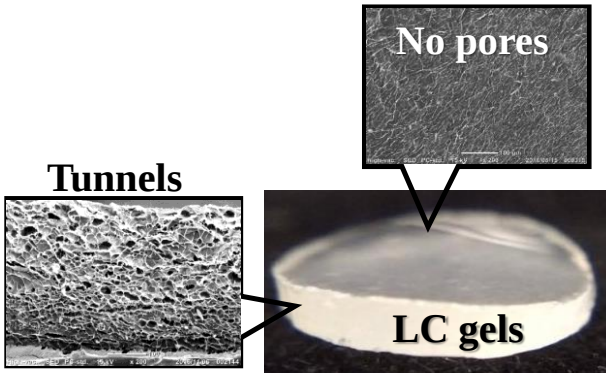

Figure 2. Surface selective porous hydrogels with tunnels on side surface while did not showed porous morphology on the top surface.

process. The final products revealed an in-plane porous structure like a tunnel with pore size and porosity of 10-35 μm and 42-80 %, respectively. This is due to the sublimation of water on side surface parallel to the in-plane orientation of sacran polymer chains. In addition, they showed proper mechanical properties in a broad application. At high cross-linking temperature, the anisotropic porous materials showed low porosity, fine-size pores, and minimal water adsorption. Conversely, the mechanical properties value such as moduli, cross-linking degree and toughness were very high. For low temperature cross-linking, the opposite set of values were observed. The water adsorption was between 9 to 186 times to that of dry material, and the elastic modulus was 3 to 585 kPa. The results reveals that the properties of the materials depends on temperature cross-linking. The surface selective microporous hydrogels were successfully prepared and precisely controlled for their properties.

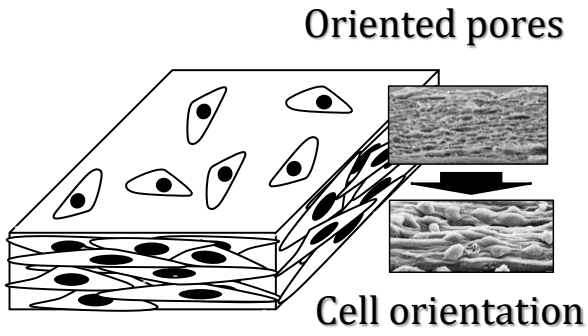

Figure 3. Fibroblast L929 cells attached on surface selective porous scaffold. Randomly orientation is presented on the top surface whereas perfectly orientation is revealed side surface. Additionally, the cell density on the top surface was lower than that of side surface.

There are various applications of porous materials, and the tissue engineering scaffold is considered to be one of the most significant. **In chapter III,** the biocompatibility and cell orientation capacity were studied using mouse fibroblast cell L929 as a model in the cell culture experiment. The surface selective microporous hydrogels showed favorable cell compatibility property. The morphology of cells attachment was analyzed. The cells orientation on side surfaces is parallel to the in-plane orientation of polymer chains. The scaffolds can be altered to mimic the

native tissue that represents uni-direction of the muscle orientation (Figure 3). Moreover, the water contact angle and protein adsorption were studied on the materials which were annealed at 100, 120 and 140 °C. The water contact angle was revealed to be 95 to 37°, and the protein adsorption were 36 to 96 μg per 1 mg. In the results, water contact angle, protein adsorption and cell orientation are related to cross-linking temperature, similar to the above-mentioned properties. However, the cell attached on top of the surface were randomly oriented. Another method was employed to control the cell orientation on the top surface of the scaffolds.

In **chapter IV** the scaffolds were casted on polystyrene, with micro-patterned on its surface. The pattern was set in a bar-shape mold with a diameter of 400 μm. The bars were arranged in parallel. The space between bars was fixed at 200, 250 and 300 μm. Sacran scaffolds with surface orientation were prepared with the same procedure to that of surface selective porous scaffolds except for the mentioned patterned substrate surface. The pattern of the scaffold revealed orientation perpendicular to that of bar molds. During the drying process, LC domains were slightly arranged to form an in-plane orientation like a layer. Looking at the side of bar molds, the top point of each bar has the sacran layer accumulated. The point is called nucleation point of orientation. Then the ends of polymer chains are aligned between bars. Polarization optical

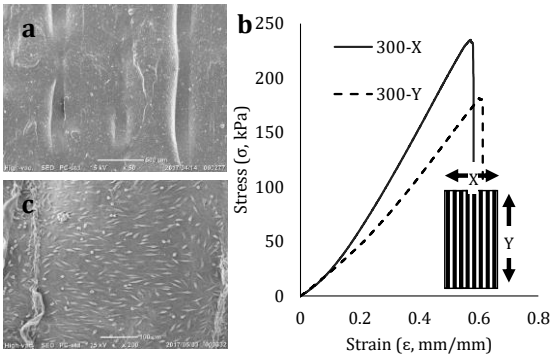

Figure 4. Sacran film with micro-patterned on the top surface (a) showed anisotropic mechanical property (b) and one direction of fibroblast L929 cells orientation (c).

microscope technique was used to confirm the orientation of LC domains, and the results showed a clear and complete visible orientation. After that, the mouse fibroblast cell L929 was used in cell culture experiment. The distribution of cell orientation degree mimics the polymer orientation on the top surface. Finally, the orientation of cell was efficiently controlled on sacran LC polymer (Figure 4).

Conclusions

The microporous scaffolds with cell-orientation capacity was successfully prepared using sacran LC polymer. They revealed favorable results of pore properties, water adsorption capacity and mechanical properties. Furthermore biocompatibility and cell alignment were also confirmed. The angle of cell attached on materials was highly oriented, mimicking the native tissue behavior. According to the development of technology for human's bioengineering, the field of tissue engineering scaffolds is growing and progressing continuously. Today, the scaffolds are mainly the work of laboratory and research. However, it has the potential to be utilized, especially to save many lives on this planet, in the future.

Keywords: sacran, scaffold, liquid crystalline gels, cell-orientation, cell-engineering

CONTENTS

Chapter I: General Introduction

1. Cyanobacterial polysaccharide

Cyanobacteria are a group of photosynthetic prokaryotes that live in a wide variety of moist soils and in the water[1]. They can be regarded as the most eco-friendly microreactors of all the photosynthetic creatures because they perform not only carbon fixation by using the energy of sunlight but also nitrogen fixation in an anaerobic condition, to produce various kinds of metabolites such as polysaccharides in an aqueous milieu. Among these products, exopolysaccharide (EPS) is a secondary metabolite attracting researchers' attention[2-5].

According to a review of the literature[6], more than 100 cyanobacteria belonging to sections I, III, IV, and V have been reported to synthesize large quantities of EPS. These EPS possess functional groups such as hydroxyls, carboxyls, sulfates, phosphates, and amines that are responsible for ionic adsorption[2, 7-12] and tissue enginerring[13-14]. The molecular weight of EPSs ranges from 2×10^5 to 3×10^7 g/mol, and more than 75 % of those characterized thus far are heteropolysaccharides comprising six or more different kinds of sugar residues. When the molecular weight of macromolecule is very high, their solubility in water is generally too poor to extract or to analyze the structures. However most of the cyanobacterial EPS is water soluble, owing to the wide variety of sugar residues, because heterogeneity of the constituents for the macromolecuels can raise the solution entropy to make easy the dissolution. Most of EPSs show anionic property because of the presence of uronic acids and/or sulfated sugars. Additionally, their functional groups can be modified for extend the application.

In order to develop the bio-application in tissue engineering they have used cyanobacterial polysaccharides, sacran, which is a recently-developed supergiant polysaccharide extracted from the edible cyanobacteria *Aphanothece sacrum* which is mass-cultivated in natural rivers[15-16]. As described in next section, sacran has a weight-average

molecular weight of 2.35×10^7 g/mol determined by light scattering as absolute molecular weight, and they believe that this value of molecular weight can be regarded as a world record of extracted molecules. Even if DNA have a M_w in the range of 10^8 g/mol in living body, its M_w was remarkably reduced to a scale of 10^6 g/mol by its extraction process[17].

1.1 *Aphanothece sacrum* polysaccharides

Aphanothece sacrum (*A. sacrum*) is mass-cultured in fresh water in Japan, and its extracellular matrix includes metal ions that create a jelly-like material (gel) which protects the cells, and may be useful as a scaffold for cell proliferation. Sacran was extracted from *A. sacrum* biomaterials by the following procedure[15-16]. The *A. sacrum* samples were freeze-thawed in order to break the cell membranes and then washed with pure water to remove water-soluble materials such as aqueous pigments (phycobiliproteins). Because phycobiliproteins show strong colors due to their ultra-high absorption coefficients, the de-coloration of the washing solution was a sign that water-washing was completed. The samples were then washed using a large amount of isopropanol with shaking at least three times until de-coloration of the washing solution (green) was confirmed, and then collected by filtration using gauze. The isopropanol-washed samples were put into 0.1 M NaOH aq. at around 70-80 °C, and agitated at a constant temperature for 8 h to yield a transparent solution. The solution was neutralized with HCl until the pH value decreased to 8.0–9.0, and then filtrated. The filtrate solution was slowly poured into isopropanol to precipitate a white fibrous material. The fibrous precipitates in isopropanol were collected and dried in a vacuum oven. The resulting aqueous solution of sacran showed no specific absorption in the wavelength range of 220-600 nm using ultraviolet-visible (UV-vis) spectroscopy, confirming that it was not contaminated by proteins, nucleic acids, chromophores, and/or other chemicals with UV-vis absorption. The extracted yield of sacran was very high at ca. 70 wt % in dried materials of *A. sacrum*.

Sacran is a heteropolysaccharide composed of various sugar residues such as Glc, Gal, Man, Xyl, Rha, and Fuc with a composition of 25.9: 11.0: 10.0: 16.2: 10.2: 6.9, and contains 20-25 % of uronic acids and trace amounts (ca. 1.0 %) of Ara, GalN (cationic), and Mur (amphoteric), which were mainly determined by gas-chromatography mass-spectroscopy (GC-MS). Sacran is sulfated in ca. 10 mol % to monosaccharide residues, determined by X-ray photoelectron spectroscopy (XPS) and CHNS elemental analyses. The main structure which was partially determined by fragment determination by Fourier-transformed ion-cyclotron resonance mass-spectroscopy (FT-ICR-MS) is shown in **Figure 1**. The absolute molecular weight, *Mw*, which was measured by multi-angle static light scattering (MALLS; detection angle from 15 ° to 40 °) was greater than10^7 g/mol. As shown in **Figure 2**, we obtained a typical Zimm-Berry plot with a very small error of 1.4 %, and the absolute M_w, radius of gyration, R_g, and second virial coefficient, A_2, for sacran were estimated at 2.35×10^7 g/mol, 402 nm, and 4.53×10^{-4} mol·cm^3/g^2, respectively. As a result of repeated extraction of sacran under different elution conditions of alkaline concentration, elution time, agitation speed, and solvent for reprecipitation, we concluded that the M_w of sacran extracted ranged between 1- 3 x 10^7 g/mol. The M_w range indicated that sacran are supergiant chains. If sacran chains are so giant, the appearance is visible easily by Atomic Force Microscopy (AFM). We therefore tried to observe the sacran appearance using the cast sample from the aqueous solution (10 ppm) in dynamic force modulation mode, and captured them as shown in the inset image of Figure 2 [18].In this image, one can confirm that the network architecture was formed by long sacran ropes with a several micrometer range.

1.2 Liquid crystalline gels

Liquid crystals are anisotropic fluids, which exhibit spontaneous orientational order of rod-like molecules, called the nematic phase. The orientated phase existing between the solid and liquid phases, which are oriented and random phases, respectively (Figure 3). There are

two distinct types of behavior in liquid crystals, thermotropic and lyotropic. In the case of thermotropic liquid crystals a mesophase appears as a result of thermal effects. By either heating above the crystalline solid phase or cooling from the isotropic liquid phase a liquid crystal mesophase will appear. The temperature on heating at which the state of matter changes from that of a solid to that of a liquid crystal is called the melting point. For the liquid crystal-isotropic liquid transition the respective temperature is referred to as the clearing point. Lyotropic liquid crystals differ in that a mesophase is observed when the concentration of the solvent is just enough to disrupt the crystal order to promote fluidity but not enough so that all order is lost and the solution becomes isotropic.

Investigation of the lyotropic liquid crystalline (LC) properties of macromolecules which are long enough to observe optically has a potential significance in self-orientation of the biological materials. Most plants have giant polysaccharides, celluloses, whose derivatives have been widely studied as LC polymers[19-22] and it has been reported that the LC structure in plant cell walls composed mainly of cellulose fibers with a high orientation degree may play a role in supporting the plant bodies[23-25]. DNA, which are representative megamolecules, could form LC structures to store themselves in chromosomes efficiently according to the literaure[17, 26].

Since the M_w of sacran is much higher than that of these macromolecules, it should be expected that investigation of their liquid crystallinity would provide important information in the nanocomposite field, because molecular orientation is very important in the development of tailor-made materials. Birefringence change as a function of sacran concentration was checked and self-orientation behavior was confirmed at over 0.3 wt%[17]. We estimated that mesogenic chains of sacran have extremely high aspect ratios of 1,600 for highly persistent lengths of 32 μm based on Flory's simple lattice theory[27-28]. The value of persistence length showed good consistency with the fully-extended length of sacran chains of ca. 50 μm but is

too much higher than other molecules so the solution structures of sacran chains were investigated in more detail. Measurements of the electrical conductivity and the zero shear viscosity demonstrated three crossover concentrations at 0.004, 0.02, and 0.1 wt %. The viscosity was found to be scaled as $\sim c^{1.5}$, $\sim c^{0.5}$, $\sim c^{1.5}$, and $\sim c^{3.0}$ with increasing concentrations of sacran. At 0.1 wt %, the sacran chain formed a weak gel which exhibited macroscopic liquid crystal domains including Schlieren texture (taken at 0.5 wt%, **Figure 4** inset). These crossover concentrations are considered to be the overlap concentration, entanglement concentration, and gelation concentration (or critical polyelectrolyte concentration), respectively. Dielectric relaxation analysis has shown that the sacran has two types of counterions with different counterion-polyion interaction, i.e. strongly bound and loosely bound counterions. The dielectric parameters such as relaxation time or relaxation strength are sensitive to both the entanglement concentration and the gelation concentration, but not the overlap concentration. The number density of bound counterions calculated from the relaxation strength revealed that the counterion is condensed around the sacran chains. The decrease in the charge density of the sacran chains reduces the repulsive force between the chains and this would cause the helix transformation (observed by electron microscopy[17]) or gelation behavior. The chain conformation of sacran in pure water and the gelation mechanism are related to the behavior of liquid crystalline polyelectrolytes, and are illustrated in **Figure 4**.

Based on this efficient liquid crystallization ability, physically and chemically cross-linked LC gels have been developed. We fabricated LC hydrogels from cast films of sacran cross-linked by a thermal treatment. The cast films formed a layer structure which was driven by LC domains.[29] During the drying process, nanoplatelets of sacran were formed as a result of self-assembly.[30] The nanoplatelets oriented along the in-plane direction during condensation of the sacran solution to produce a layered arrangement in the cast films[31]. The LC hydrogels were formed by rehydration of the thermally-cross-linked cast films and had the ability to swell

uniaxially as the thickness was increased as water molecules diffused through the layers[32]. Furthermore, chemical cross-linked hydrogels were prepared by using divinyl sulfone as a cross-linker, which increased the swelling anisotropy[38]. Thus, the LC properties of sacran led to the unique characteristics of hydrogels, making them suitable for a wide range of applications such as drug carriers[33-35], catalyst adsorbents[36-37], and filters[38-39].

1.3 Scaffolds for tissue engineering

The regenerative treatment, tissue engineering (TE) is a multidisciplinary field that aims to provide therapeutic treatments to maintain, restore, or replace damaged or diseased tissues, and provide better alternatives for whole organ transplantation also[40-42]. Nowadays, TE have been made in the regeneration of various tissues such as skin[43], bone[44-45], cartilage[46], tendons[47], ligaments[48], liver[49], cardiac tissues[50], blood vessels[51], esophagus[52], adipose[53], renal[54], lung[55], and neural tissues[56].

The fundamental concept underlying tissue engineering is to combine a supporting matrix with living cells and/or biologically active molecules to form a tissue engineering construct which promotes the repair and/or regeneration of tissues[41] (Figure 5). In general, the main components of tissue engineering systems that decide its properties are cells, scaffolds, and bioactive factor (Figure 6).

1. Cells are isolated from native tissue, that can produce three-dimensional artificial tissue.

2. Scaffolds are supported materials for cells.

3. Bioactive molecule such as growth factor, that regulate and induce cellular behavior in a controlled manner.

The isolated cells (from autologous/allogenic source) need some kind of supporting structure to grow on and form new tissues. The supporting structures are often called “scaffolds” in which biomaterials are used to mimic a specific microenvironment. In this regard, scaffolds

play a key role in accommodating cells and directing their growth into specific tissues. The scaffold is expected to perform various functions, including the support of cell colonization, migration, growth, and differentiation. Therefore, the development of a suitable supporting base for both *in vitro* and *in vivo* applications of implants is the key point for successful cell transplantation therapy, emphasizing the importance of scaffolds in tissue engineering.

Scaffolds are three-dimensional materials for cell supported in tissue engineering.[57] The fundamental concept underlying tissue engineering is to combine a scaffold with living cells which promotes the repair or regeneration of tissues. The scaffolds always are biomaterials, which use to mimic a native environment for cells. In regeneration tissue, scaffolds play a key important role in accommodating cells and guiding their growth direction into specific tissue.[58] The native muscle comprises of fibers formed through orientation of cells. Therefore, a major part of tissue engineering research has been devoted to designing biomaterials that can provide instructive cues for cells and tissues. To design such well-organized tissue, many fabrication approaches, such as electrospinning[59-62], spin coating[63], three-dimension printing[64-66], surfaced pattern[67-69], and so on. Furthermore, oriented scaffolds on the molecular level, which effectively controlled by using liquid crystalline (LC) polymers.[70]

Scaffolds materials need basic requirement such as biocompatible property they should not to produce an unfavorable physiological response. Biodegradable property, the rate of degradation should match with the healing rate of new tissues and the broken down polymer should not toxic molecules. Scaffolds should have congruent mechanical properties with the native tissue which can adjust by preparation techniques and precursor. Furthermore, scaffolds will play a property like extra cellular matrix for serving the formation of new tissue.

To achieve muscle function, the cells orientation was important factor. Because native tissue revealed one direction of cell orientation. To controlled the cells orientation, the scaffolds

were fabricated using various methods, such as electrospinning, groove/ridge micro- and nano-patterns by photolithography, spin coating, and 3D-printing.

1.3.1 Oriented scaffold prepared by electrospinning technique

Electrospinning, as a simple yet versatile manufacturing method to process a rich variety of biomaterials into nanofibers, has recently been garnering a lot of attention as the scaffolds obtained through electrospinning possess many attractive features, such as high surface area to volume ratio, formation of interconnected porous networks, similarity in fiber size scale to those of the extra cellular matrix (ECM) of native vasculature, and adjustable surface structure. These advantages make the electrospun nanofibrous scaffolds a favorable candidate for tissue engineering. However, the traditional electrospun scaffolds showed randomly deposited electrospun nanofibers. To achieve an electrospun vascular scaffold with uni-direction alignment structure. By modify a template collector nanofiber will deposit with the unique structure of the wire spring collector, electrospun vascular scaffolds with aligned nanofibrous structures.

Figure 7 and 8 showed aligned fiber scaffolds prepared by electrospinning technique. In 2015 Anneng Yang et al prepared aligned fiber scaffolds from poly *L*-lactic acid polymer using electrospinning technique[59, 71]. The rotation collector device was used to collect the align fiber while a flat aluminum foil was used for random fiber. Besides, the morphology of fiber was adjusted by the concentration of poly *L*-lactic acid polymer. Moreover, the wire springs collector also usage for alignment controlling[72].

1.3.2 Oriented scaffold prepared by Photo and chemical cross-linking technique[73].

Photochemical surface modification has high potential in *in situ* patterning and controlling living cells, whose developments are introduced and recent progresses by utilizing laser. The patterning was started by introducing photolithography which needs photomasks to fabricate fine structures on a substrate. The photolithography was developed to soft lithography

and it has been widely applied for patterning proteins and living cells. On the other hand, photochemical and photothermal methods for surface modification enable us to form various patterning, through which cell control is realized. These are well achieved spatio-temporally by introducing laser ablation which is of superior features.

Figure 9 showed gelatin methacrylate (GelMA) hydrogels with hexagonal geometry on surface. The GelMA solution was mixed with irgacure 2959 photoinitiator then using UV photo cross-linking under the virtual mask in the form of hexagonal pattern. The GelMA hydrogels showed anisotropic swelling due to cross-linking density. The patterning was controlled by the shape of mask. Therefore, GelMA hydrogel with surface patterning has potential for oriented scaffolds[74].

1.3.3 Oriented scaffold prepared by surface topography technique[75-76].

Surface topography has been introduced as a new tool to coordinate cell selection, growth, morphology, and differentiation. A precise control of cell alignment and organization in vitro relies on a robust micro/nano-fabrication technique to construct a synthetic extracellular environment mimicking the native biological environment. To address this need, one popular technique is to fabricate and use a culture substrate with microscopic features that impose a defined cell adhesion pattern. This technique has been used to study the influence of cell shape on its architecture, migration, differentiation, and growth.

Figure 10-11 showed scaffolds with micro-grooved structure. These scaffolds were prepared by gelation the collagen on ice template. The collagen was added to container with ice template, after cross-linked the hydrogels were frozen dry. Result in sponge scaffolds with micro-pattern groove like ice template. They showed high precisely controlled the shape and size of groove. For cell culture, they showed orientation of cell depend on size of grooved and cells density. Moreover, by using ice template, scaffolds with various type of pattern was successful prepared[67].

1.3.4 Oriented scaffold prepared by LC polymer[70, 75].

One of the most effective methods for controlling the substrate orientation on the molecular level is to use liquid crystalline (LC) polymers. The orientation was controlled by the LC domains polymers, which can be revealed in different of orientation degree.

LC hydrogel was prepared from poly(2,2′-disulfonyl-4,4′-benzidine terephthalamide) (PBDT) and poly(N-[3-(*N*,*N*-dimethylamino)propyl] acrylamide methyl chloride quaternary) (PDMAPAA-Q). Due to LC property of PBDT, the highly oriented molecule is seen on the structure of hydrogel (Figure 12)[75]. There are two possible directions of orientation, parallel and vertical, which depends on swelling behavior. Moreover, the LC hydrogel presents anisotropic mechanical property in parallel and vertical direction due to the orientation direction of the molecule.

LC polymers synthesis needs a complex process for preparation. To overcome the problem in this research, natural polysaccharide LC polymer, sacran, was used.

1.4 Objective

As previously mentioned, scaffolds play as an important substrate in regenerative tissue engineering. The orientation of scaffolds is an essential property for tissue engineering but there are only a few numbers of study on the topic. To evaluate the new methodology of preparing the sacran-based LC polymer, my research aims are setting up as following:

1. To prepared anisotropic porous materials using sacran LC polymer.
2. To study the biocompatibility of anisotropic porous sacran.
3. To prepare sacran hydrogels with micro-patterned on the surface.
4. To study the orientation property of sacran anisotropic porous and micro-patterned hydrogels.
5. To evaluate the orientation of cell on sacran materials.

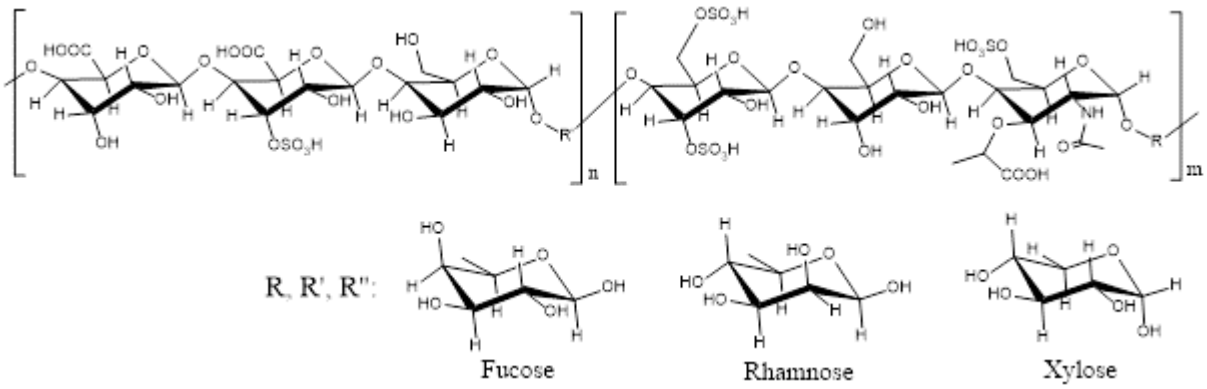

Figure 1. Chemical structure of sacran LC molecules.

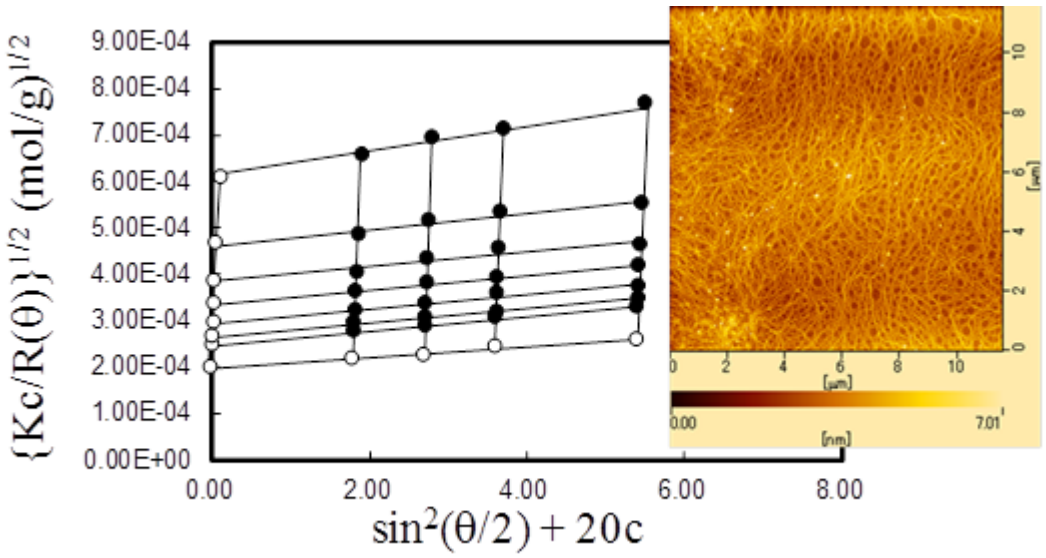

Figure 2. Zimm-Berry plots of the sacran solution. Inset picture: AFM height image of the dried specimen cast from the sacran solution (10 ppm) onto a mica substrate[16].

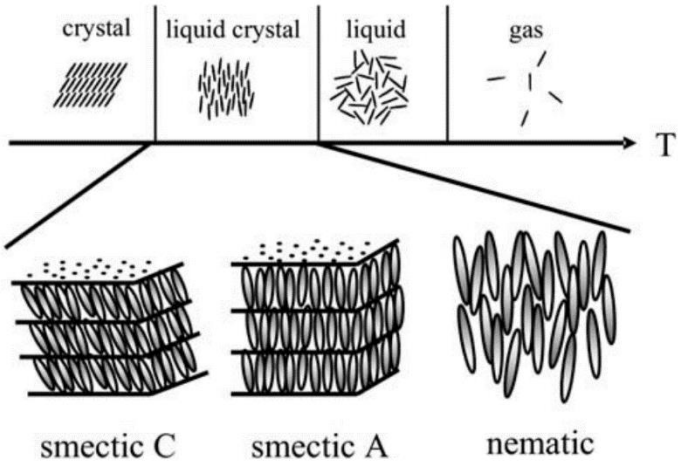

Figure 3. Schematic illustration of the occurrence of thermotropic liquid crystal phases as an intermediate state between the solid crystal and the isotropic liquid. LC exhibit both, anisotropy of physical properties, alongside with flow properties of a viscous liquid. A large variety of liquid crystal phases are distinguished, the most prominent being shown; the nematic phase with only orientation order of the long axis of elongated molecules, and the fluid smectic phases (smectic A andsmectic C) which exhibit additional one-dimensional positional order.[77]

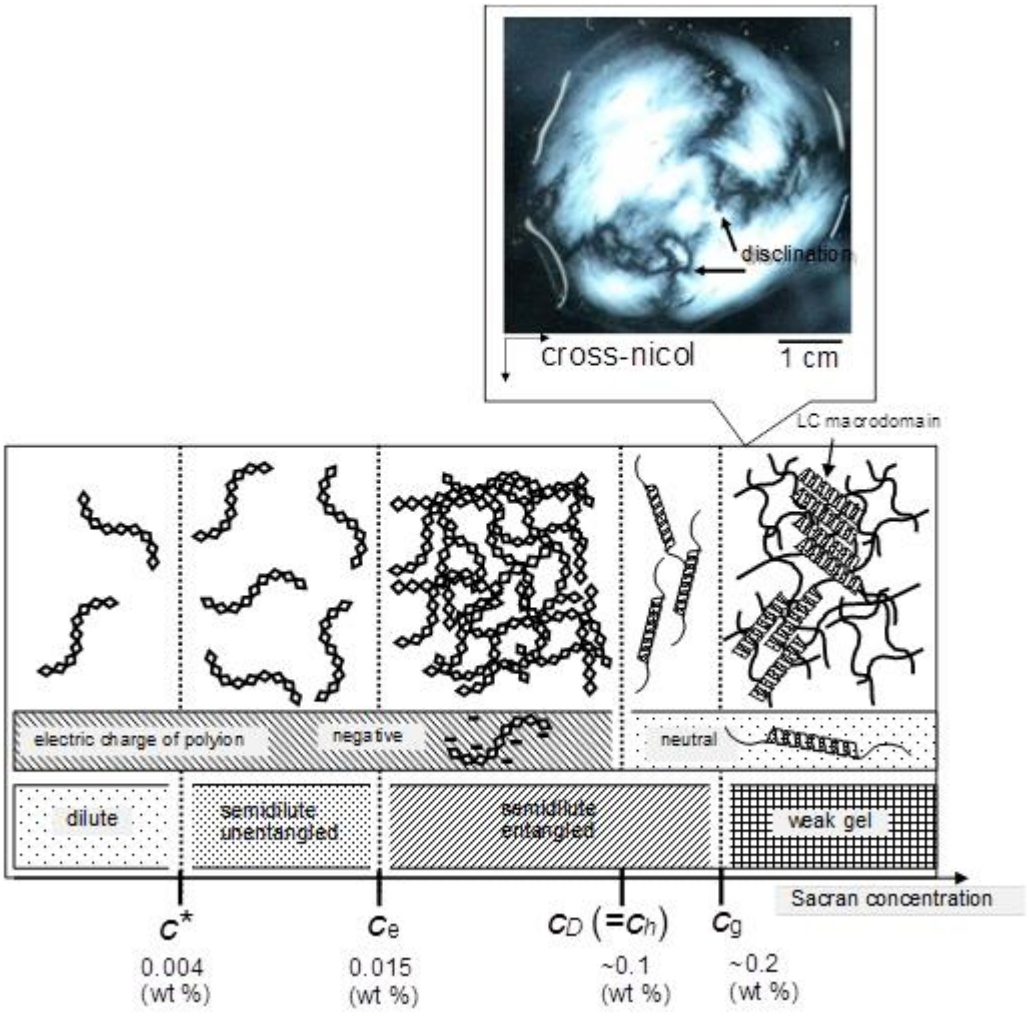

Figure 4. Schematic illustrations representing the chain conformation of sacran in salt-free solutions (c^*: overlap concentration, c_e: entanglement concentration, c_D: critical polyelectrolyte solution, c_h: helix transition concentration, c_g: gelation concentration). Inset microscopic picture is Schlieren texture taken under cross-Nicol polarimetry in a concentration of 0.5 wt%[78].

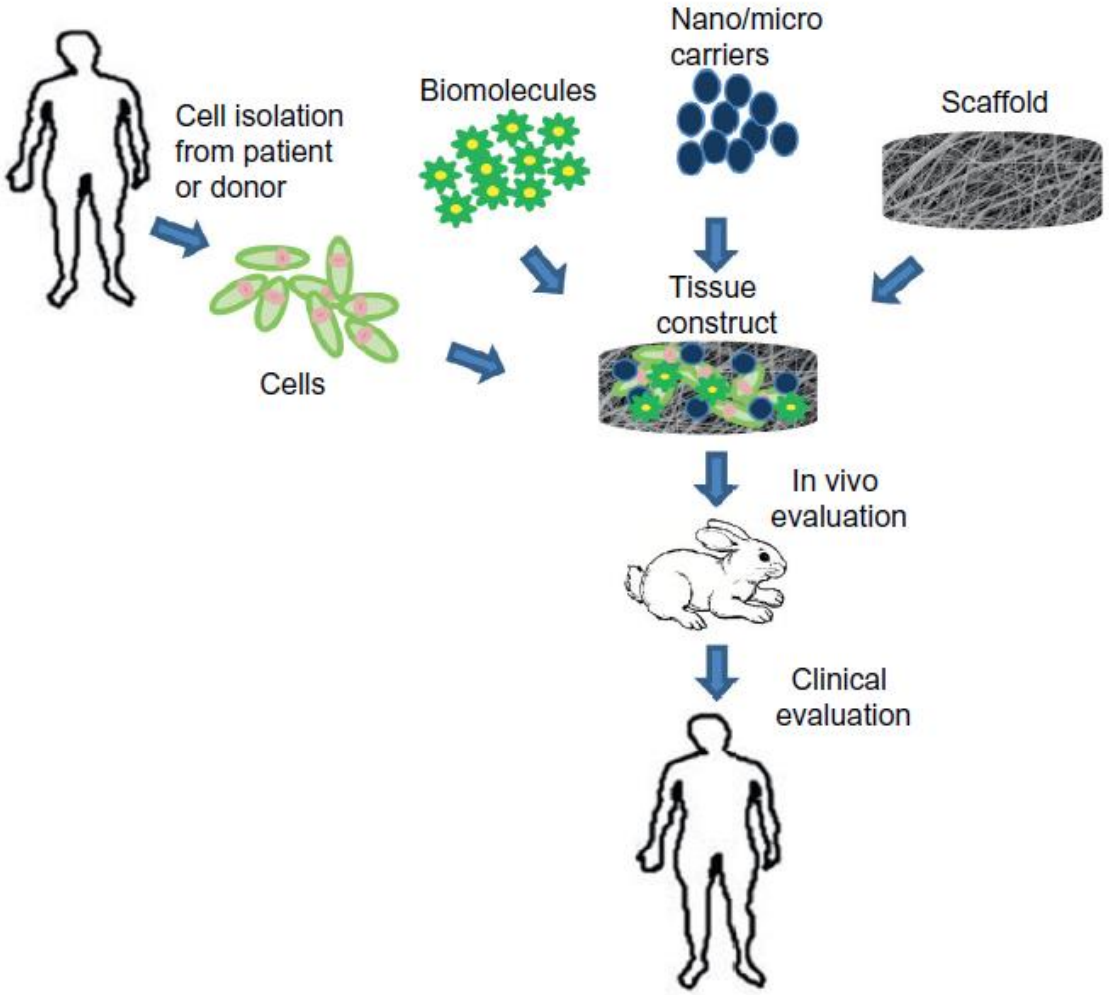

Figure 5. Schematic diagram of scaffold-based tissue engineering[41].

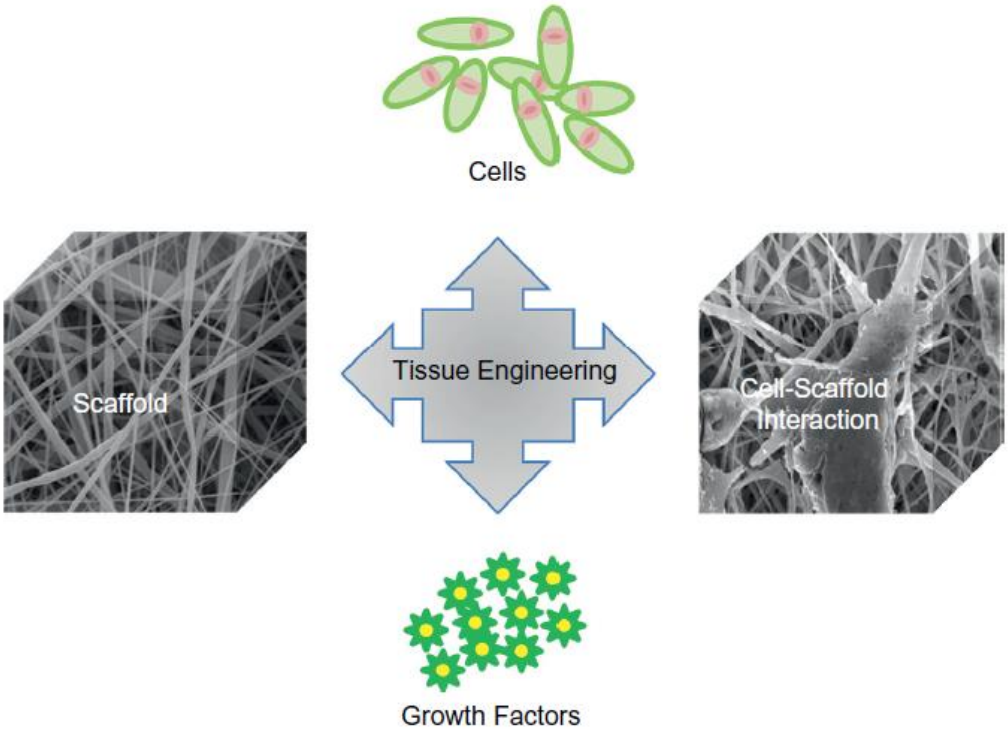

Figure 6. Schematic diagram showing key components of scaffold-based tissue engineering[41].

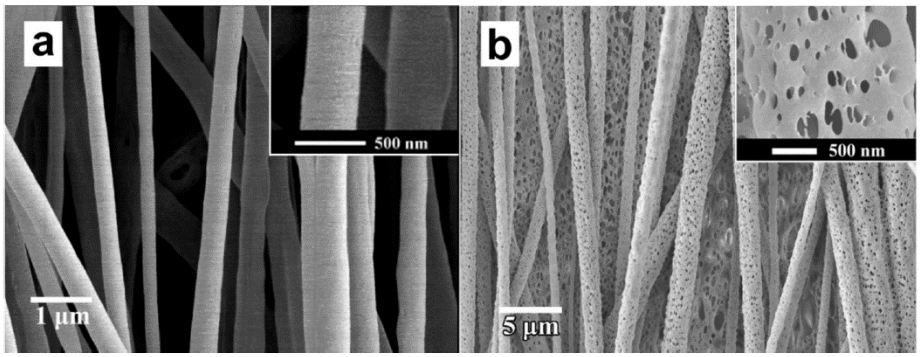

Figure 7. SEM images of electrospun aligned fibers without pores (a) and with pores (b). The upper right corner inset for the corresponding enlargements[59].

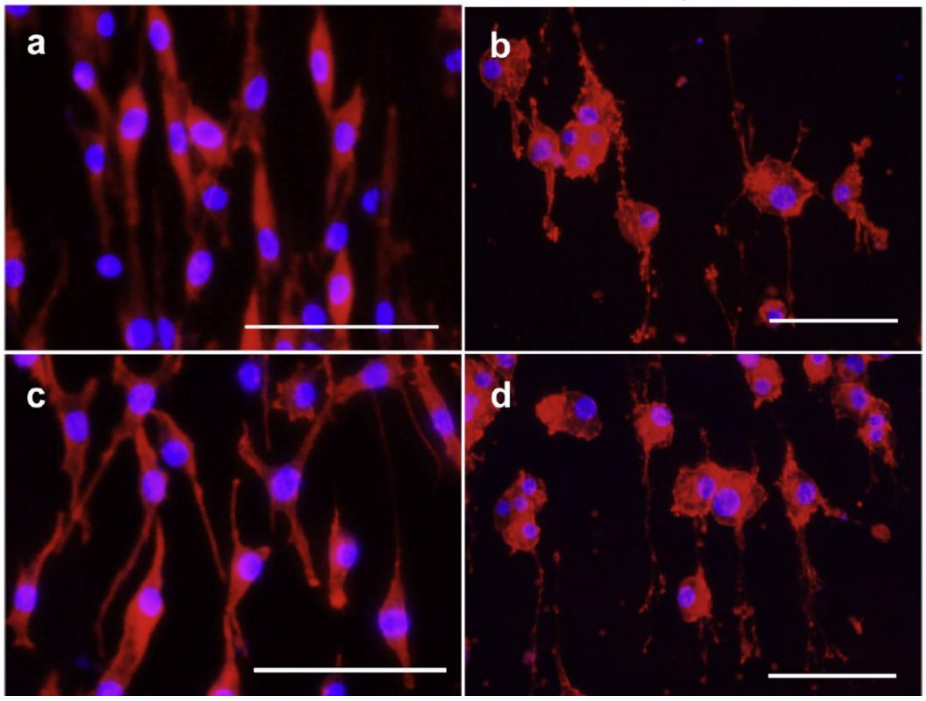

Figure 8. Immunofluorescence micrograph of L929 cells and PC12 cells stained by phalloidin/DAPI on polypyrrole aligned fibers (a, b) and polypyrrole aligned porous fibers (c, d). Scale bar = 100 μm[59].

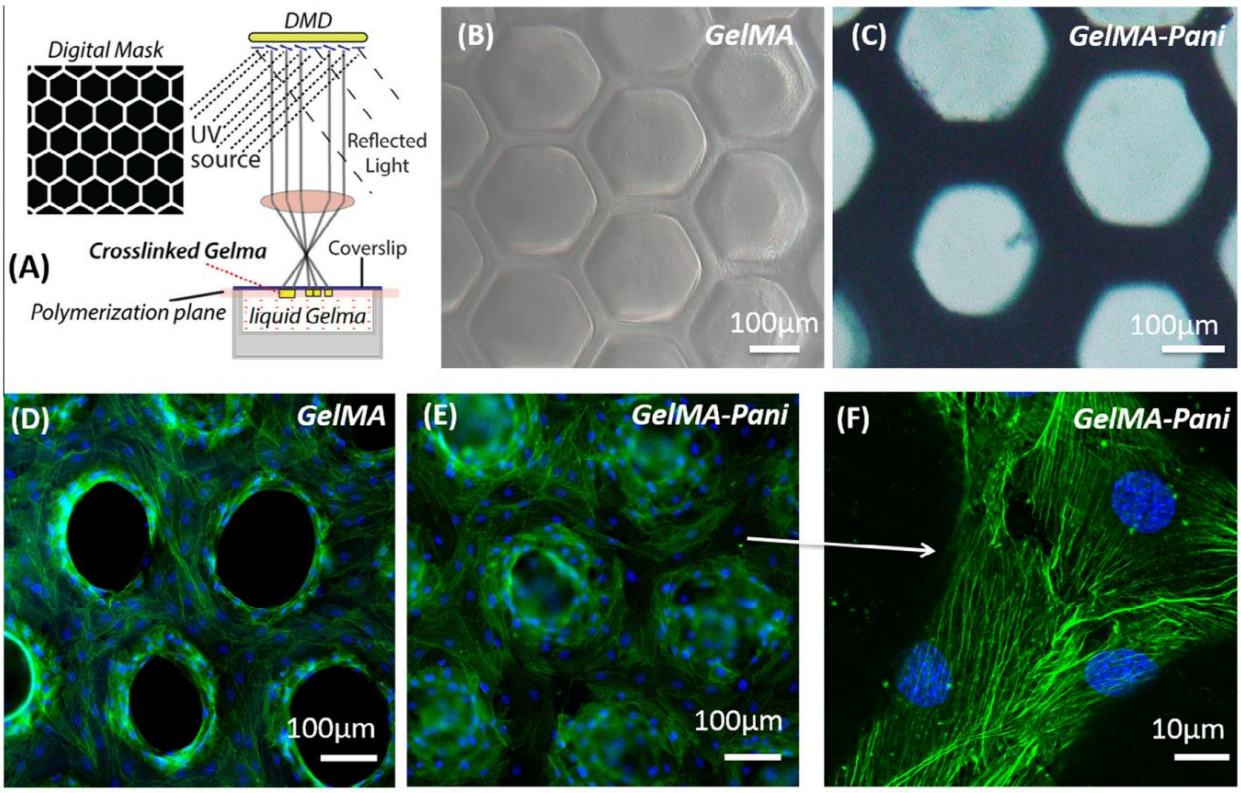

Figure 9. Fabrication of GelMA–Pani using user-defined hexagonal geometry: (A) Schematic of digital projection micro-stereolithography: Liquid GelMA precursor solution is placed in a chamber covered by a methacrylated glass coverslip. Computer aided design (CAD)-based digital mask with hexagonal pattern is used to modulate UV light, and selectively polymerize GelMA. (B and C) Brightfield images of GelMA (semi-transparent) and GelMA–Pani (dark-green) with hexagonal geometry. (D–F) Fluorescence and confocal images of GelMA and GelMA–Pani samples seeded with 10T1/2 cells, and labelled for actin (green) and nucleus (blue)[74].

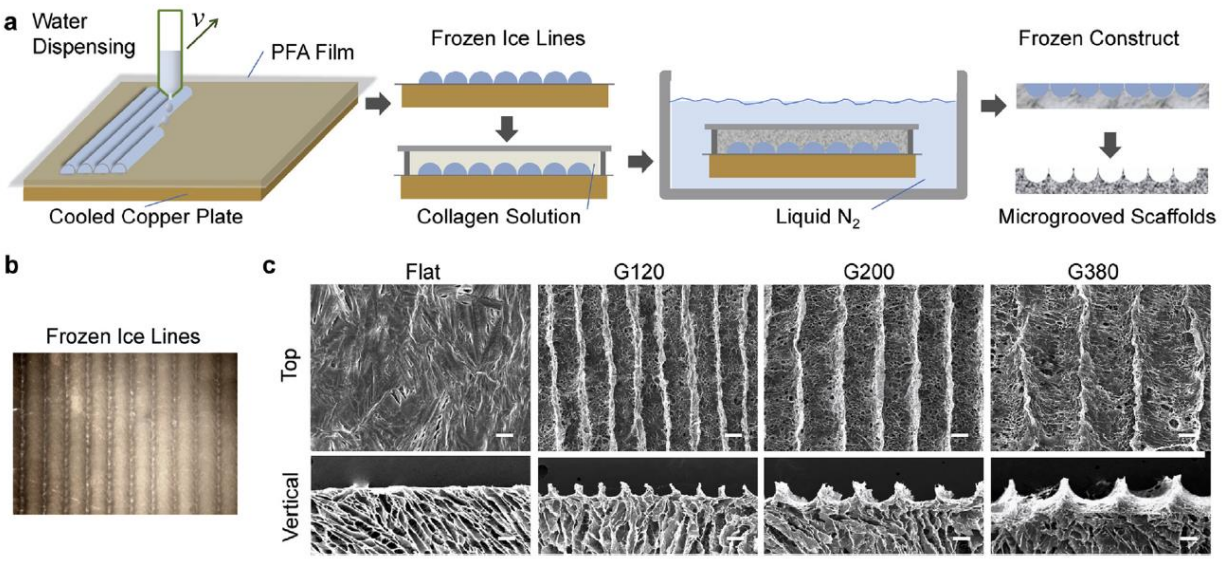

Figure 10. Preparation of micro-grooved collagen scaffolds. (a) A schematic for the preparation of micro-grooved collagen scaffolds. (b) Image of frozen ice lines prepared from water dispensing. (c) SEM images of different micro-grooved collagen scaffolds. Flat: control collagen scaffolds with a flat surface; G120, G200, G380: collagen scaffolds with mean microgroove widths of 120, 200, 380 mm, respectively. Upper images show the top view and lower images show the vertical cross-sectional view of different scaffolds. Scale bar : 100 mm[67].

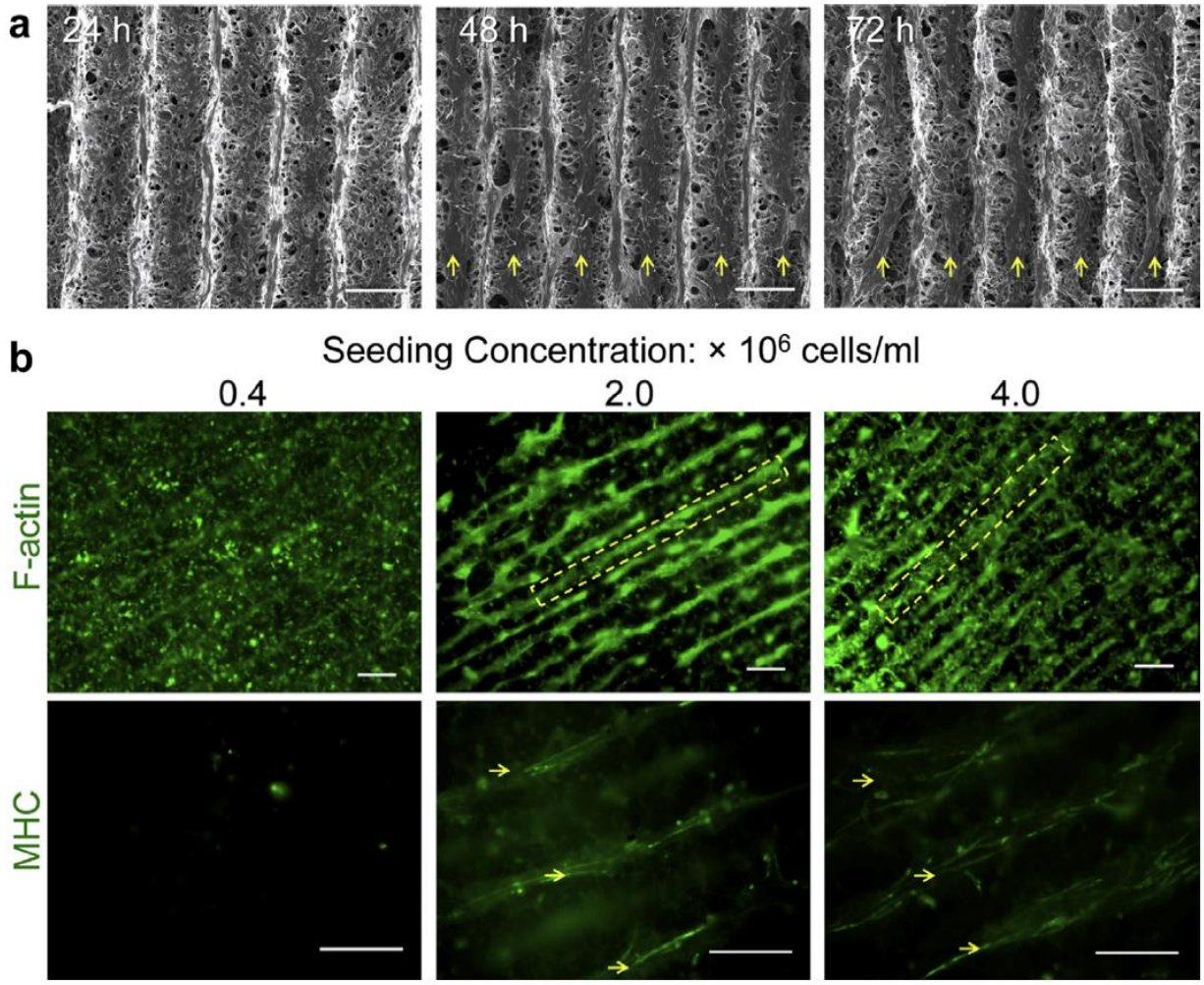

Figure 11. Formation of cell bundles in micro-grooved scaffolds. (a) SEM images of cell-seeded scaffolds (G200, seeding concentration: 2.0×10^6/ml) after 24 h, 48 h and 72 h culture. Arrows mark cell bundles formed in the microgrooves. (b) Cell bundle formation in scaffolds (G200) seeded with different concentrations of myoblasts (0.4, 2.0, 4.0×10^6/ml) after 7 d culture. Myoblasts were visualized using F-actin staining; myotube formation was shown using MHC staining. Dashed squares mark cell bundle in the microgrooves and arrows mark myotubes in microgrooves. Scale bar: 200 mm[67].

Figure 12. Orientation characterization of superstructure formed in patterned hydrogels. Observation of superstructure of PBDT in patterned PDMAPAA-Q hydrogels at as-prepared (a,b) and swollen (c,d) states. The gels were observed under POM from top (a,c) and side (b,d) directions. The thickness of the observation direction from side was unified into B2 mm. The images in column (i) were observed under the parallel polarizers, columns (ii) and (iii) were observed under the crossed polarizers without and with 530-nm tint plate, respectively. The column (iv) is a schematic illustration of the orientation of PBDT molecules within the gel, where the green bars represent PBDTs with weak orientation, the green circles represent PBDTs orientation of vertical direction to the sheet, the orange and blue bars represent highly ordered PBDTs. A: Analyzer; P: Polarizer; X' : fast axis of the tint plate; Z' : slow axis of the tint plate. Scale bar, 1 mm[75].

References:

1. Dodds, W. K.; Gudder, D. A.; Mollenhauer, D., The ecology of Nostoc. *Journal of Phycology* **1995,** *31* (1), 2-18.
2. De Philippis, R.; Vincenzini, M., Exocellular polysaccharides from cyanobacteria and their possible applications. *FEMS Microbiology Reviews* **1998,** *22* (3), 151-175.
3. De Philippis, R.; Sili, C.; Paperi, R.; Vincenzini, M., Exopolysaccharide-producing cyanobacteria and their possible exploitation: a review. *Journal of Applied Phycology* **2001,** *13* (4), 293-299.
4. Li, P.; Harding, S. E.; Liu, Z., Cyanobacterial exopolysaccharides: their nature and potential biotechnological applications. *Biotechnology and Genetic Engineering Reviews* **2001,** *18* (1), 375-404.
5. Pereira, S.; Zille, A.; Micheletti, E.; Moradas-Ferreira, P.; De Philippis, R.; Tamagnini, P., Complexity of cyanobacterial exopolysaccharides: composition, structures, inducing factors and putative genes involved in their biosynthesis and assembly. *FEMS microbiology reviews* **2009,** *33* (5), 917-941.
6. Rippka, R.; Deruelles, J.; Waterbury, J. B.; Herdman, M.; Stanier, R. Y., Generic assignments, strain histories and properties of pure cultures of cyanobacteria. *Microbiology* **1979,** *111* (1), 1-61.
7. Kaplan, D.; Christiaen, D.; Arad, S. M., Chelating properties of extracellular polysaccharides from Chlorella spp. *Applied and Environmental Microbiology* **1987,** *53* (12), 2953-2956.
8. Kurek, E.; Francis, A.; Bollag, J.-M., Immobilization of cadmium by microbial extracellular products. *Archives of Environmental Contamination and Toxicology* **1991,** *21* (1), 106-111.
9. Li, P.; Liu, Z.; Xu, R., Chemical characterisation of the released polysaccharide from the cyanobacterium Aphanothece halophytica GR02. *Journal of applied phycology* **2001,** *13* (1), 71-77.
10. Sutherland, I. W., Structure-function relationships in microbial exopolysaccharides. *Biotechnology advances* **1994,** *12* (2), 393-448.
11. Tease, B. E.; Walker, R. W., Comparative composition of the sheath of the cyanobacterium Gloeothece ATCC 27152 cultured with and without combined nitrogen. *Microbiology* **1987,** *133* (12), 3331-3339.
12. De Philippis, R.; Sili, C.; Tassinato, G.; Vincenzini, M.; Materassi, R., Effects of growth conditions on exopolysaccharide production by Cyanospira capsulata. *Bioresource Technology* **1991,** *38* (2-3), 101-104.
13. Schenck, T. L.; Hopfner, U.; Chávez, M. N.; Machens, H.-G.; Somlai-Schweiger, I.; Giunta, R. E.; Bohne, A. V.; Nickelsen, J.; Allende, M. L.; Egaña, J. T., Photosynthetic biomaterials: A pathway towards autotrophic tissue engineering. *Acta biomaterialia* **2015,** *15*, 39-47.
14. Chávez, M. N.; Schenck, T. L.; Hopfner, U.; Centeno-Cerdas, C.; Somlai-Schweiger, I.; Schwarz, C.; Machens, H.-G.; Heikenwalder, M.; Bono, M. R.; Allende, M. L., Towards autotrophic tissue engineering: photosynthetic gene therapy for regeneration. *Biomaterials* **2016,** *75*, 25-36.

15. Okajima-Kaneko, M.; Ono, M.; Kabata, K.; Kaneko, T., Extraction of novel sulfated polysaccharides from Aphanothece sacrum (Sur.) Okada, and its spectroscopic characterization. *Pure and Applied Chemistry* **2007,** *79* (11).
16. Okajima, M. K.; Bamba, T.; Kaneso, Y.; Hirata, K.; Fukusaki, E.; Kajiyama, S. i.; Kaneko, T., Supergiant ampholytic sugar chains with imbalanced charge ratio form saline ultra-absorbent hydrogels. *Macromolecules* **2008,** *41* (12), 4061-4064.
17. Okajima, M. K.; Kaneko, D.; Mitsumata, T.; Kaneko, T.; Watanabe, J., Cyanobacteria That Produce Megamolecules with Efficient Self-Orientations. *Macromolecules* **2009,** *42* (8), 3057-3062.
18. Okajima, M. K.; Kumar, A.; Fujiwara, A.; Mitsumata, T.; Kaneko, D.; Ogawa, T.; Kurata, H.; Isoda, S.; Kaneko, T., Anionic complexes of MWCNT with supergiant cyanobacterial polyanions. *Biopolymers* **2013,** *99* (1), 1-9.
19. Gilbert, R.-D.; Patton, P., Liquid crystal formation in cellulose and cellulose derivatives. *Progress in Polymer Science* **1983,** *9* (2-3), 115-131.
20. Greiner, A.; Hou, H.; Reuning, A.; Thomas, A.; Wendorff, J.; Zimmermann, S., Synthesis and opto-electronic properties of cholesteric cellulose esters. *Cellulose* **2003,** *10* (1), 37-52.
21. Takada, A.; Fujii, K.; Watanabe, J.; Fukuda, T.; Miyamoto, T., Chain-length dependence of the mesomorphic properties of fully decanoated cellulose and cellooligosaccharides. *Macromolecules* **1994,** *27* (6), 1651-1653.
22. Giraud-Guille, M.-M., Twisted liquid crystalline supramolecular arrangements in morphogenesis. *International review of cytology* **1996,** *166*, 59-101.
23. Vincent, J., From cellulose to cell. *Journal of Experimental Biology* **1999,** *202* (23), 3263-3268.
24. Mitov, M.; Dessaud, N., Going beyond the reflectance limit of cholesteric liquid crystals. *Nature materials* **2006,** *5* (5), 361.
25. Giraud-Guille, M.-M., Twisted plywood architecture of collagen fibrils in human compact bone osteons. *Calcified tissue international* **1988,** *42* (3), 167-180.
26. Sundaresan, N.; Suresh, C. H.; Thomas, T.; Thomas, T.; Pillai, C., Liquid crystalline phase behavior of high molecular weight DNA: a comparative study of the influence of metal ions of different size, charge and binding mode. *Biomacromolecules* **2008,** *9* (7), 1860-1869.
27. Flory, P. J. In *Phase equilibria in solutions of rod-like particles*, Proceedings of the Royal Society of London A: Mathematical, Physical and Engineering Sciences, The Royal Society: 1956; pp 73-89.
28. Flory, P. J., Molecular theory of liquid crystals. In *Liquid crystal polymers I*, Springer: 1984; pp 1-36.
29. Okajima, M. K.; Mishima, R.; Amornwachirabodee, K.; Mitsumata, T.; Okeyoshi, K.; Kaneko, T., Anisotropic swelling in hydrogels formed by cooperatively aligned megamolecules. *RSC Adv.* **2015,** *5* (105), 86723-86729.
30. Okeyoshi, K.; Joshi, G.; Rawat, S.; Sornkamnerd, S.; Amornwachirabodee, K.; Okajima, M. K.; Ito, M.; Kobayashi, S.; Higashimine, K.; Oshima, Y., Drying-Induced Self-Similar Assembly of Megamolecular Polysaccharides through Nano and Submicron Layering. *Langmuir* **2017,** *33* (20), 4954-4959.

31. Okeyoshi, K.; Okajima, M. K.; Kaneko, T., Milliscale Self-Integration of Megamolecule Biopolymers on a Drying Gas-Aqueous Liquid Crystalline Interface. *Biomacromolecules* **2016,** *17* (6), 2096-103.
32. Joshi, G.; Okeyoshi, K.; Okajima, M. K.; Kaneko, T., Directional control of diffusion and swelling in megamolecular polysaccharide hydrogels. *Soft Matter* **2016,** *12* (25), 5515-8.
33. Liu, J.; Qi, C.; Tao, K.; Zhang, J.; Zhang, J.; Xu, L.; Jiang, X.; Zhang, Y.; Huang, L.; Li, Q.; Xie, H.; Gao, J.; Shuai, X.; Wang, G.; Wang, Z.; Wang, L., Sericin/Dextran Injectable Hydrogel as an Optically Trackable Drug Delivery System for Malignant Melanoma Treatment. *ACS Applied Materials & Interfaces* **2016,** *8* (10), 6411-6422.
34. Weaver, C. L.; LaRosa, J. M.; Luo, X.; Cui, X. T., Electrically Controlled Drug Delivery from Graphene Oxide Nanocomposite Films. *ACS Nano* **2014,** *8* (2), 1834-1843.
35. Yuan, X.; Marcano, D. C.; Shin, C. S.; Hua, X.; Isenhart, L. C.; Pflugfelder, S. C.; Acharya, G., Ocular Drug Delivery Nanowafer with Enhanced Therapeutic Efficacy. *ACS Nano* **2015,** *9* (2), 1749-1758.
36. Li, Z.; Zheng, Z.; Su, S.; Yu, L.; Wang, X., Preparation of a High-Strength Hydrogel with Slidable and Tunable Potential Functionalization Sites. *Macromolecules* **2016,** *49* (1), 373-386.
37. Zhao, Y.; Zhang, Y.; Liu, A.; Wei, Z.; Liu, S., Construction of Three-Dimensional Hemin-Functionalized Graphene Hydrogel with High Mechanical Stability and Adsorption Capacity for Enhancing Photodegradation of Methylene Blue. *ACS Applied Materials & Interfaces* **2017,** *9* (4), 4006-4014.
38. Liu, H.; Zuo, K.; Vecitis, C. D., Titanium Dioxide-Coated Carbon Nanotube Network Filter for Rapid and Effective Arsenic Sorption. *Environmental Science & Technology* **2014,** *48* (23), 13871-13879.
39. Wang, H.; Zhang, L.; Li, Y.; Hu, C., Influence of Filtration Aids on Continuous Filtration in Membrane Bioreactors. *Industrial & Engineering Chemistry Research* **2014,** *53* (17), 7202-7208.
40. Venkatesan, J.; Kim, S.-K.; Wong, T. W., Chitosan and Its Application as Tissue Engineering Scaffolds. In *Nanotechnology Applications for Tissue Engineering*, 2015; pp 133-147.
41. Rana, D.; Arulkumar, S.; Vishwakarma, A.; Ramalingam, M., Considerations on Designing Scaffold for Tissue Engineering. In *Stem Cell Biology and Tissue Engineering in Dental Sciences*, 2015; pp 133-148.
42. Ravichandran, R.; Sundarrajan, S.; Venugopal, J. R.; Mukherjee, S.; Ramakrishna, S., Advances in polymeric systems for tissue engineering and biomedical applications. *Macromolecular bioscience* **2012,** *12* (3), 286-311.
43. Eaglstein, W. H.; Falanga, V., Tissue engineering and the development of Apligraf®, a human skin equivalent. *Clinical Therapeutics* **1997,** *19* (5), 894-905.
44. Hutmacher, D. W., Scaffolds in tissue engineering bone and cartilage. *Biomaterials* **2000,** *21* (24), 2529-2543.
45. Hu, Y.-C., Bone and Cartilage Tissue Engineering. In *Gene Therapy for Cartilage and Bone Tissue Engineering*, Springer Berlin Heidelberg: Berlin, Heidelberg, 2014; pp 1-15.
46. Marcacci, M.; Berruto, M.; Brocchetta, D.; Delcogliano, A.; Ghinelli, D.; Gobbi, A.; Kon, E.; Pederzini, L.; Rosa, D.; Sacchetti, G. L., Articular Cartilage Engineering with

Hyalograft (R) C: 3-Year Clinical Results. *Clinical orthopaedics and related research* **2005,** *435*, 96-105.
47. Calve, S.; Dennis, R. G.; Kosnik, P. E.; Baar, K.; Grosh, K.; Arruda, E. M., Engineering of functional tendon. *Tissue engineering* **2004,** *10* (5-6), 755-761.
48. Vunjak-Novakovic, G.; Altman, G.; Horan, R.; Kaplan, D. L., Tissue engineering of ligaments. *Annu. Rev. Biomed. Eng.* **2004,** *6*, 131-156.
49. Kulig, K. M.; Vacanti, J. P., Hepatic tissue engineering. *Transplant Immunology* **2004,** *12* (3), 303-310.
50. Jawad, H.; Ali, N.; Lyon, A.; Chen, Q.; Harding, S.; Boccaccini, A., Myocardial tissue engineering: a review. *Journal of tissue engineering and regenerative medicine* **2007,** *1* (5), 327-342.
51. Koike, N.; Fukumura, D.; Gralla, O.; Au, P.; Schechner, J. S.; Jain, R. K., Tissue engineering: creation of long-lasting blood vessels. *Nature* **2004,** *428* (6979), 138-139.
52. Penkala, R. A.; Kim, S. S., Gastrointestinal tissue engineering. *Expert review of medical devices* **2007,** *4* (1), 65-72.
53. Stosich, M. S.; Mao, J. J., Adipose tissue engineering from human adult stem cells: clinical implications in plastic and reconstructive surgery. *Plastic and reconstructive surgery* **2007,** *119* (1), 71.
54. Fiegel, H. C.; Kaufmann, P. M.; Bruns, H.; Kluth, D.; Horch, R. E.; Vacanti, J. P.; Kneser, U., Hepatic tissue engineering: From transplantation to customized cell-based liver directed therapies from the laboratory. *Journal of cellular and molecular medicine* **2008,** *12* (1), 56-66.
55. Wagner, W. R.; Griffith, B. P., Reconstructing the lung. *Science* **2010,** *329* (5991), 520-522.
56. Chalfoun, C.; Wirth, G.; Evans, G., Tissue engineered nerve constructs: where do we stand? *Journal of cellular and molecular medicine* **2006,** *10* (2), 309-317.
57. Molinos, M.; Carvalho, V.; Silva, D. M.; Gama, F. M., Development of a hybrid dextrin hydrogel encapsulating dextrin nanogel as protein delivery system. *Biomacromolecules* **2012,** *13* (2), 517-527.
58. Madhurakkat Perikamana, S. K.; Lee, J.; Lee, Y. B.; Shin, Y. M.; Lee, E. J.; Mikos, A. G.; Shin, H., Materials from mussel-inspired chemistry for cell and tissue engineering applications. *Biomacromolecules* **2015,** *16* (9), 2541-2555.
59. Yang, A.; Huang, Z.; Yin, G.; Pu, X., Fabrication of aligned, porous and conductive fibers and their effects on cell adhesion and guidance. *Colloids and Surfaces B: Biointerfaces* **2015,** *134*, 469-474.
60. Wang, Y.; Shi, H.; Qiao, J.; Tian, Y.; Wu, M.; Zhang, W.; Lin, Y.; Niu, Z.; Huang, Y., Electrospun Tubular Scaffold with Circumferentially Aligned Nanofibers for Regulating Smooth Muscle Cell Growth. *ACS Applied Materials & Interfaces* **2014,** *6* (4), 2958-2962.
61. Asran, A. S.; Razghandi, K.; Aggarwal, N.; Michler, G. H.; Groth, T., Nanofibers from Blends of Polyvinyl Alcohol and Polyhydroxy Butyrate As Potential Scaffold Material for Tissue Engineering of Skin. *Biomacromolecules* **2010,** *11* (12), 3413-3421.
62. Ahmed, F.; Choudhury, N. R.; Dutta, N. K.; Zannettino, A.; Knott, R., Near Superhydrophobic Fibrous Scaffold for Endothelialization: Fabrication, Characterization and Cellular Activities. *Biomacromolecules* **2013,** *14* (11), 3850-3860.

63. Watanabe, H.; Fujimoto, A.; Yamamoto, R.; Nishida, J.; Kobayashi, M.; Takahara, A., Scaffold for Growing Dense Polymer Brushes from a Versatile Substrate. *ACS Applied Materials & Interfaces* **2014,** *6* (5), 3648-3653.
64. Zhao, H.; Yang, F.; Fu, J.; Gao, Q.; Liu, A.; Sun, M.; He, Y., Printing@Clinic: From Medical Models to Organ Implants. *ACS Biomaterials Science & Engineering* **2017**.
65. Bakarich, S. E.; Gorkin, R.; in het Panhuis, M.; Spinks, G. M., Three-Dimensional Printing Fiber Reinforced Hydrogel Composites. *ACS Applied Materials & Interfaces* **2014,** *6* (18), 15998-16006.
66. Luo, Y.; Zhai, D.; Huan, Z.; Zhu, H.; Xia, L.; Chang, J.; Wu, C., Three-Dimensional Printing of Hollow-Struts-Packed Bioceramic Scaffolds for Bone Regeneration. *ACS Applied Materials & Interfaces* **2015,** *7* (43), 24377-24383.
67. Chen, S.; Nakamoto, T.; Kawazoe, N.; Chen, G., Engineering multi-layered skeletal muscle tissue by using 3D microgrooved collagen scaffolds. *Biomaterials* **2015,** *73*, 23-31.
68. McCormick, A. M.; Maddipatla, M. V.; Shi, S.; Chamsaz, E. A.; Yokoyama, H.; Joy, A.; Leipzig, N. D., Micropatterned Coumarin Polyester Thin Films Direct Neurite Orientation. *ACS applied materials & interfaces* **2014,** *6* (22), 19655-19667.
69. Hu, Y.; You, J.-O.; Aizenberg, J., Micropatterned hydrogel surface with high-aspect-ratio features for cell guidance and tissue growth. *ACS applied materials & interfaces* **2016,** *8* (34), 21939-21945.
70. Kaneko, T.; Tran, H. T.; Matsusaki, M.; Akashi, M., Biodegradable LC oligomers with cranked branching points form highly oriented fibrous scaffold for cytoskeletal orientation. *Chemistry of materials* **2006,** *18* (26), 6220-6226.
71. Yang, A.; Huang, Z.; Yin, G.; Pu, X., Fabrication of aligned, porous and conductive fibers and their effects on cell adhesion and guidance. *Colloids Surf B Biointerfaces* **2015,** *134*, 469-74.
72. Xu, H.; Li, H.; Ke, Q.; Chang, J., An anisotropically and heterogeneously aligned patterned electrospun scaffold with tailored mechanical property and improved bioactivity for vascular tissue engineering. *ACS Appl Mater Interfaces* **2015,** *7* (16), 8706-18.
73. Okano, K.; Hsu, H.-Y.; Li, Y.-K.; Masuhara, H., In situ patterning and controlling living cells by utilizing femtosecond laser. *Journal of Photochemistry and Photobiology C: Photochemistry Reviews* **2016,** *28*, 1-28.
74. Wu, Y.; Chen, Y. X.; Yan, J.; Quinn, D.; Dong, P.; Sawyer, S. W.; Soman, P., Fabrication of conductive gelatin methacrylate–polyaniline hydrogels. *Acta biomaterialia* **2016,** *33*, 122-130.
75. Takahashi, R.; Wu, Z. L.; Arifuzzaman, M.; Nonoyama, T.; Nakajima, T.; Kurokawa, T.; Gong, J. P., Control superstructure of rigid polyelectrolytes in oppositely charged hydrogels via programmed internal stress. *Nat Commun* **2014,** *5*, 4490.
76. Oh, H. H.; Ko, Y. G.; Lu, H.; Kawazoe, N.; Chen, G., Preparation of porous collagen scaffolds with micropatterned structures. *Advanced Materials* **2012,** *24* (31), 4311-4316.
77. Dierking, I., Recent developments in polymer stabilised liquid crystals. *Polymer Chemistry* **2010,** *1* (8), 1153-1159.
78. Mitsumata, T.; Miura, T.; Takahashi, N.; Kawai, M.; Okajima, M. K.; Kaneko, T., Ionic state and chain conformation for aqueous solutions of supergiant cyanobacterial polysaccharide. *Phys Rev E Stat Nonlin Soft Matter Phys* **2013,** *87* (4), 042607.

Chapter II: Preparation of anisotropic porous materials

1. Introduction

Porous hydrogels have been widely applied in the fields of artificial muscles, microfluidic valves, actuators, soft robotics, drug carriers, microlenses, supported catalysis, and chromatography.[1-8] Modulation of pore size and their distribution are essential for controlling hydrogel properties. Several strategies such as gas foaming, fiber bonding, and porogen leaching have been developed to fabricate hydrogels with homogeneous macropores for rapid stimuli-response. [2] One of the simplest methods for forming the pores in hydrogels is freeze-drying and re-swelling. The drawback of this method is that pore formation worsens the mechanical properties of the hydrogels, limiting their application.

Sacran is a newly developed sulfated polysaccharide extracted from a cyanobacterium, *Aphanothece sacrum*, which grows in underground freshwater. Sacran contains various sugar residues, such as Glc, Gal, Man, Xyl, Rha, Fuc, uronic acids, and muramic acids, where the chains are sulfated at a degree of 10-20 mol% to sugar residues. The sacran chain has a very high molecular weight of over 2.0 x 10^7 g/mol (molecular length over 30 μm), and shows self-assembly with increases in the solution concentration to become a rigid-rod structure at around 0.1%. In thicker solutions with concentrations ranging over 0.3 %, the sacran solution exhibits a liquid crystalline (LC) phase.[9] Sacran has various properties such as super-high water-absorbent capacity, and has potential for wound healing functions, anti-inflammatory effects, and anti-allergic activities.[10-12] Another unique behavior of sacran is film formation with an in-plane orientation structure which shows anisotropic swelling. These properties of sacran and

the above-mentioned importance of porous hydrogels motivated us to create tough and porous gels with molecular orientation of sacran LC chains. [13-14]

Here we report a new, simple method of preparing the layered sacran hydrogels with anisotropic pore structures using a casting and freeze-drying method, although many other complicated methods have been reported for the preparation of porous hydrogels such as metal-organic frameworks (MOFs)[15-17], electrospinning [18-23], gas foaming [24], 3D printing [25-28] and porogen leaching [29-31]. In particular, optimization of the hydrogelation condition creates tough hydrogels with a high porosity even in a water-swollen state.

2. Materials and methods

2.1 Materials.

Sacran was dedicated from Green Science Material Inc. (Kumamoto, Japan) and used as received. Tetralin was purchased from TCI, Japan.

2.2 Hydrogel preparation.

Hydrogels used here were prepared by the procedure shown in Figure 1. First non-porous sacran hydrogels were prepared as precursors for porous ones by a previously-reported procedure.[32] The sacran aqueous solution with a concentration of 0.5 % (50 ml) prepared by agitating at 80 °C for 8 h was cast into a polypropylene case (50 × 50 × 50 mm^3) and dried in an oven at 60 °C for 72 h to form translucent films with a thickness of 44 ± 9 μm. The films were punched into disk-like samples with a diameter of 5 mm and were thermally treated at 60, 80, 100, 120, and 140 °C, in order to cross-link the sacran chains in a dry film state. When the films were immersed in deionized water at room temperature and kept for 24 h, the translucent self-standing hydrogels were of an almost constant diameter, whereas the thickness was increased.

Next porous sacran hydrogels were prepared by the following procedure. The precursor hydrogels were frozen by keeping in liquid nitrogen for about 10 min and then drying in a

freeze-drying apparatus (EYELA, FDU-1200) for 72 hrs. We were able to confirm their complete drying because the samples spontaneously attached to the glass wall by electrostatic force. As a result of freeze-drying, spongy materials were formed. When the sponges were immersed in deionized water, self-standing hydrogels were recovered.

For comparison, non-porous sacran hydrogels were additionally prepared via the following freezing procedure. If the precursor hydrogels frozen by keeping in liquid nitrogen for about 10 min were thawed by leaving at room temperature for 1 hr, the hydrogels were recovered. The obtained hydrogels were immersed in deionized water and were kept for 24 h to reach an equilibrium swelling state. The freeze-thawed hydrogels were used for comparison to those that were freeze-dried because the former have a simple layer structure with no pores.

2.3 Pore size measurement.

Scanning electron microscopy (SEM, JEOL, JCM-6000PLUS) was used to investigate the sample structures. The samples were mounted onto metal stubs using carbon tape. The stubs were then coated with gold using a sputter coater machine. ImageJ analysis software was used to determine the averaged pore sizes of twenty randomly selected samples. Three different images of one freeze-dried sample were used for the mean pore size calculation.

2.4 Porosity measurement.

Porosity was evaluated using the tetralin displacement method as follows. Freeze-dried samples were cut into 5 mm diameter disk-like samples and were then immersed in tetralin which is slightly viscous solvent with a high boiling point. After keeping the samples for 3 days, the weight was measured by electronic balance. The porosity was then evaluated by the equation:

$$\%Porosity = \frac{(W_s - W_d)/\rho_{\text{tetraline}}}{V_s} \times 100 \quad (1)$$

where W_d is dry weight, W_s is weight in the swollen state, and V_s is the total volume of the swollen sample. The density of tetralin, $\rho_{tetralin}$, was 0.97 g/cm^3. The evaluations were repeated 5 times and the data were averaged.

2.5 Swelling properties.

The degrees of swelling were measured by the following method. The weights of dry precursor films or sponges were measured before hydrogel formation. The hydrogels swollen in an equilibrated state were weighed after the water on the sample surfaces was removed by wiping. The degree of swelling, *Q*, was evaluated by the ratio of the swollen weight, W_s, to the dry one, W_d:

$$Q = \frac{W_s}{W_d} \quad (2)$$

The water content, *A*, of the hydrogels was also evaluated by the following equation:

$$A = \frac{W_s - W_d}{W_d} \quad (3)$$

The values of 5 specimens were averaged.

2.6 Mechanical properties of the hydrogels. [33-35]

The mechanical properties of the sacran hydrogels were investigated in an elongation test. The elongation probe was set up on an Instron 3365 machine using a 5 kN load cell with a crosshead speed of 1.0 mm/min. Elastic modulus (*E*) of each sample was calculated using the following neo-Hookean equation applied to unidirectional elongation measurements:

$$\tau = \frac{F}{A} = E(\lambda - \lambda^{-2}) \quad (4)$$

where τ is the stress, *F* is the applied force, *A* is the original cross-sectional area of the hydrogels, and *E* is the elastic modulus. $\lambda = h/h_0$, where *h* is the hydrogel length under strain and h_0 is the hydrogel length before elongation. Plotting *F/A* versus $(\lambda - \lambda^{-2})$ resulted in a straight line with a slope of *E*, which is the modulus of elasticity of the swelling hydrogel.

The effective cross-link density, V_e, was calculated from the swelling ratio and modulus using the equation:

$$V_e = \frac{E\sqrt[3]{Q}}{RT} \quad (5)$$

where E is the elastic modulus, Q is the swelling degree, R is the gas constant, and T is the absolute temperature of the hydrogels.

The average molecular weight between cross-linking points, M_c, was calculated using the cross-link density as shown in the following equation:

$$M_c = \frac{\rho_p}{V_e} \quad (6)$$

where ρ_p is the density of the dry polymer (sacran ≈ 0.83 g/cm^3).

The average molecular length between cross-linking points, L, was calculated using the molecular weight between the cross-linking points as shown in the following equation:

$$L = \frac{M_c L_0}{M_0} \quad (7)$$

where L_0 is the molecular length of the polymer repeating unit (8.6 Å) and M_0 is the molecular weight of the polymer repeating unit.

The degree of cross-linking, X, can be estimated theoretically using M_c as given in the following equation:

$$X = \frac{M_0}{2M_c} \quad (8)$$

3. Results and discussion

3.1 Pore formation in hydrogels.

We made the porous sacran material using the freeze-drying technique which is a conventional and simple method widely used for pore preparation in hydrogels [36]. The rationale was that sacran, having an ultra-high molecular weight (>20 MDa) and a rigidity high enough to exhibit a LC phase where sacran chains are intrinsically self-oriented in a very low concentration (> 0.3 wt%) as stated in the introduction, might demonstrate the ability to form

strong networks of hydrogels. At first, the sacran solution was simply subjected to freeze-drying in order to form spongy materials (representative picture, Figure 2a) and then the spongy sacran was annealed at 60°C and 140°C in order to examine the thermal cross-linking behavior in the dried sponge state. SEM images of the sacran sponges were taken to observe the porous structure on their surfaces as shown in Figures 3a and 3b. The pore size of the sponges annealed at 60°C was about 6.0±1.5 μm which was higher than those annealed at 140 °C (2.3±0.9 μm). The pores created by freeze-drying shrunk with successive annealing treatments, which suggested that the thermal crosslinking occurred due to the annealing treatment as demonstrated previously in the cast film test.[32] The sponge annealed at 60°C was immersed in deionized water for 24 h to turn it into a viscous solution but not into gels (Figure 2b), while the other at 140°C created the intended gels (Figure 2c) after immersion in deionized water for 24 h. These results indicated that the high annealing temperature is important for the gelation of the sacran sponges. The swelling degree of the sacran sponges at 140 °C was 57±6 g/g which is higher than that of non-porous hydrogels derived from sacran cast films due to the pores. As discussed previously, because sacran chains contain numerous carboxylic and hydroxyl groups, intermolecular hydrogen bonds might be generated by annealing.[37-39] Moreover, it is possible to form ester or ether bonds among these functional groups. This is why the annealing temperature of the sacran sponge affected the gelation behavior. The pores were successfully formed by freeze-drying and the subsequent thermal treatment method but actually the hydrogels did not exhibit appropriate toughness. Such an unexpected result of hydrogel brittleness could be due to randomly-directed LC domains as illustrated in Figure 1a, where the interdomain boundary might induce the brittleness. Moreover, thermal crosslinking of sacran chains beyond the boundaries is probably difficult because the sacran chains attached in different directions. In summary, simple freeze-drying of the sacran solution is not suitable for the production of tough and porous sacran hydrogels. Consequently, our efforts have been

devoted to improving the physical properties of porous sacran hydrogels. We developed a method for obtaining tough sacran hydrogels using a solvent casting method. The toughness was induced by uniaxial orientation of the sacran chains in LC mono-domains formed though fusing small orientation domains under interfacial effects (Figure 1).[32]

3.2 Preparation of layered/porous hydrogels.

The porous hydrogels with a layered structure were prepared from the sacran LC solution (Figure 1a). The LC solution was dried on a flat substrate such as plastic to form a cast film with an in-plane orientation of sacran chains and then the film was thermally-crosslinked at 60, 80, 100, 120, and 140 ^{o}C (Figure 1b). When the film was immersed in water, hydrogels with a layered structure were formed which are regarded here as original hydrogels (Figure 1c). The porous hydrogels were prepared by freeze-drying to form sponges which were then re-swollen in water (Figure 1d). Freeze-thawed examples of the original hydrogels were prepared for comparison to those that were freeze-dried. Figure 4 and 5 representative SEM images of sacran films cast from a LC solution and then annealed at 60 ^{o}C (a and c) and 140 ^{o}C (b and d). Regardless of annealing temperatures, the SEM images of the top view of the film show that they are very smooth with no particular structure (4a and 4b) while the images of the side view for cross-sectional samples (Figure 5) show striped lines, which revealed that in-plane orientation of sacran molecules formed layered structures in micrometer scale. No distinct difference in the layered structure on these SEM images was observed. From this observation, we confirmed that the layered structure was formed throughout the films. The film was swollen in water and freeze-dried to produce white sponges whose appearances in the Figure 6. Sponges looked more dense in the case of the higher thermal cross-linking temperature, which agrees with the above-mentioned phenomenon using a sacran solution. Figure 7 shows SEM images of freeze-dried samples of the original hydrogels with layered structures, where the porous pattern can be observed only in the side view whereas both top and bottom surfaces show some

unclear wrinkle-like structures but no pore structures. The porous patterns can be observed in all of the cross-sections of these sponges cut by a very sharp surgical knife, revealing the interconnection of pore structures like tunnels. The interconnected pore structures were observed in samples cross-linked at all annealing temperatures. The absence of pores in the top and bottom surfaces is interesting because a simple freeze-drying treatment induced such oriented tunnel structures. The pores were formed by ice sublimation and the vapor appeared to preferentially vent out of the side faces but never break the top and bottom surfaces. This phenomenon strongly suggests that the sacran primary layers should be very tough intrinsically owing to strong interchain interactions. At the same time, the wrinkled structures on the top and bottom surfaces were formed on the surface because of the pressure change due to the outflow of water.[40] When the sponges were immersed in deionized water, translucent hydrogels were prepared as shown in the Figure 6. The hydrogels were somewhat opaque because of the LC phase. As abovementioned, at first, freeze-dried samples of sacran LC solutions were annealed but failed to form porous hydrogels having layer structure. Thus, the timing for thermal cross-linking is important to form stable hydrogels. This suggests that sacran molecular chains should be strongly interacted in oriented domains to make thermal cross-linking efficient.

Even after immersion in water, the hydrogels still kept in-plane orientation which was suggested by the following test; samples were torn from the edges of porous hydrogels by two pairs of tweezers and fracture regions were observed. When they are torn, the hydrogels were not very smoothly fractured to get rough fracture area while regular hydrogels are very easily broken by such a strong twisting stress. Figure 8 shows representative photographs of the fracture area of the hydrogels derived from the films thermally cross-linked at 60 ^{o}C. One can see many steps in the fracture areas marked by dotted lines in Figure 8a, strongly suggesting the layered structure formation in hydrogels. The hydrogels prepared by a freeze-thawing

method, which is widely-used to prepare hydrogel-type tissue engineering scaffolds and so on,[41-45] were also prepared for comparison to clarify the freezing effects on hydrogel structures and properties. The freeze-thawed hydrogels also showed steps, suggesting the maintenance of the layered structure (Figure 8b), but had no pores. They are good examples for comparison to the freeze-dried hydrogels.

3.3 Pore structures.

Figure 9a shows that the pores in the side face observed by SEM seem smaller in the hydrogels prepared from the films cross-linked at higher temperatures. The pore size was estimated from these SEM images and found to range between 10-35 μm. The size was plotted against the thermal cross-linking temperature from 60 to 140 °C to obtain Figure 9a, showing a quantitative tendency of pore size decrease with increasing thermal cross-linking temperature. The tendency corresponds to the shrinking of pores by thermal-treatment for freeze-dried sponges and the layered structure remaining at 140 ^{o}C can be easily identified in the picture in Figure 7j. We therefore conjecture that annealing the film can enhance intra-layer interaction of the sacran chains to make the layers stiff. The water vapor should make pores around the portions where sacran chains interact weakly between layers.

Figure 9b shows the relationship between annealing temperature and porosity which was measured by taking the volume of voids over the total volume inside xerogels. If freeze-dried sponges were immersed in tetralin, which is not a solvent for sacran chains, the sponges readily absorbed the tetralin. This phenomenon could have occurred due to capillary effects, allowing water to intrude through pores to hydrate the sacran chains. The porosity values of all freeze-dried hydrogels were higher than 40 % and were affected by the annealing temperature. The porosity was 79 % at an annealing temperature of 60 °C. These results indicate that the pore size and porosity in hydrogels can be controlled by varying the annealing temperature of sacran films. Because pore structures are important for applications such as filters[3-5], catalyst

supports[6], and tissue engineering scaffolds[7-8, 46], the good controllability is an advantage in these applications. The porosity values are higher than those reported by Nasri-Nasrabadi et al.(25-50 %) on a porous composite of starch/cellulose[47]. The porous starch/cellulose was prepared by the combination of film casting, salt leaching, and freeze drying methods. By this method, it is difficult to use big salt particles as a porogen due to brittleness or homogeneity. The results of the method in the present study were characterized by high pore size, high porosity, and interconnected pores.

3.4 Swelling behaviors.

The annealing temperature's effect on pore structures should have a great influence on swelling behavior. We therefore investigated the swelling degree of porous hydrogels with comparison to nonporous hydrogels prepared by freeze-thawing methods. The swelling degree, *Q*, (g/g) was determined as the weight ratio of absorbed water to dried polymer is shown in Table 1. The porous hydrogel from the film cross-linked at 60 °C showed a *Q* value of 186 g/g which decreased to 9 g/g at 140 °C. The higher cross-linking temperature yielded smaller pore sizes and a stronger intra-layer interaction to disturb the water molecule absorption into the hydrogels.

We prepared the freeze-thawed hydrogels in order to examine the freezing effects on hydrogel properties by comparing them to original hydrogels and to examine the drying effects by comparing them to porous hydrogels from freeze-dried sponges. The freeze-thawed samples showed a lower degree of water swelling than porous hydrogels at all thermal-crosslinking temperatures (Table 1), presumably due to the strong effects of interconnected pores on enhancing water absorption through capillary force. On the other hand, the swelling degree of the network matrix of sacran chains was calculated using the data on porosity, and resulting values are shown in parentheses. These values were lower than those for freeze-thawed hydrogels, suggesting that the drying process also has an effect on decreasing the

degree of swelling. For the comparison of freeze-thawed hydrogels with original hydrogels, the swelling degree increased only slightly, indicating that freezing effects are very weak at controlling the degree of swelling. Poly(vinyl alcohol)s, PVA, are well-known for showing the physical cross-linking accomplished by the freeze-thawing technique.[48-49] However, sacran chains have more complex structures that avoids the crystallization than PVA. Water content, *A*, was also calculated in order to estimate the network structure quantitatively which will be described in detail later. In summary, thermal cross-linking temperature controlled the swelling behavior well in the present method for producing sacran hydrogels.

3.5 Mechanical properties.

The mechanical properties of swollen hydrogels were measured by stress-strain tests in elongation mode. Generally, the compression mode is widely used for the hydrogel mechanical test because the elongation mode requires an intrinsic toughness of the samples. Figure 10a shows stress-strain curves of water-swollen sacran networks in porous hydrogels, which were obtained by normalization of the curves for porous hydrogels (Figure 10b) using porosity. The curves show a typical shape including initial Hookean regions. Elongation tests of freeze-thawed hydrogels were conducted (Figure 11b), and Figure 11a represented the stress-strain curves of original hydrogels. Elastic modulus, E, tensile strain at fracture, σ, elongation at fracture, ε, and strain energy density are summarized in Table 2. While mechanical properties and network analysis of original hydrogels were summarized in Table 3.

E and σ were increased because of the cross-linking temperature increase. The increasing temperature of cross-linking resulted in proportionally higher E and σ of the sacran layer porous hydrogels, suggesting that the establishment of an increasing cross-linking temperature enlarged the cross-linking point. E and σ values of porous hydrogels showed an increasing trend from 3 kPa (60 °C) to 585 kPa (140 °C) and from 1 kPa (60 °C) to 210 kPa (140 °C), respectively, by an increase in annealing temperature. On the other hand, ε values were highest

at an annealing temperature of 120 °C. Thermal cross-linking can induce the strength and hardness of hydrogels but too many cross-linking points cause brittleness. E and σ values of freeze-thawed hydrogels also increased from 5 kPa (60 °C) to 1,745 kPa (140 °C) and from 2 kPa (60 °C) to 758 kPa (140 °C). Porous hydrogels showed 210 and 195 fold increases whereas those that were freeze-thawed showed 379 and 349 fold increases for σ and E, respectively. The difference in the rate of increases may be related with no cross-linking inside the pores. Actually σ and E values of sacran chain networks in porous hydrogels which were re-estimated using matrix cross-sectional areas by subtracting pore areas (shown in parentheses of Table 2) are higher than those of porous hydrogels but lower than those of freeze-thawed ones, except for the case of 60 °C annealing. The high mechanical strength of freeze-thawed hydrogels may be attributable to interlayer interaction breakage by the pore generation. Strain energy density, which can be regarded as the measure of toughness in materials science and calculated by the area under the stress–strain curves, showed a continual increase from 1 kJ/m^3 (60 °C) to 208 kJ/m^3 (140 °C) for freeze-thawed hydrogels while the porous hydrogels showed a maximum of 91 kJ/m^3 at 120 °C and decreased to 43 kJ/m^3 at 140 °C. The maximum was caused by the ε value tendency. Although the strain energy densities of porous hydrogels were lower than those of freeze-thawed hydrogels, the values were comparable with those of polymethacrylate derivative hydrogels[50] applied practically for contact lens and were higher than those of poly(acrylic acid) hydrogels prepared using silica nanoparticle porogens.[51]

Moreover, the porous hydrogel from sacran sponges had a maximum E value of 585 kPa, which is higher than other reported hydrogels derived from dextrin [52] chitosan/collagen [53], a natural silk protein [54], hyaluronic acid[55], and cellulose/alginate [56] which were prepared by chemical cross-linking. This is owing to the in-plane orientation of the sacran LC structures.

Network structure analyses were performed from A and E values. Table 4 summarizes cross-link density, V_e, molecular weight between the cross-linking points, M_c, molecular length

between the cross-linking points, *L*, and degree of effective cross-linking, *X*. When the temperature was increased from 60 °C to 140 °C, the values of V_e and *X* increased 81 and 74 fold, while M_c and *L* dropped dramatically by 82 fold for porous hydrogels. Similarly, freeze-thawed hydrogels showed increases in V_e and *X* with a cross-linking temperature increase but the rate of increase was 176 and 153 fold higher than porous hydrogels, respectively, while M_c and *L* decreased 174 fold. It can be seen that freeze-thawed hydrogels had higher *E* values than those of porous hydrogels and their water-swollen sacran networks (in parentheses in the table 4) in spite of a higher swelling degree than those of water-swollen sacran networks. As a result, V_e and *X* values of freeze-thawed hydrogels increased sufficiently to induce high toughness over 100 kJ/m^3 at thermal cross-linking temperatures of 120 and 140 ^{o}C. Owing to a layered structure, porous hydrogels retained high toughness although the strain energy density values decreased. In the drying step, the ice was substituted by air to make pore gaps which broke the interlayer cross-linking however intralayer cross-linking should be kept to some extent as clearly illustrated in the SEM image in Figure 7j. As reported by Kováčik, J, not only cross-linking density but also the pore shape and size also show a significant effect on the mechanical properties of porous materials[57]. In our porous hydrogels of sacran LC chains, the tunnel-like pores along the layers were very effective at keeping high strain energy density in highly-porous hydrogels.

4. Conclusions

Freeze-drying of water-swollen layered hydrogels of a supergiant LC polysaccharide, sacran, which are prepared by thermal cross-linking of film cast over a sacran LC solution, forms pores only on the side faces of spongy materials where layer edges are located but no pores on the top and bottom faces as revealed by SEM. The pore size is decreased from 35 to 10 μm by an increase in temperature for thermal cross-linking from 60 to 140 °C depending on the annealing temperature of the film cast. The anisotropic sponge absorbs an oily solvent, tetralin, although

sacran does not dissolve in it, presumably owing to capillary force. From the amount of tetralin absorbed, the porosity of the sacran sponge materials was estimated to range between 40-80%, decreasing with an increase in the thermal cross-linking temperature of the cast films. The anisotropic sponges swell in water to form hydrogels. The swelling degrees are estimated as weight ratios of the water-swollen hydrogel to the dry sponge and range between 9-186 g/g which is higher than those of the original hydrogels (8-51 g/g), indicating that the porous structures are retained in hydrogels. The swelling degree of the network matrix is calculated to be 6-40 g/g by subtracting the water amount in pores from the whole swelling degree, which was lower than the non-porous hydrogels prepared by freeze-thawing of the original hydrogels. The swelling degrees of freeze-thawed hydrogels are between those of original hydrogels (from cast films) and those of the network matrix, suggesting that both freezing and successive drying are effective on additional cross-linking of original networks. The porous hydrogels are tough enough to tear at their edges, and many steps appeared around torn parts, suggesting the layer structures from the layered cast film are maintained. Elastic moduli of the porous hydrogels range from 3 to 585 kPa while tensile strengths at fracture range from 1 to 200 kPa. Moreover, strain energy density of porous hydrogels cross-linked thermally at 120 ^{o}C is high at around 91 kJ/m^{3}. The high toughness might be attributable to pores arranging between the layers and not reducing the mechanical toughness when the gels are stretched along the longitudinal direction of the layer.

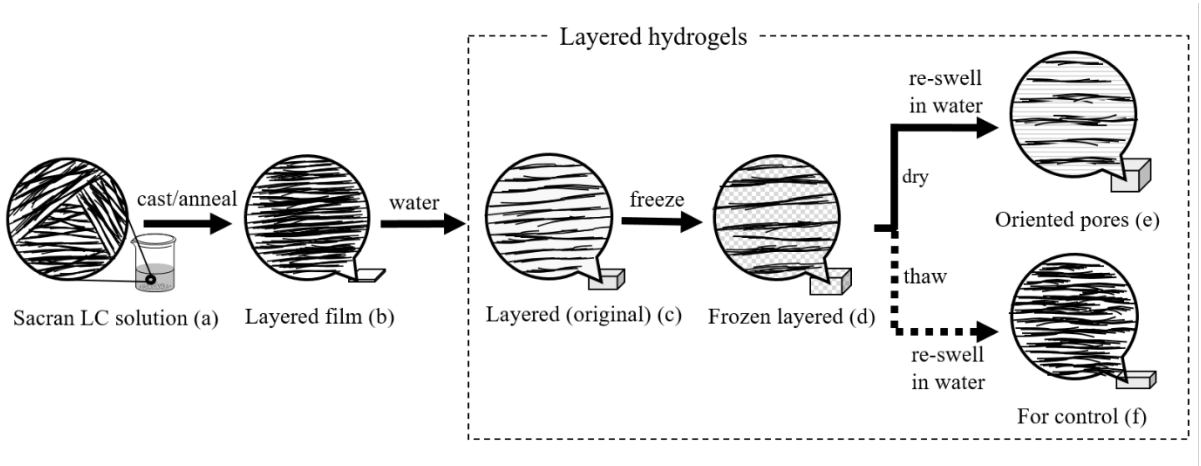

Figure 1. Schematic illustration of the preparation process for hydrogels with a layered structure and oriented pores. a) Sacran liquid crystalline (LC) solution with a concentration of 0.5 w/v %. b) Film with layered structures where sacran chains were oriented in-plane, formed by casting of a. c) Hydrogels having a layered structure formed by water-immersion of b after thermal cross-linking at various temperatures, which are basis of subsequently produced layered hydrogels. d) Frozen hydrogels keeping a layer structure of sacran chains surrounded by ice crystal. e) Hydrogels having the layered structure and oriented pores formed by freeze-drying and successive water-immersion of d. f) d was thawed and immersed in water to prepare non-dried hydrogels for comparison to e.

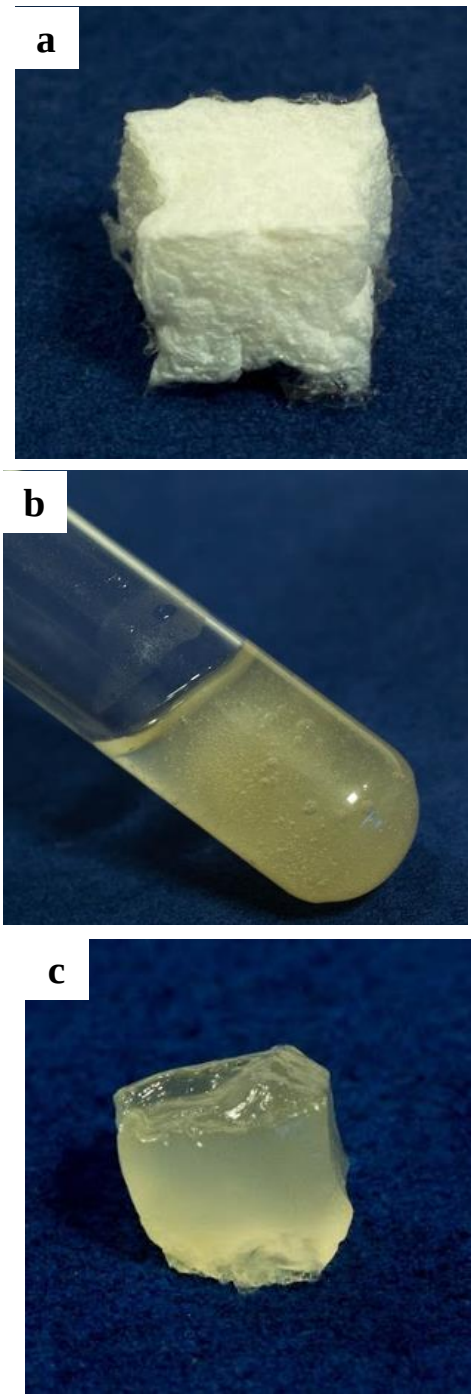

Figure 2. a) Photograph of the sacran sponge prepared by freeze-drying of the sacran LC solution with a concentration of 0.5%. b) The sacran sponge was immersed in pure water and was kept for 24 h after annealing at 60 ^{o}C, to form a viscous solution. c) Self-standing hydrogel prepared by water-immersion of the sacran sponge and kept for 24 h after thermal cross-linking at 140 ^{o}C.

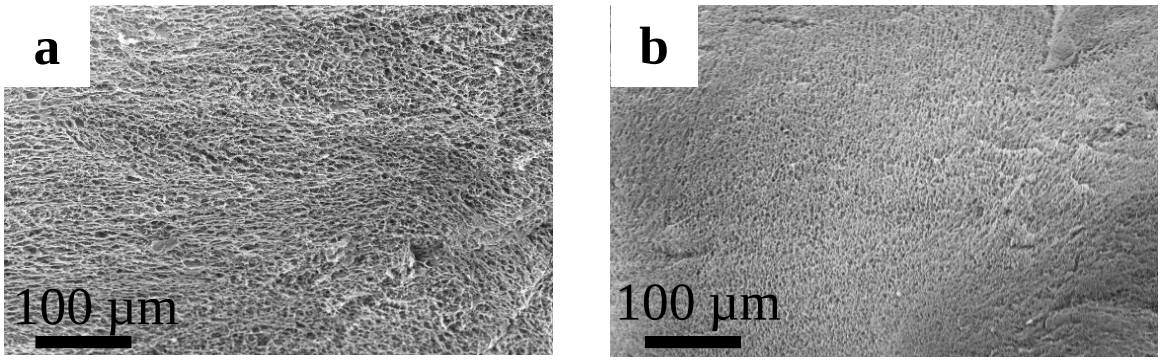

Figure 3. SEM images of sacran sponge surfaces prepared by freeze-drying the sacran solution with a concentration of 0.5% and successive annealing at 60 a) and 140 °C b).

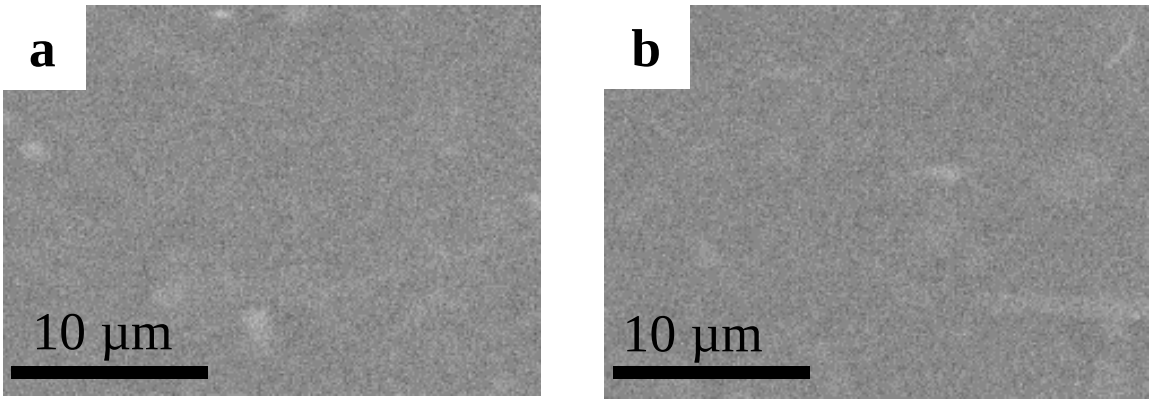

Figure 4. SEM images of the surface of sacran films cast from the LC solution and then thermally cross-linked at 60 ^{o}C (a) and 140 ^{o}C (b).

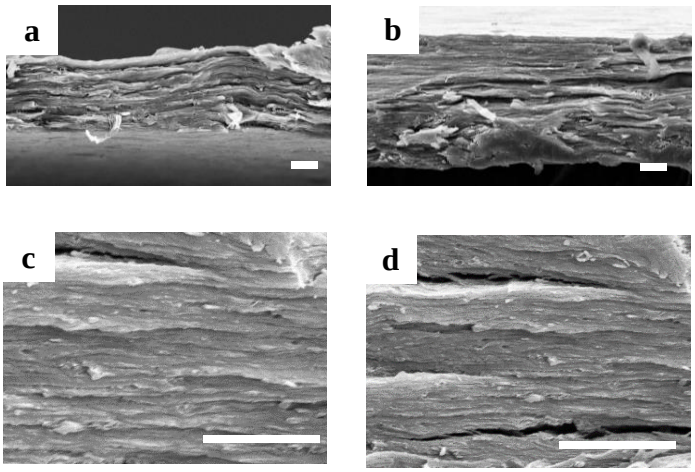

Figure 5. SEM images of cross-section sacran films cast from the LC solution and then thermally cross-linked at 60 ºC (a and c) and 140 ºC (b and d). Higher magnification image (c and d) obviously revealed layered structures. Scale bar: 10 μm.

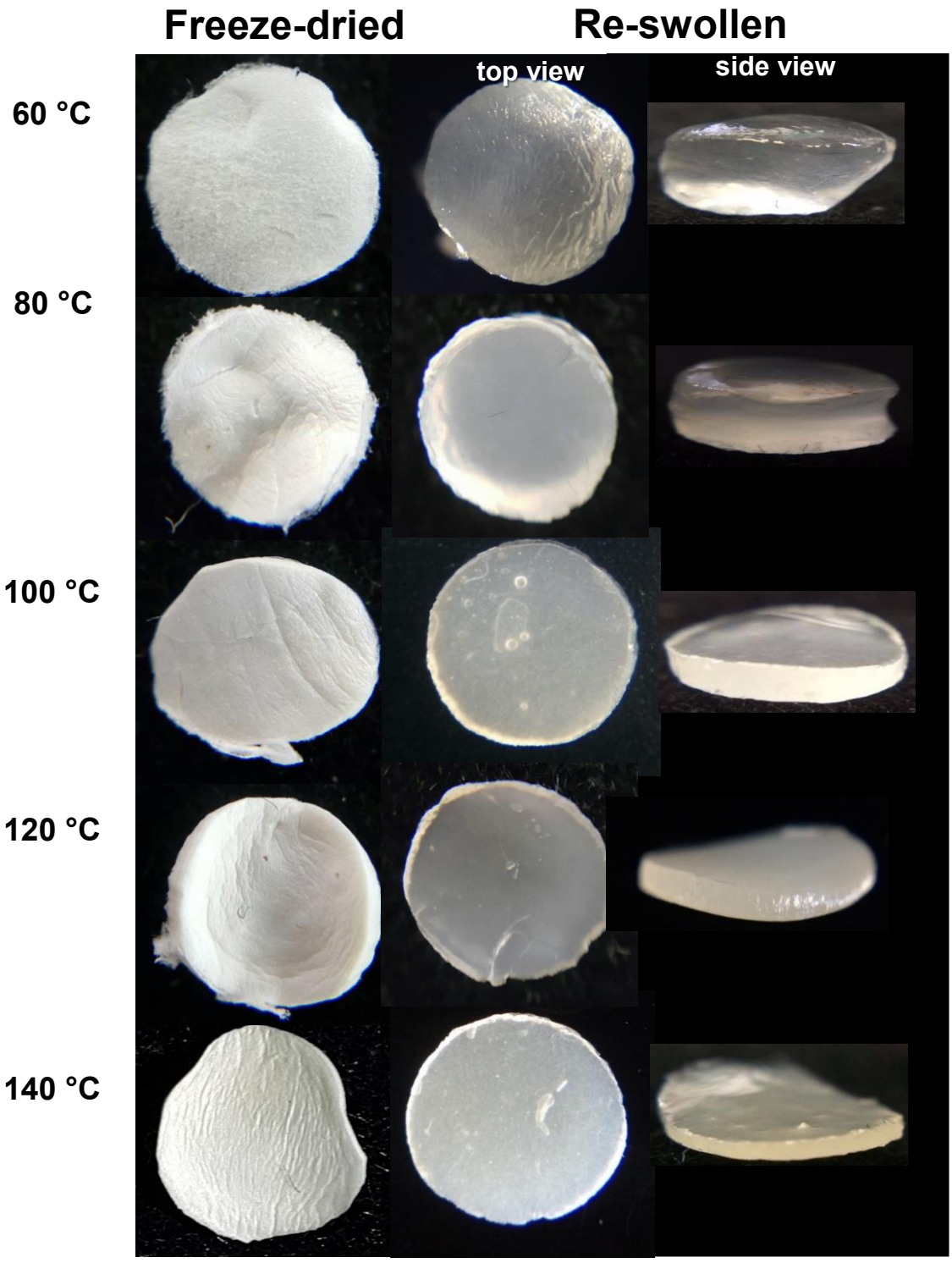

Figure. 6 Photographs of freeze-dried samples (porous materials) and successive re-swollen samples of layered hydrogels which were prepared by casting the sacran LC solution with a concentration of 0.5 w/v% and then cross-linking thermally at 60, 80, 100, 120 and 140 °C. Scale bar: 1 mm.

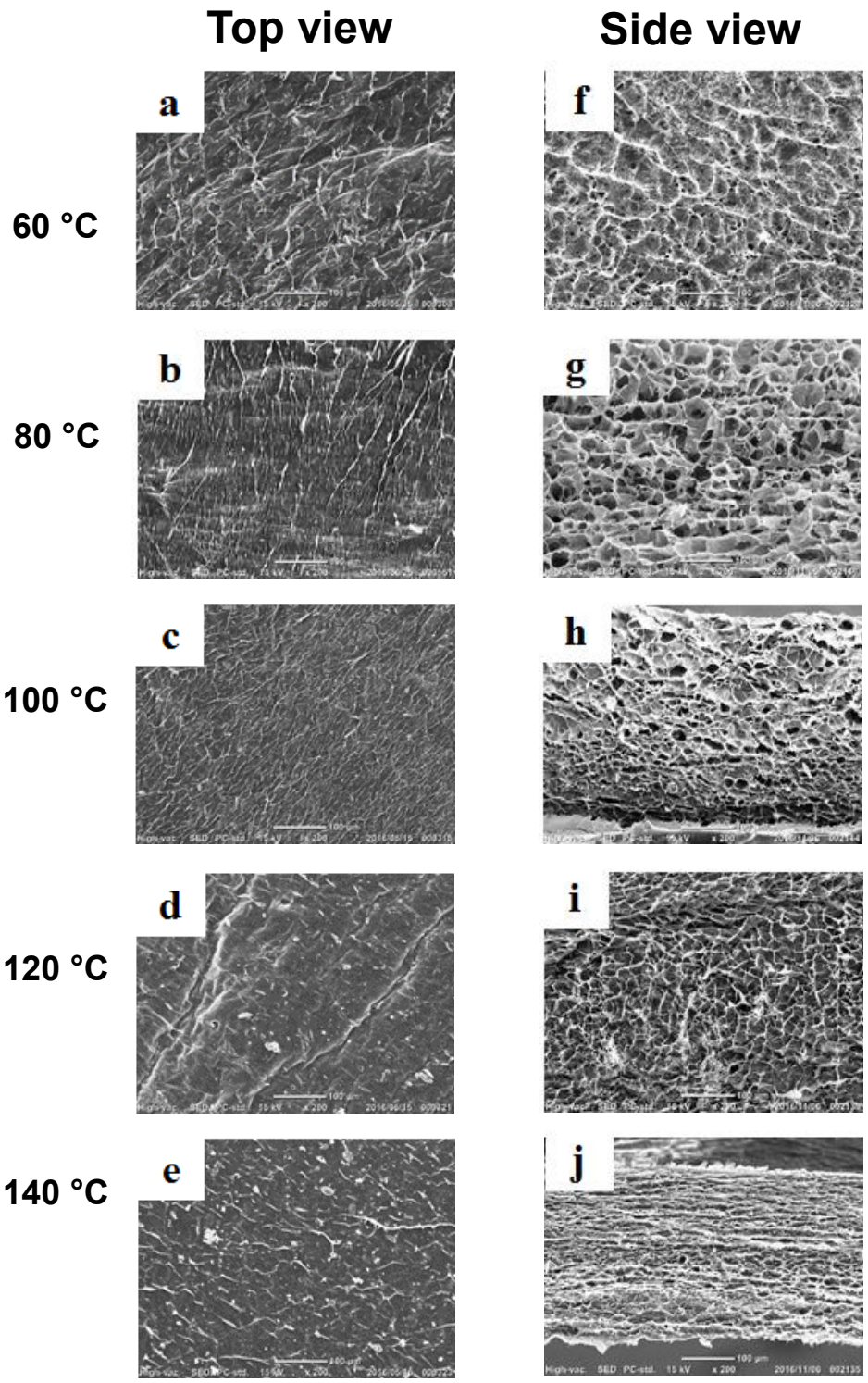

Figure 7 SEM images of freeze-dried samples of layered hydrogels which were prepared by casting the sacran LC solution with a concentration of 0.5 w/v%, and then thermally cross-linking at 60 (a, f), 80 (b, g), 100 (c, h), 120 (d, i), and 140 °C (e, j). Side views (f-j) reveal pore structure, while top views (a-e) reveal no pore structure. Scale bar: 100 μm.

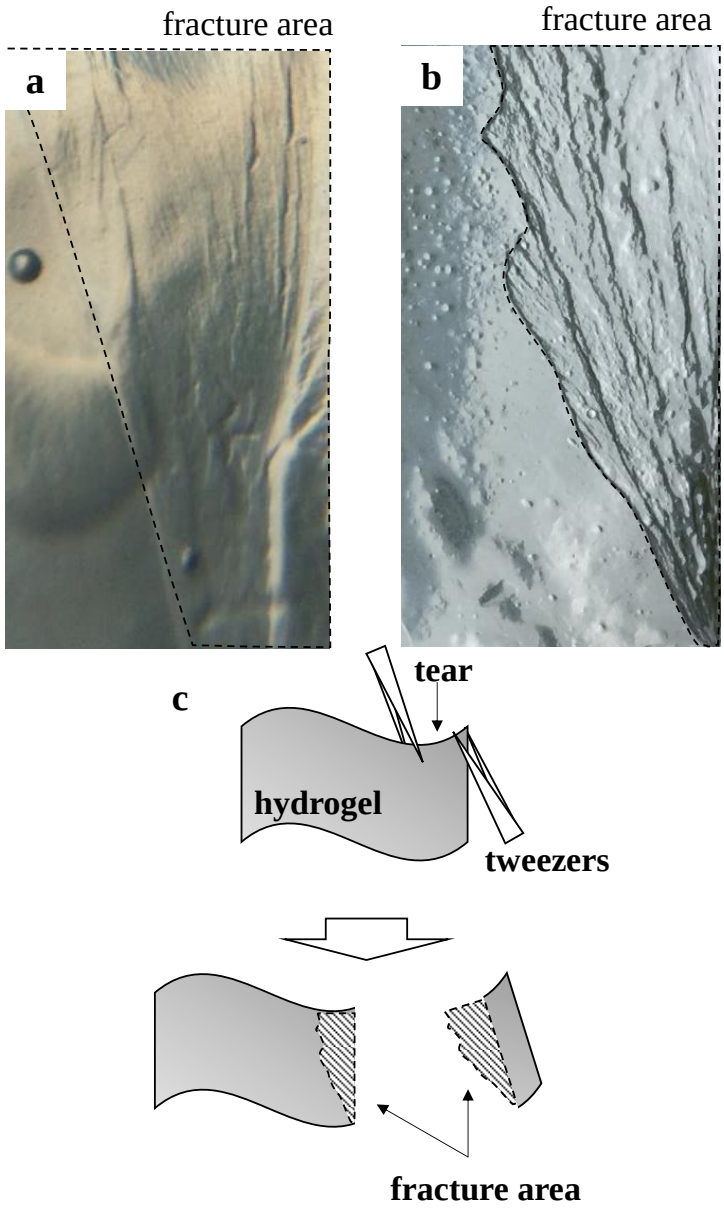

Figure 8. Photographs of partially torn samples from the edges of hydrogels derived from the films thermally cross-linked at 60 ºC, by freeze-drying a) and freeze-thawing b) methods. Illustration c) shows how to conduct a tear test of hydrogels. Fracture areas are marked by dotted lines. Both photographs show steps in the fracture area of hydrogels suggesting layered structures.

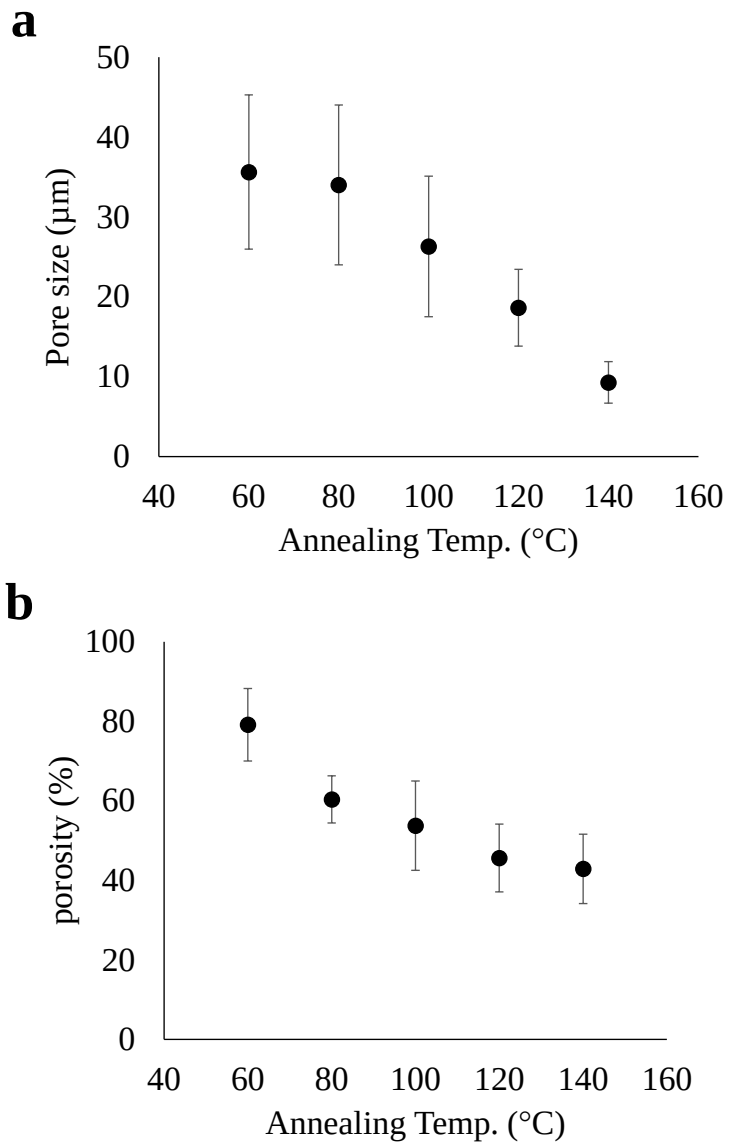

Figure 9. Pore size a) and porosity b) of freeze-dried samples of layered hydrogels which were prepared by casting the sacran LC solution with a concentration of 0.5 w/v% and then thermally cross-linking at 60, 80, 100, 120 and 140 ˚C. Pore size a) was estimated from side views of SEM images (Figure 4f-j), and porosity b) was evaluated from the amount of tetralin intruding into sample pores.

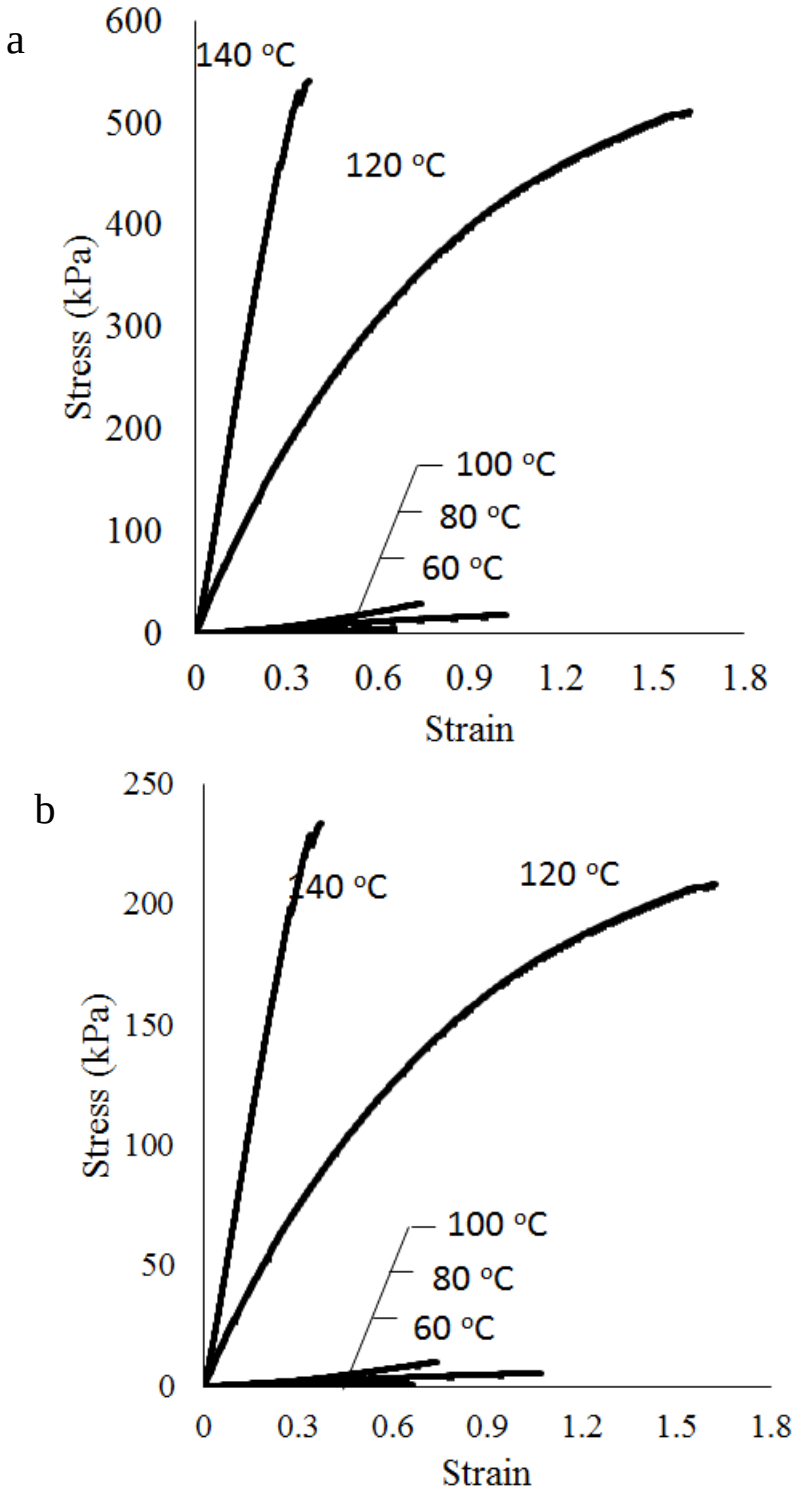

Figure 10. Representative stress-strain curves of sacran hydrogels derived from layered films cross-linked thermally at the indicated temperatures. a) Stress-strain curves of porous hydrogels, where stress values were normalized by using matrix areas of water-swollen networks. b) original stress-strain curves.

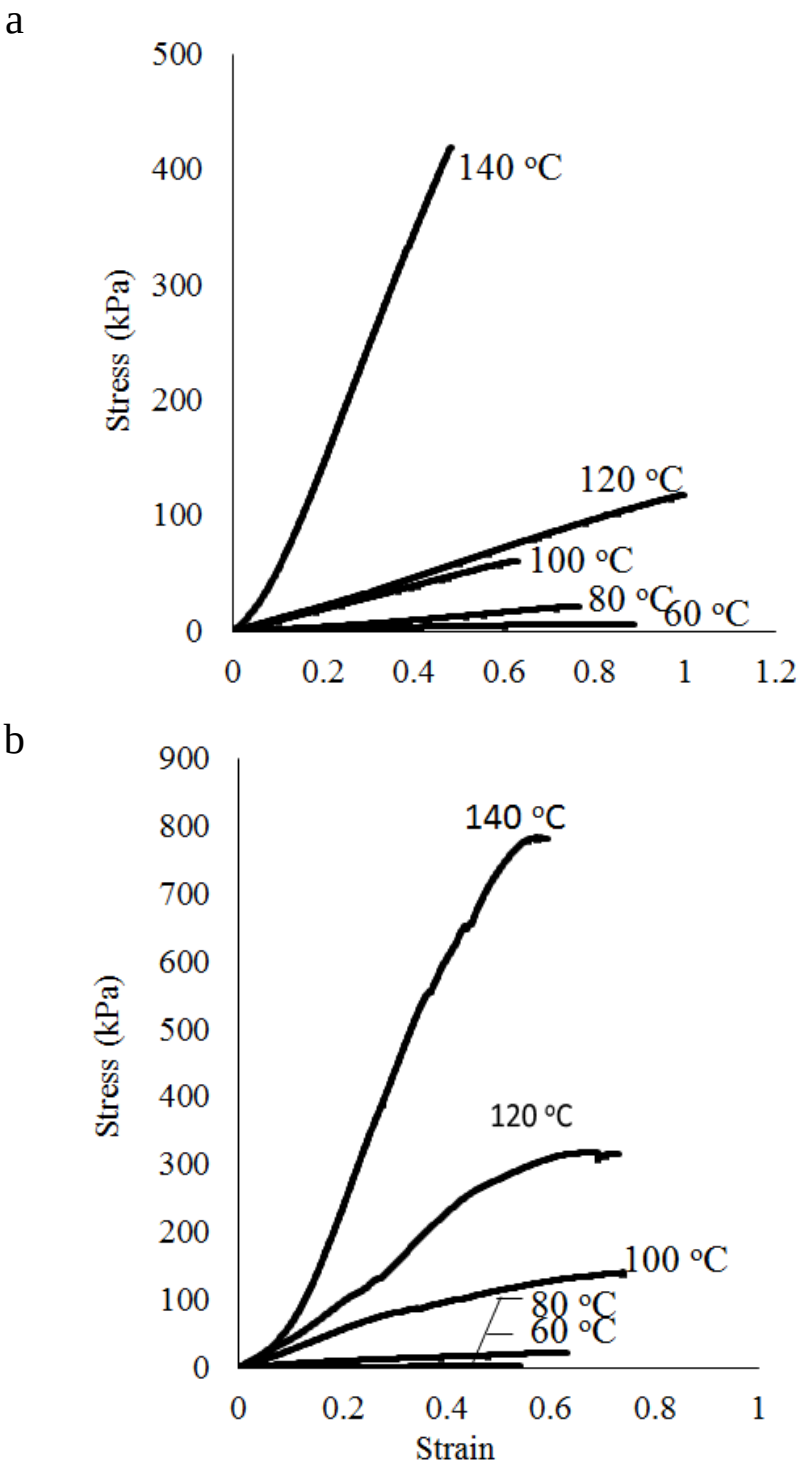

Figure 11. Representative stress-strain curves of sacran hydrogels derived from layered films cross-linked thermally at the indicated temperatures. a) Stress-strain curves of original hydrogels. b) Freeze-thawed and equilibrated-swollen ones hydrogels.

Table 1. Swelling degrees of porous and freeze-thawed sacran hydrogels[a].

cross-linking temperatures[b] (°C)	porous hydrogels (g/g)	freeze-thawed hydrogels (g/g)
60	186±16 (40±3)	77±3
80	95±6 (38±3)	43±2
100	32±3 (15±1)	23±3
120	16±2 (9±1)	12±1
140	9±0.2 (6±0.1)	9±2

[a]Swelling degrees (Q) in distilled water were estimated at room temperature. Values in parentheses refer to matrix swelling degrees estimated by subtracting pore volumes from entire swelling. [b]Thermal cross-linking temperatures of layered film as precursors of layered hydrogels.

Table 2. Mechanical properties of porous and freeze-thawed sacran hydrogels[a]

cross-linking temperatures[b] (°C)	porous hydrogels				freeze-thawed hydrogels			
	E[c] (kPa)	σ[d] (kPa)	ε[e] (mm/mm)	strain energy density[f] (kJ/m^3)	E[c] (kPa)	σ[d] (kPa)	ε[e] (mm/mm)	strain energy density[f] (kJ/m^3)
60	3±1 (18±5)	1±0.1 (7±1)	0.60±0.06	0.3±0.1 (1±0.2)	5±0.2	2±1	0.65±0.09	1±0.1
80	5±1 (19±3)	5±1 (17±3)	0.94±0.47	1±0.1 (4±2)	46±6	28±9	0.74±0.33	13±5
100	21±5 (62±16)	13±3 (38±8)	0.88±0.19	10±4 (19±11)	250±37	120±18	0.75±0.02	52±12
120	220±410 (540±98)	210±44 (520±110)	1.46±0.32	91±7 (550±140)	610±50	330±40	0.68±0.14	140±13
140	590±130 (1360±290)	200±30 (470±70)	0.40±0.09	43±12 (120±11)	1750±430	760±40	0.52±0.08	210±32

[a]Mechanical properties were determined from stress-strain curves recorded at room temperature using a tensiometer in an elongation mode. Values in parentheses are mechanical properties re-estimated using matrix cross-sectional areas with subtracting pore areas. [b]Thermal cross-linking temperatures of layered film as precursors of layered hydrogels. [c]E values refer to elastic modulus. [d]σ values refer to tensile strength at fracture. [e]ε values refer to elongation at fracture. [f]Strain energy density values were estimated from area surrounded by stress-strain curves.

Table 3. Swelling degrees, mechanical properties, and network structure analyses of original sacran hydrogels.

cross-linking temperatures[a] (°C)	Q[b] (g/g)	E[c] (kPa)	σ[d] (kPa)	e[e] (mm/mm)	strain energy density[f] (kJ/m^3)	V_e [g] (mol·m^{-3})	M_c [h] (kg·mol^{-1})	L[i] (Å)	X[j] (x10^{-3})
60	51±2	8±1	6±1	0.86±0.10	3±1	11±1	73±7	3494±353	1±0.1
80	33±3	40±8	38±6	0.92±0.16	16±3	52±10	17±3	791±155	6±1
100	20±2	100±25	40±14	1.06±0.43	10±6	108±27	8±2	383±76	12±3
120	11±0.2	779±204	120±31	1.03±0.21	50±14	688±180	1±0.3	61±17	75±20
140	8±2	1177±188	402±14	0.41±0.06	79±14	918±147	1±0.2	44±8	100±16

[a]Thermal cross-linking temperatures of layered film as precursors of layered hydrogels. [b]Q values refer to swelling ratio estimated by weight ratios of swollen hydrogel to dried ones. Mechanical properties were determined from stress-strain curves recorded at room temperature using a tensiometer in an elongation mode. [c]E values refer to elastic modulus. [d]σ values refer to tensile strength at fracture. [e]e values refer to elongation at fracture. [f]Strain energy density values were estimated from area surrounded by stress-strain curves. [g]V_e values refer to cross-linking density. [h]M_c values refer to molecular weight between cross-linking points. [i]L valeus refer to molecular length between cross-linking points. [j]X values refer to degree of cross-linking.

Table 4. Network structure analyses of freeze-dried and freeze-thawed sacran hydrogels

cross-linking temperatures[a] (°C)	porous hydrogels				freeze-thawed hydrogels			
	V_e[b] (mol·m^{-3})	M_c[c] (kg·mol^{-1})	L[d] (Å)	X[e] (x10^{-3})	V_e[b] (mol·m^{-3})	M_c[c] (kg·mol^{-1})	L[d] (Å)	X[e] (x10^{-3})
60	6±2 (25±7)	145±40 (35±10)	6900±1900 (1680±470)	0.7±0.2 (3±1)	8±1	105±11	5000±520	1±0.1
80	9±2 (24±6)	92±23 (36±9)	4400±1120 (1700±440)	1±0.2 (3±1)	63±11	14±3	650±130	7±1
100	26±7 (59±17)	34±8 (15±4)	1610±400 (710±170)	3±1 (6±2)	270±31	3±0.4	150±19	30±3
120	220±45 (430±90)	4±1 (2±0.4)	190±38 (89±20)	23±5 (47±10)	530±72	2±0.2	76±10	58±8
140	480±89 (930±170)	2±0.3 (1±0.2)	84±14 (44±7)	52±10 (100±18)	1410±350	1±0.1	29±7	150±38

[a]Thermal cross-linking temperatures of layered film as precursors of layered hydrogels. [b]V_e values refer to cross-linking density. [c]M_c values refer to molecular weight between cross-linking points. [d]L valeus refer to molecular length between cross-linking points. [e]X values refer to degree of cross-linking. Values in parentheses are calculated using elastic moduli and water contents for matrix areas of water-swollen networks with neglecting water amount in pores and pore areas.

References

1. Zhang, H.; Edgar, D.; Murray, P.; Rak-Raszewska, A.; Glennon Alty, L.; Cooper, A. I., Synthesis of porous microparticles with aligned porosity. *Advanced Functional Materials* **2008,** *18* (2), 222-228.

2. Luo, R.; Wu, J.; Dinh, N. D.; Chen, C. H., Gradient Porous Elastic Hydrogels with Shape-Memory Property and Anisotropic Responses for Programmable Locomotion. *Advanced Functional Materials* **2015,** *25* (47), 7272-7279.

3. Keckes, J.; Burgert, I.; Frühmann, K.; Müller, M.; Kölln, K.; Hamilton, M.; Burghammer, M.; Roth, S. V.; Stanzl-Tschegg, S.; Fratzl, P., Cell-wall recovery after irreversible deformation of wood. *Nature materials* **2003,** *2* (12), 810-813.

4. Colombo, P., In praise of pores. *Science* **2008,** *322* (5900), 381-383.

5. Pyzik, A. J.; Li, C. G., New design of a ceramic filter for diesel emission control applications. *International Journal of Applied Ceramic Technology* **2005,** *2* (6), 440-451.

6. Twigg, M. V.; Richardson, J. T., Fundamentals and applications of structured ceramic foam catalysts. *Industrial & engineering chemistry research* **2007,** *46* (12), 4166-4177.

7. Hench, L. L.; Polak, J. M., Third-generation biomedical materials. *Science* **2002,** *295* (5557), 1014-1017.

8. Hollister, S. J., Porous scaffold design for tissue engineering. *Nature materials* **2005,** *4* (7), 518-524.

9. Mitsumata, T.; Miura, T.; Takahashi, N.; Kawai, M.; Okajima, M. K.; Kaneko, T., Ionic state and chain conformation for aqueous solutions of supergiant cyanobacterial polysaccharide. *Phys Rev E Stat Nonlin Soft Matter Phys* **2013,** *87* (4), 042607.

10. Wathoni, N.; Motoyama, K.; Higashi, T.; Okajima, M.; Kaneko, T.; Arima, H., Enhancing effect of γ-cyclodextrin on wound dressing properties of sacran hydrogel film. *International Journal of Biological Macromolecules* **2017,** *94*, 181-186.

11. Wathoni, N.; Motoyama, K.; Higashi, T.; Okajima, M.; Kaneko, T.; Arima, H., Physically crosslinked-sacran hydrogel films for wound dressing application. *International Journal of Biological Macromolecules* **2016,** *89*, 465-470.

12. Ngatu, N. R.; Okajima, M. K.; Yokogawa, M.; Hirota, R.; Eitoku, M.; Muzembo, B. A.; Dumavibhat, N.; Takaishi, M.; Sano, S.; Kaneko, T.; Tanaka, T.; Nakamura, H.; Suganuma, N., Anti-inflammatory effects of sacran, a novel polysaccharide from Aphanothece sacrum, on 2,4,6-trinitrochlorobenzene–induced allergic dermatitis in vivo. *Annals of Allergy, Asthma & Immunology* **2012,** *108* (2), 117-122.

13. Okajima, M. K.; le Nguyen, Q. T.; Tateyama, S.; Masuyama, H.; Tanaka, T.; Mitsumata, T.; Kaneko, T., Photoshrinkage in polysaccharide gels with trivalent metal ions. *Biomacromolecules* **2012,** *13* (12), 4158-63.

14. Okeyoshi, K.; Okajima, M. K.; Kaneko, T., Milliscale Self-Integration of Megamolecule Biopolymers on a Drying Gas-Aqueous Liquid Crystalline Interface. *Biomacromolecules* **2016,** *17* (6), 2096-103.

15. Kaneti, Y. V.; Tang, J.; Salunkhe, R. R.; Jiang, X.; Yu, A.; Wu, K. C. W.; Yamauchi, Y., Nanoarchitectured Design of Porous Materials and Nanocomposites from Metal-Organic Frameworks. *Advanced Materials* **2016**.

16. Alezi, D.; Belmabkhout, Y.; Suyetin, M.; Bhatt, P. M.; Weseliński, Ł. J.; Solovyeva, V.; Adil, K.; Spanopoulos, I.; Trikalitis, P. N.; Emwas, A. H.; Eddaoudi, M., MOF Crystal Chemistry Paving the Way to Gas Storage Needs: Aluminum-Based soc-MOF for CH4, O2, and CO2 Storage. *Journal of the American Chemical Society* **2015,** *137* (41), 13308-13318.

17. Zhao, Y.; Lee, S. Y.; Becknell, N.; Yaghi, O. M.; Angell, C. A., Nanoporous Transparent MOF Glasses with Accessible Internal Surface. *Journal of the American Chemical Society* **2016,** *138* (34), 10818-10821.

18. Rieger, K. A.; Cho, H. J.; Yeung, H. F.; Fan, W.; Schiffman, J. D., Antimicrobial Activity of Silver Ions Released from Zeolites Immobilized on Cellulose Nanofiber Mats. *ACS Applied Materials & Interfaces* **2016,** *8* (5), 3032-3040.

19. Klossner, R. R.; Queen, H. A.; Coughlin, A. J.; Krause, W. E., Correlation of Chitosan's Rheological Properties and Its Ability to Electrospin. *Biomacromolecules* **2008,** *9* (10), 2947-2953.

20. Tayi, A. S.; Pashuck, E. T.; Newcomb, C. J.; McClendon, M. T.; Stupp, S. I., Electrospinning Bioactive Supramolecular Polymers from Water. *Biomacromolecules* **2014,** *15* (4), 1323-1327.

21. Pol, V. G.; Koren, E.; Zaban, A., Fabrication of Continuous Conducting Gold Wires by Electrospinning. *Chemistry of Materials* **2008,** *20* (9), 3055-3062.

22. Tang, C.; Saquing, C. D.; Harding, J. R.; Khan, S. A., In Situ Cross-Linking of Electrospun Poly(vinyl alcohol) Nanofibers. *Macromolecules* **2010,** *43* (2), 630-637.

23. Dong, Z.; Wu, Y.; Clark, R. L., Thermodynamic Modeling and Investigation of the Formation of Electrospun Collagen Fibers. *Langmuir* **2011,** *27* (20), 12417-12422.

24. Colosi, C.; Costantini, M.; Barbetta, A.; Pecci, R.; Bedini, R.; Dentini, M., Morphological Comparison of PVA Scaffolds Obtained by Gas Foaming and Microfluidic Foaming Techniques. *Langmuir* **2013,** *29* (1), 82-91.

25. Mannoor, M. S.; Jiang, Z.; James, T.; Kong, Y. L.; Malatesta, K. A.; Soboyejo, W. O.; Verma, N.; Gracias, D. H.; McAlpine, M. C., 3D Printed Bionic Ears. *Nano Letters* **2013,** *13* (6), 2634-2639.

26. Zhu, F.; Cheng, L.; Yin, J.; Wu, Z. L.; Qian, J.; Fu, J.; Zheng, Q., 3D Printing of Ultratough Polyion Complex Hydrogels. *ACS Applied Materials & Interfaces* **2016,** *8* (45), 31304-31310.

27. Bhattacharjee, T.; Gil, C. J.; Marshall, S. L.; Urueña, J. M.; O'Bryan, C. S.; Carstens, M.; Keselowsky, B.; Palmer, G. D.; Ghivizzani, S.; Gibbs, C. P.; Sawyer, W. G.; Angelini, T. E., Liquid-like Solids Support Cells in 3D. *ACS Biomaterials Science & Engineering* **2016,** *2* (10), 1787-1795.

28. Lim, K. S.; Schon, B. S.; Mekhileri, N. V.; Brown, G. C. J.; Chia, C. M.; Prabakar, S.; Hooper, G. J.; Woodfield, T. B. F., New Visible-Light Photoinitiating System for Improved Print Fidelity in Gelatin-Based Bioinks. *ACS Biomaterials Science & Engineering* **2016,** *2* (10), 1752-1762.

29. Plikk, P.; Målberg, S.; Albertsson, A. C., Design of Resorbable Porous Tubular Copolyester Scaffolds for Use in Nerve Regeneration. *Biomacromolecules* **2009,** *10* (5), 1259-1264.

30. Mecerreyes, D.; Grande, H.; Miguel, O.; Ochoteco, E.; Marcilla, R.; Cantero, I., Porous Polybenzimidazole Membranes Doped with Phosphoric Acid: Highly Proton-Conducting Solid Electrolytes. *Chemistry of Materials* **2004,** *16* (4), 604-607.

31. Lin-Gibson, S.; Cooper, J. A.; Landis, F. A.; Cicerone, M. T., Systematic Investigation of Porogen Size and Content on Scaffold Morphometric Parameters and Properties. *Biomacromolecules* **2007,** *8* (5), 1511-1518.

32. Okajima, M. K.; Mishima, R.; Amornwachirabodee, K.; Mitsumata, T.; Okeyoshi, K.; Kaneko, T., Anisotropic swelling in hydrogels formed by cooperatively aligned megamolecules. *RSC Adv.* **2015,** *5* (105), 86723-86729.

33. Zhu, C.; Bettinger, C. J., Photoreconfigurable Physically Cross-Linked Triblock Copolymer Hydrogels: Photodisintegration Kinetics and Structure–Property Relationships. *Macromolecules* **2015,** *48* (5), 1563-1572.

34. Salinas, C. N.; Anseth, K. S., Mixed Mode Thiol−Acrylate Photopolymerizations for the Synthesis of PEG−Peptide Hydrogels. *Macromolecules* **2008,** *41* (16), 6019-6026.

35. Baier Leach, J.; Bivens, K. A.; Patrick Jr, C. W.; Schmidt, C. E., Photocrosslinked hyaluronic acid hydrogels: natural, biodegradable tissue engineering scaffolds. *Biotechnology and bioengineering* **2003,** *82* (5), 578-589.

36. Madihally, S. V.; Matthew, H. W. T., Porous chitosan scaffolds for tissue engineering. *Biomaterials* **1999,** *20* (12), 1133-1142.

37. Kanimozhi, K.; Khaleel Basha, S.; Sugantha Kumari, V., Processing and characterization of chitosan/PVA and methylcellulose porous scaffolds for tissue engineering. *Mater Sci Eng C Mater Biol Appl* **2016,** *61*, 484-91.

38. Li, G.; Zhao, Y.; Zhang, L.; Gao, M.; Kong, Y.; Yang, Y., Preparation of graphene oxide/polyacrylamide composite hydrogel and its effect on Schwann cells attachment and proliferation. *Colloids and Surfaces B: Biointerfaces* **2016,** *143*, 547-556.

39. Wu, J.; Meredith, J. C., Assembly of Chitin Nanofibers into Porous Biomimetic Structures via Freeze Drying. *ACS Macro Letters* **2014,** *3* (2), 185-190.

40. Yang, C. H.; Lin, Y. Y., Surface wrinkles of swelling gels under arbitrary lateral confinements. *European Journal of Mechanics-A/Solids* **2014,** *45*, 90-100.

41. Mitsumata, T.; Hasegawa, C.; Kawada, H.; Kaneko, T.; Takimoto, J.-i., Swelling and viscoelastic properties of poly(vinyl alcohol) physical gels synthesized using sodium silicate. *Reactive and Functional Polymers* **2008,** *68* (1), 133-140.

42. Lin, C.; He, G.; Dong, C.; Liu, H.; Xiao, G.; Liu, Y., Effect of Oil Phase Transition on Freeze/Thaw-Induced Demulsification of Water-in-Oil Emulsions. *Langmuir* **2008,** *24* (10), 5291-5298.

43. Zhao, J.; Bolisetty, S.; Adamcik, J.; Han, J.; Fernández-Ronco, M. P.; Mezzenga, R., Freeze–Thaw Cycling Induced Isotropic–Nematic Coexistence of Amyloid Fibrils Suspensions. *Langmuir* **2016,** *32* (10), 2492-2499.

44. Niven, R. K.; Singh, K., Mobilization and Rupture of LNAPL Ganglia during Freeze-Thaw: Two-Dimensional Cell Experiments. *Environmental Science & Technology* **2008,** *42* (15), 5467-5472.

45. Liu, B.; Mazouchi, A.; Gradinaru, C. C., Trapping Single Molecules in Liposomes: Surface Interactions and Freeze−Thaw Effects. *The Journal of Physical Chemistry B* **2010,** *114* (46), 15191-15198.

46. Lanza, R.; Langer, R.; Vacanti, J. P., *Principles of tissue engineering*. Academic press: 2011.

47. Nasri-Nasrabadi, B.; Mehrasa, M.; Rafienia, M.; Bonakdar, S.; Behzad, T.; Gavanji, S., Porous starch/cellulose nanofibers composite prepared by salt leaching technique for tissue engineering. *Carbohydrate polymers* **2014,** *108*, 232-8.

48. Ricciardi, R.; Auriemma, F.; Gaillet, C.; De Rosa, C.; Lauprêtre, F., Investigation of the Crystallinity of Freeze/Thaw Poly(vinyl alcohol) Hydrogels by Different Techniques. *Macromolecules* **2004,** *37* (25), 9510-9516.

49. Ricciardi, R.; Auriemma, F.; De Rosa, C.; Lauprêtre, F., X-ray Diffraction Analysis of Poly(vinyl alcohol) Hydrogels, Obtained by Freezing and Thawing Techniques. *Macromolecules* **2004,** *37* (5), 1921-1927.

50. Jackson, A. P., Measurement of the fracture toughness of some contact lens hydrogels. *Biomaterials* **1990,** *11* (6), 403-407.

51. Yang, J.; Han, C. R.; Duan, J. F.; Xu, F.; Sun, R. C., In situ grafting silica nanoparticles reinforced nanocomposite hydrogels. *Nanoscale* **2013,** *5* (22), 10858-10863.

52. Molinos, M.; Carvalho, V.; Silva, D. M.; Gama, F. M., Development of a hybrid dextrin hydrogel encapsulating dextrin nanogel as protein delivery system. *Biomacromolecules* **2012,** *13* (2), 517-27.

53. Martínez, A.; Blanco, M. D.; Davidenko, N.; Cameron, R. E., Tailoring chitosan/collagen scaffolds for tissue engineering: Effect of composition and different crosslinking agents on scaffold properties. *Carbohydrate polymers* **2015,** *132*, 606-619.

54. Wang, Z.; Wang, J.; Jin, Y.; Luo, Z.; Yang, W.; Xie, H.; Huang, K.; Wang, L., A Neuroprotective Sericin Hydrogel As an Effective Neuronal Cell Carrier for the Repair of Ischemic Stroke. *ACS applied materials & interfaces* **2015,** *7* (44), 24629-24640.

55. Collins, M. N.; Birkinshaw, C., Morphology of crosslinked hyaluronic acid porous hydrogels. *Journal of Applied Polymer Science* **2011,** *120* (2), 1040-1049.

56. Kirdponpattara, S.; Khamkeaw, A.; Sanchavanakit, N.; Pavasant, P.; Phisalaphong, M., Structural modification and characterization of bacterial cellulose–alginate composite scaffolds for tissue engineering. *Carbohydrate polymers* **2015,** *132*, 146-155.

57. Kováčik, J., Correlation between Young's modulus and porosity in porous materials. *Journal of materials science letters* **1999,** *18* (13), 1007-1010.

Chapter III Biocompatibility and cell-orientation controlling property of sacran biopolymer

1. Introduction

Hydrogels are three-dimension of polymer network that is capable of absorbing a large amount of water or biological solutions as well as keeping their structure integrity[1-2]. They show a variety of biomedical application such as cell carrier[3], drug delivery[4-5], and engineering scaffolds[6-8] due to their similarities with the extracellular matrix, excellent biological performance, and inherent cellular interaction capacity[9-11]. Scaffolds are biomaterials which are used for cell supported materials to grow on and form the new tissues. The most important property of scaffolds is biocompatible[12], which is not produce an unfavorable physiological response. Moreover, they should have selfsame mechanical properties with the native tissues[13]. The architecture such as pore size, porosity, pore interconnectivity and permeability also required[14-15].

Previously I successful prepared anisotropic porous hydrogels of sacran bio-renewable polymer[16]. Our hydrogels showed inter-connected porous structure however pores were presented only side faces like a tunnel. Besides, mechanical properties were an appropriate performance in scaffolds materials. Sacran[17-18] is a megamolecular of polysaccharide (Mw: 1.6×10^7 g/mol), extracted from *Aphanothece sacrum* cyanobacteria. Sacran composed of various sugar residues such as Glc, Gal, Man, Xyl, Rha, and Fuc. On the polysaccharide chain contain carboxylate groups, sulfate groups and the most important is amide groups. Due to the presence of amide, sacran could be showed bioactivity like a glycosaminoglycan, the extensive

proteoglycans present in the extracellular matrix and on cell surfaces in animal tissues[19]. Thus, we believe the sacran hydrogels were proper properties for scaffolds candidate.

Herein we exploit the opportunity sacran hydrogels to employ in tissue engineering field. The significant issues regarding scaffolds were studied, surface morphology, hydrophobicity, and the ability to adsorb protein. Furthermore, culturing of fibroblast L929 cells on these hydrogels showed biocompatibility as well and the morphology of attached cell also good-looking oriented.

2. Materials and methods

2.1 Materials.

Sacran was dedicated from Green Science Material Inc. (Kumamoto, Japan) and used as received.

2.2 Sacran scaffolds fabrication

Sacran scaffolds with porous layered pattern were prepared freeze-drying of hydrogels which were fabricated by solvent casting process as reported before. Briefly, 50 ml of 0.5 % w/v sacran solution was casted on polystyrene mold with micro-patterned on a polypropylene case ($50 \times 50 \times 50$ mm^3) and dried in an oven at 60 °C for 24 h to form translucent films. The films were thermally treated at 100, 120, and 140 °C, for 6 h in order to cross-link the sacran chains in a dry film state. When the films were immersed in deionized water at room temperature for 24 h became equilibrium state hydrogels. Next, sacran hydrogels were frozen by keeping in liquid nitrogen for about 10 min and then drying in a freeze-drying apparatus (EYELA, FDU-1200) for 72 h to form porous sacran scaffolds.

2.3 Characterization of sacran scaffolds

To investigate the surface morphology, the microscopic images were examined using scanning electron microscopy (SEM, JEOL, JCM-6000PLUS). The samples were mounted onto metal stubs using carbon tape. The stubs were then coated with gold using a sputter coater machine.

Water contact angle experiment of the sacran scaffolds were performed on top surface using a contact angle meter (Drop Master, Kyowa Interface Science Co., Ltd., Japan) at room temperature.

To measure the protein adsorption, sacran scaffolds were placed in 96 well plate having Dulbecco's Modified Eagle's Medium (DMEM) + 10% FBS and was incubated at 37 °C for 24 h. After incubation, the scaffolds were washed with PBS solution thrice. The washed scaffolds were then incubated with the 2 % w/v of sodium dodecyl sulfate solution (Wako, Japan) at room temperature for 3 h. Total protein was calculated using Bicinchoninic acid (BCA) assay[20].

2.4 Cell Culture

A mouse fibroblast-like cell line (L929) was selected for all biological assays in order to evaluate the biocompatibility and cell adhesion behavior on sacran scaffolds. The L929 fibroblast cell line was obtained from the American Type Culture collection (Manassas, VA). The cells were cultured in Dulbecco's Modified Eagle's Medium (DMEM, Sigma, USA) supplemented with 10% heat-inactivated fetal bovine serum (FBS, Biochrom AG, Germany) incubated at 37 °C in a humidified atmosphere with 5% CO_2.

2.5 Cell Adhesion

Prior to biological assays, all scaffolds were sterilized under UV radiation overnight[21], then immersed in ethanol 70% (v/v) for 3 days. Subsequently, the 1 ml of 1.0×10^5 cells·ml^{-1}

cell suspension was seed on each scaffolds and cultured for 1, 2, and 3 days at 37 °C. After each incubation period, the samples were rinsed with a buffer saline (PBS, Sigma-Aldrich, USA). The number of cells adhering to the porous scaffold was then counted.

2.6 CCK-8 assay [22]

Cell Counting Kit-8 (CCK-8, dojinb, Japan) was applied to evaluate cell number according to the manufacturer's instruction. Each sample, after rince with PBS, was incubated in 0.1 ml of growth medium supplemented with 10 µl of CCK-8 stock solution for 3 h at 37 °C in a humidified atmosphere of 5% CO2, in air. The absorbance at 450 nm was measured.

2.7 Cell morphology

The morphology of the cultured L929 (1.0×10^5 cell/scaffold) was observed by SEM images. After 3 days of cultured, the cells were fixed by 10% formalin neutral buffer solution (Wako, Japan) for 24 hours. Dehydration process was performed on each specimen in ethanol (60%, 70%, 80%, 90%, 100% and 100%) and 2 time of *t*-Butanol, each for 1 h then dry at room temperature. After that they were sputter-coated with gold and viewed by SEM.

2.8 Live/ Dead assay [7, 22]

Cell viability in sacran scaffolds was evaluated using live/dead assay. Constructs were harvested, gently rinsed twice with PBS and then incubated with calcein AM and ethidium homodimer-1 (EthD-1) for 15 min to strain live (green) and dead (red), respectively, for 15 min at 37 °C and 5% CO_2 humidified incubator. Samples were viewed using fluorescence microscope (BZ-X700, KEYENCE)

3. Results and discussion

3.1 Morphology

Sacran scaffolds were fabricated by using the simple method of solvent casting and freeze-drying. Firstly, 0.5 % w/v of sacran liquid crystalline (LC) solution was casted at 60 °C to form translucent films[23]. Then these film were cross-linked using thermal annealing strategy at 100, 120 and 140 °C. The SEM images (Figure. 1) presented the layered pattern on the side surfaces on the other hand there was not find any pattered structure on the top surface of films, thanks to the texture of sacran LC domains oriented. Afterwards, the films were immersed in de-ionize water for 24 h to form swollen hydrogels and submitted to freeze-dry process, the finalized porous scaffolds occurred (Figure. 1: inset). The porous scaffolds revealed porous structure like tunnel throughout materials. In contrast, on the top surface were unseen any pores, with the exception of wrinkle flow due to water evaporation. From above, they showed relationship between layered pattern on side surfaces of films and pores structure. Pores were generated instead of water molecule inside hydrogels, water was evaporated by freeze-drying step. The layered structure inhibited the movement direction of water molecules, thus they emanated through the gaps between layers and pores were showed only side surfaces.

The scaffold annealed at high temperature revealed small and dense pores otherwise cross-linking degree and mechanical properties were advance and vice versa. We believe that, sacran porous materials are reasonable scaffold candidate. Especially, cells could penetrate and oriented within interconnected tunnels then regenerative tissues were created with expected morphology.

3.2 Surface properties

Subsequently, water contact angle (WCA) was measured to evaluate the wettability of the sacran scaffolds. Wettability is an important characteristic of scaffolds, which was

employed to investigate cell behaviors on the materials[24]. On literatures, the moderate wettability surface from hydrophobicity to hydrophilicity preferred well-adhesion of cells[25]. Figure. 2a revealed that the WCA of scaffolds cross-linked at 100 °C was the highest (95.1°) and gradually decrease for cross-linked at 120 °C (77.9°). While WCA was changed too much at 140 °C cross-linked scaffold, only 37.4° was detected. These results indicated that the surface wettability of the sacran scaffolds could be simply controlled using cross-linking temperature. This is likely due to the fact, that chemical structure of sacran polysaccharide was tailored by annealing temperature. Another reason can be that the density of polymer increased by increasing of cross-linking temperature, sacran is hydrophilic polymer thus high density scaffold was higher hydrophobicity. Moreover, water droplet was hold by roughness surface on 100 °C scaffold, in contrast smooth surface on 140 °C scaffold cannot hold[26].

Protein adsorption has a vital role in scaffolds, serum protein including fibronectin and fibronectin have been found to promote cell adhesion and reorganization of the actin filaments[27]. Sacran scaffold cross-linked at 140 °C showed the smallest amount of protein adsorption. The amount of adsorbed protein showed a significant increase when decreasing annealing temperature (Figure 2b). Protein adsorbed by scaffolds 120 and 140 °C were approximately 2 and 3 fold respectively more adsorbed than scaffold annealed at 100 °C. By reason of porous structure, scaffold prepared at high temperature revealed small pore size and lower in porosity degree. Moreover, at high temperature annealing polymers were completely cross-linked then small amount of free functional groups such as –OH, –COOH can bind with protein[28]. Therefore, the adsorption of protein depended on the annealing temperature of sacran scaffolds. This result was an important evidence to promote possibility of sacran hydrogels in tissue engineering application.

3.3 Cell cultured

The ability of scaffolds to support cell adhesion and proliferation play a crucial role in tissue engineering application. In the following study, we continued the cell cultured experiment on sacran scaffolds. Fibroblast L929 cell was used to evaluate cell-matrix interaction. Biocompatibility results of the sacran scaffolds as evaluated by SEM and fluorescent microscopy are presented in figure 3 and 4, respectively. SEM images demonstrated that the cell was thoroughly attached to the scaffolds and exhibited an elongated shape. However, attachment patterns were different pattern between top surface and side surface. On the side surface, cells were extended in accordance with layered alignments of sacran scaffolds. Because the topology and porosity of material play a significant role in the cell attachment and the proliferation of cells[29]. The uniaxial alignment of cell showed highly oriented. The scaffold cross-linked at 140 °C revealed the clearest align due to it is the highest condense and porous structure was the highest align too. On the other hand, cells were randomly adhered on the top surface. Owing to sacran scaffolds did not present open pore on the top surface thus nothing can guide the alignment of cells on the top surface. Furthermore, both of the top and the side surface of scaffolds were covered by cells which proofed the biocompatibility of sacran scaffolds. In addition, a large number of cell muddled on scaffold 100 and 120 °C, however they were clearly showed aligning on 140 °C scaffolds. This observation was supported by the results fluorescent microscopy (Figure 4).

Figure 4, the live and dead assay was performed. The fluorescent image of fibroblast L929 cells after 72 h incubation was reported. The result showed green colour that mean majority of cells are alive, where the cell pattern on the side surface was higher order than on the top surface.

These confirmed that the sacran scaffolds facilitated the cell adhesion and promote the proper cell morphology. Besides, the anisotropic structure of pores could control the alignment of fibroblast cells and these unique characteristic may use to lead the organization of artificial tissue.

As to characterize the proliferation of L929 cells on sacran scaffolds, CCK-8 test was used to evaluate. Figure 5a depicted the absorbance values obtained after 3 days of incubation. At the first day of cell culture, the amount of cells on scaffolds highest to lowest were 140, 120 and 100 °C annealed, respectively. The number of cells on scaffold can clearly be seen that there was a large increase after 2 days of incubation for 120 °C cross-linked, while 100 and 140 °C cross-linking scaffolds revealed a slight increased. From this experiment the 120 °C cross-linked scaffold was the proper materials for cells adhesion, and scaffolds which was cross-linked at 100 °C also appropriated. Otherwise, the number of cells on scaffold cross-linked at 140 °C was decreased after 3 days of incubation however, cells orientation was highly aligning.

Figure 5b showed the density of cells which was compared between top and size surfaces. This data was analyzed from SEM images of scaffolds which were culture for 3 days (Figure 3). The density of cells on top surface was higher than side surface for all samples. However, cells density number on top surface correlates well with amount of cell on scaffolds in Figure 5a. This results suggested that amount of cells on scaffolds were preferred by cells which adhered on side surfaces. Surface area on side was lower than top, however the number of cell on side was impacted. Due to materials morphology was the main condition for cell adhesion, thus many cells were offered to attached at the side surface. In addition, scaffold annealed at 140 °C revealed side surface area, pore size and amount of protein adsorbed lower than others thus amount of cell was low.

3.4 Cell orientation

To qualify the orientation of fibroblast L929 cells in response to the layered structure of sacran scaffolds, we analyzed the angle between the growth direction of L929 cell and the surface direction of substrate scaffolds (Figure 6). The orientation angle was varied in the range from -90 to +90°. An orientation angle at 0° represents the direction of elongated cells parallel to reference axis. The reference axis was parallel to layered structure on side plane whereas horizontal line was assigned as 0° on top plane. The cell numbers were counted for incremental orientation angle intervals of 10°. Figure 6 demonstrated that most of cells on side surface were aligned, while cells on top surface were random, and the alignment increased with annealing temperature. On scaffold 100 °C annealed, most of cells aligned at orientation degree between -25 to +25°. However, 63% of cells aligned within -25 to -5° orientation. For scaffold at 120 °C annealing, 80% of cells oriented within ±25° and they showed in normal distribution pattern. In addition, all of cells on scaffold 140 °C annealing were aligned between -15 to +25°. Additionally, there was 91.5% of cells oriented in range of -5 to 15°.

The cells distribution behaviour demonstrated that increasing annealing temperature of substrate scaffolds significantly enhanced cell orientation degree. At low temperature annealing resulted in large pore size, wide space between layers and soft texture. This swollen hydrogel was high surface area, moreover the free space between layers prevented the alignment of cells. Based on these reasons, sacran layer scaffolds annealed at 100 °C revealed low orientation degree. The increasing of annealing temperature produced the sacran scaffolds with high orientation of layers. Furthermore, layers pattern was condensed and introduced the orientation behavior of fibroblast cells.

These results revealed that, cell orientation behavior was absolutely controlled by layered structure. At 140 °C annealing produced the layer of sacran scaffolds with proper pore size, high dense and well oriented resulted in the most perfectly orientation of cells.

4. Conclusion

In summary, we demonstrated that the sacran scaffolds with anisotropic porous structure was excellent materials for tissue engineering application. They showed layered pattern on pores which could guide the cell adhesion behavior. Surface property in water contact angle was presented the proper condition from 95 to 37°. Base on chemical structure protein was bind with –OH and –COOH functional groups of sacran. Both of water contact angle and protein adsorption were accompanied by thermal cross-linking temperature. Particularly, sacran scaffolds were good biocompatibility due to amide group which was a duplication of glycosaminoglycan native tissue. Not only biocompatibility, but the orientation of cells was also well oriented. Most of cells almost parallel to layered structure of scaffolds at side planar. Hence, sacran porous materials have good bio-properties and are promising biomaterials for tissue engineering scaffolds.

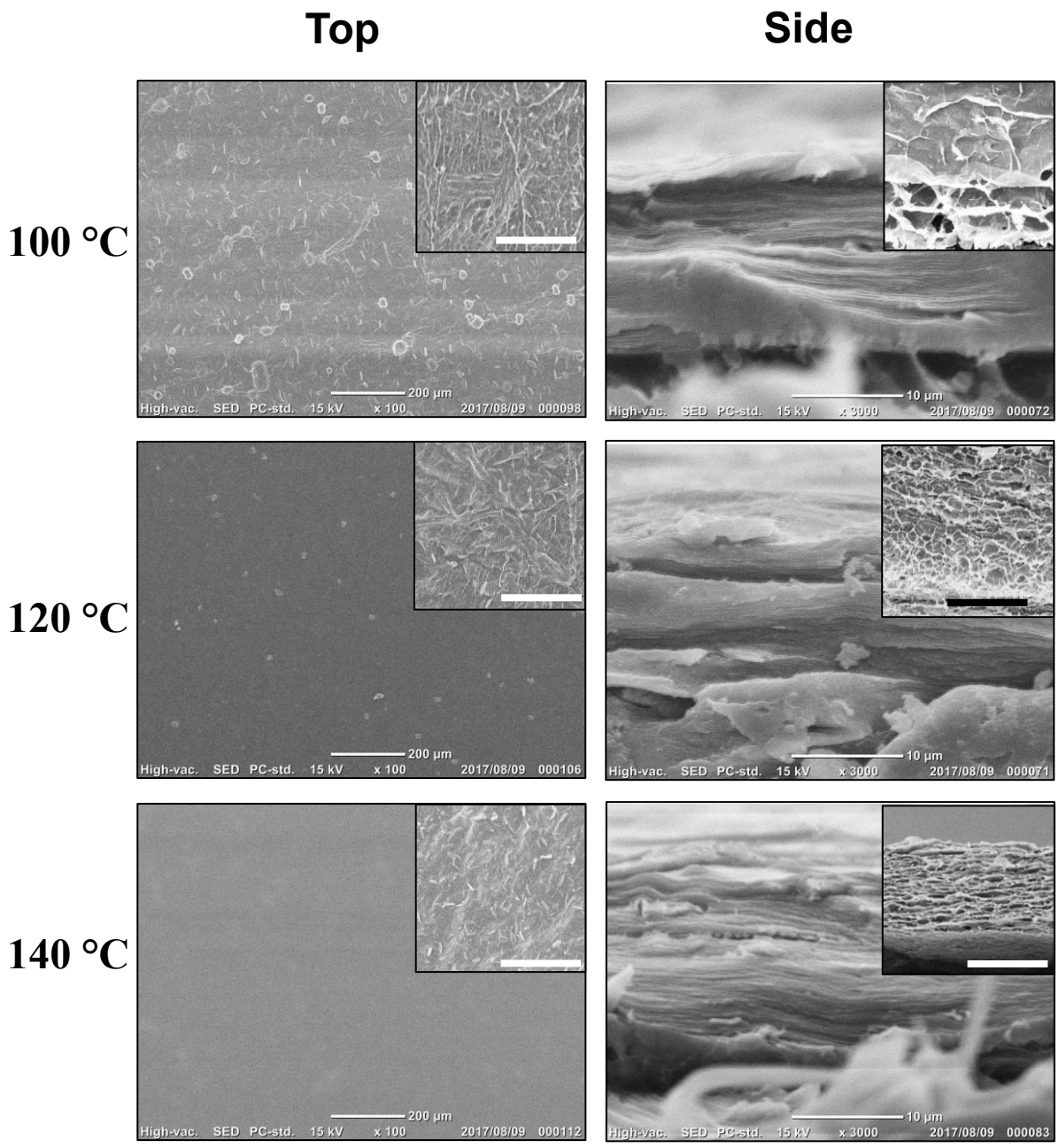

Figure 1. SEM images of layered films prepared by casting of 0.5 % w/v sacran solution and annealed at 100, 120 and 140 °C. Images revealed layered patterns on side faces while no specific pattern on top face. Inset: Porous scaffolds prepared by freeze-drying of layered films (scale bars: 200 mm).

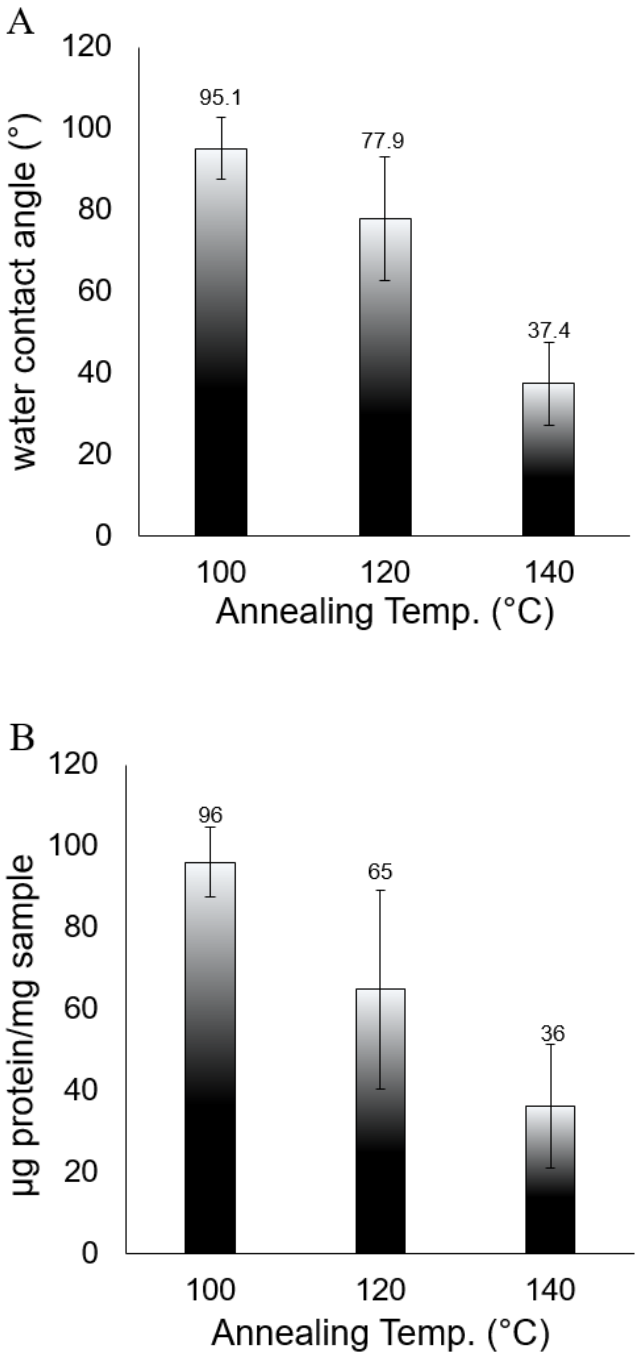

Figure 2. Surface properties of layered porous scaffolds which were prepared by freeze-drying of hydrogels from the films thermally annealed at 100, 120 and 140 ^{o}C. (A) Water contact angles on the scaffolds. (B) Protein adsorption after 24 h immersion of the scaffolds. The values are an average of data (n= 5) and error bars are standard deviation.

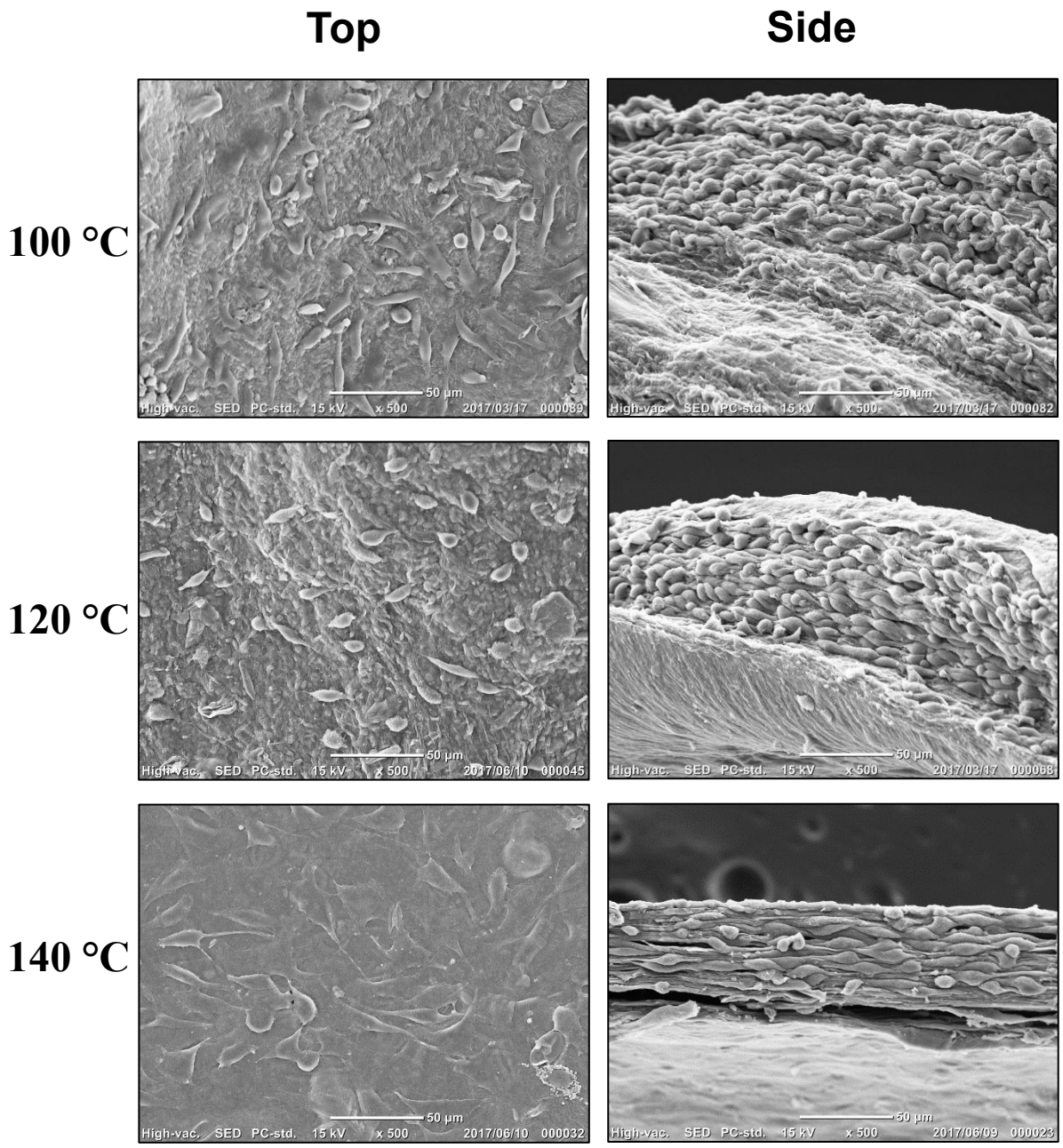

Figure 3. SEM images of L929 fibroblasts taken after incubation for 3 days on layered porous scaffolds, which were annealed at 100, 120 and 140 °C.

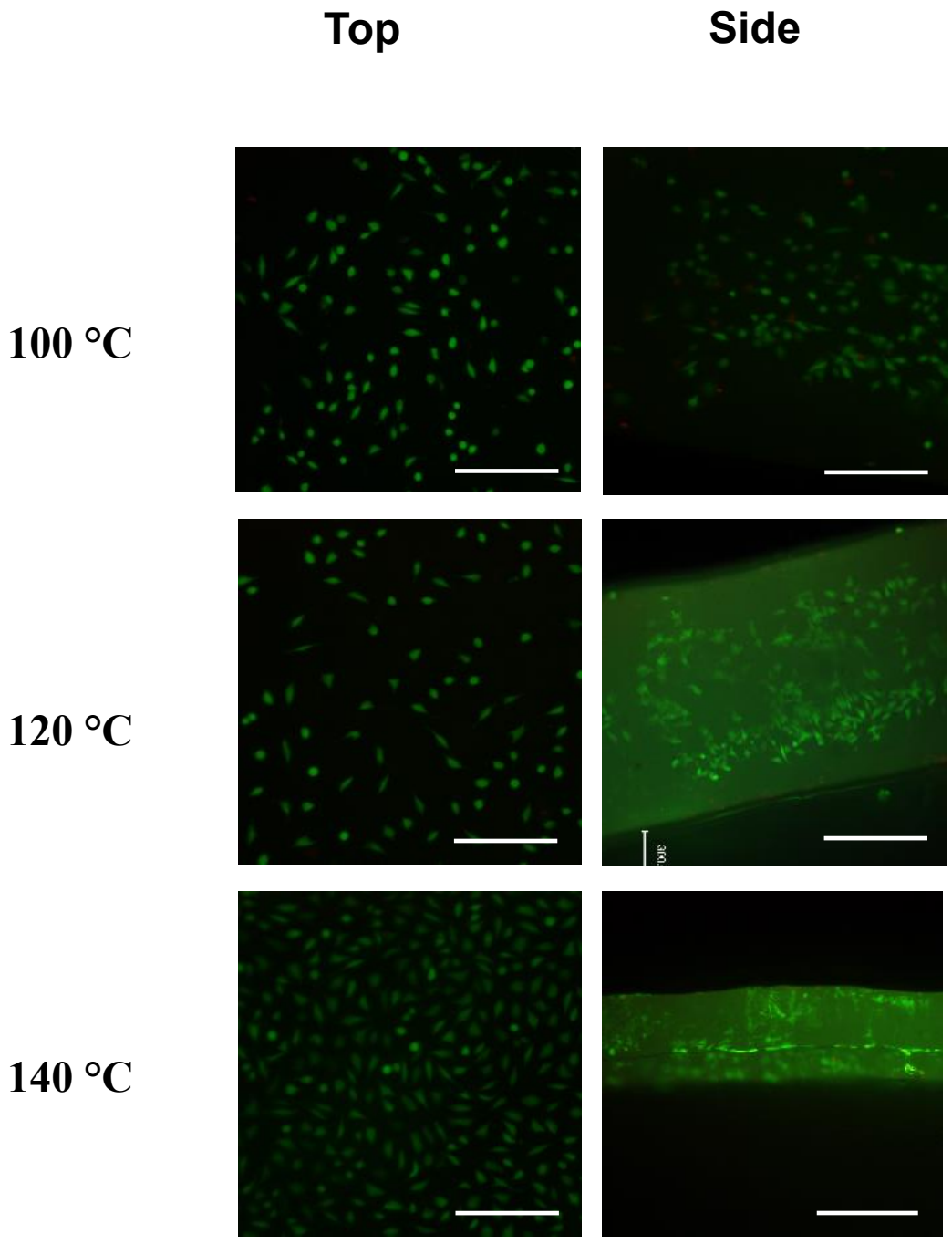

Figure 4. Resulting images of live/dead staining of fibroblast L929 after 3 days incubation on layered porous scaffolds of sacran which were prepared by freeze-drying of hydrogels from the films annealed at 100, 120 and 140 oC. Live cells are green (celcein AM) while dead cells are red (edthidium homodimer). Scale bars: 200 mm.

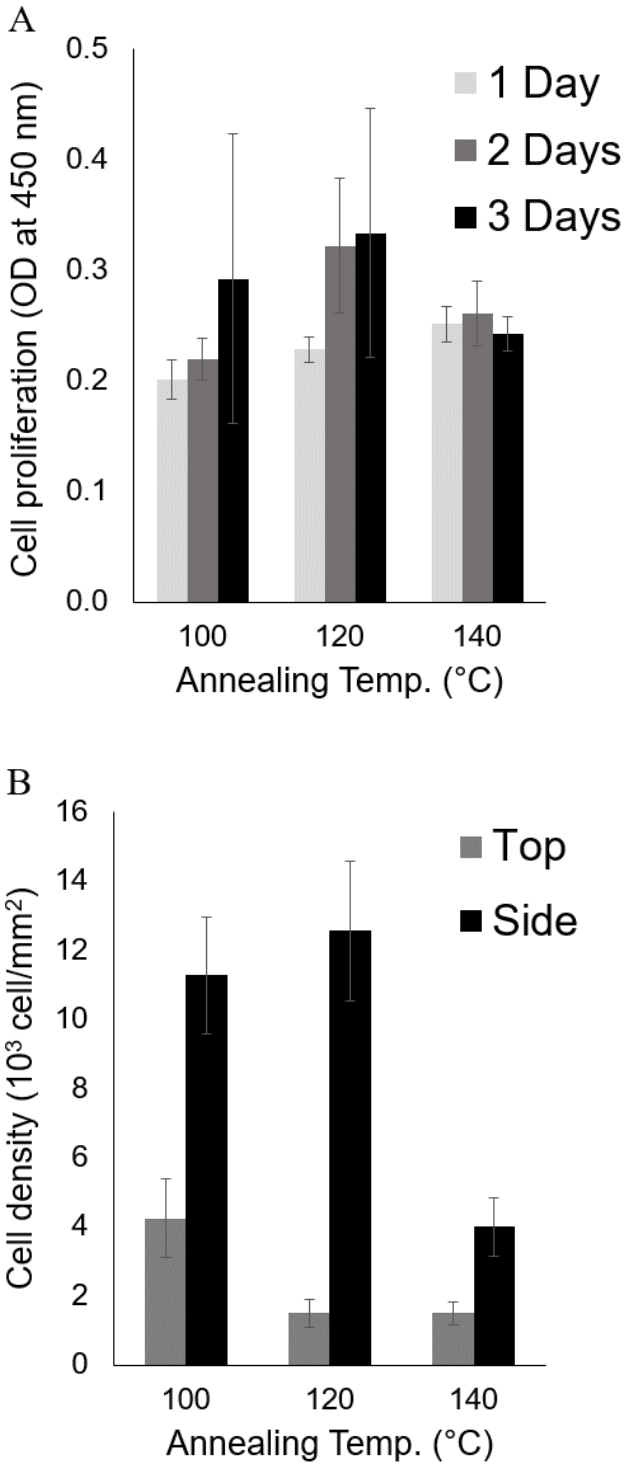

Figure 5. Proliferation data of fibroblast L929 cells on layered porous scaffolds of sacran which were prepared by freeze-drying of hydrogels from the films annealed at 100, 120 and 140 ºC. (A) Total number of cells proliferated on sacran scaffolds after 1, 2 and 3 days of incubation. (B) Cell densities on top and side faces of scaffolds after 3 days incubation. Values are an average of data (n= 5) and error bars are standard deviation.

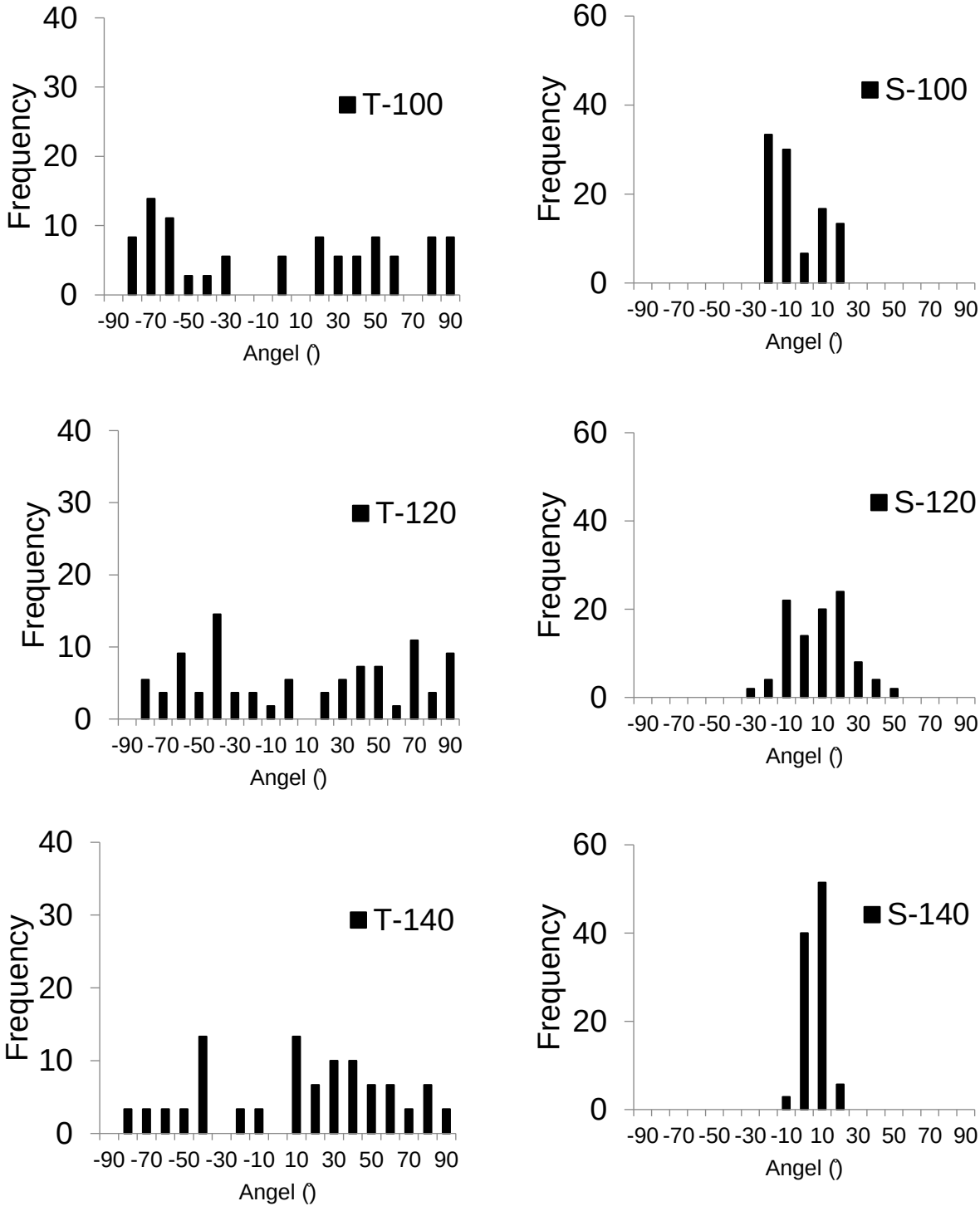

Figure 6. Histogram data showed the angle distribution of the longitudinal direction of the extended cell to the axis of scaffolds, which were annealed at 100, 120 and 140 °C. The frequency of distribution was compared between side surface (S) and top surface (T).

REFERENCES

1. Xiang, H.; Xia, M.; Cunningham, A.; Chen, W.; Sun, B.; Zhu, M., Mechanical properties of biocompatible clay/P(MEO2MA-co-OEGMA) nanocomposite hydrogels. *Journal of the Mechanical Behavior of Biomedical Materials* **2017,** *72,* 74-81.

2. Yang, Y.; Wang, C.; Wiener, C. G.; Hao, J.; Shatas, S.; Weiss, R. A.; Vogt, B. D., Tough Stretchable Physically-Cross-linked Electrospun Hydrogel Fiber Mats. *ACS Applied Materials & Interfaces* **2016,** *8* (35), 22774-22779.

3. Wang, Z.; Wang, J.; Jin, Y.; Luo, Z.; Yang, W.; Xie, H.; Huang, K.; Wang, L., A Neuroprotective Sericin Hydrogel As an Effective Neuronal Cell Carrier for the Repair of Ischemic Stroke. *ACS Applied Materials & Interfaces* **2015,** *7* (44), 24629-24640.

4. Xue, B.; Kozlovskaya, V.; Liu, F.; Chen, J.; Williams, J. F.; Campos-Gomez, J.; Saeed, M.; Kharlampieva, E., Intracellular Degradable Hydrogel Cubes and Spheres for Anti-Cancer Drug Delivery. *ACS Applied Materials & Interfaces* **2015,** *7* (24), 13633-13644.

5. Zhang, Z.; He, Z.; Liang, R.; Ma, Y.; Huang, W.; Jiang, R.; Shi, S.; Chen, H.; Li, X., Fabrication of a Micellar Supramolecular Hydrogel for Ocular Drug Delivery. *Biomacromolecules* **2016,** *17* (3), 798-807.

6. Kim, M.; Hong, B.; Lee, J.; Kim, S. E.; Kang, S. S.; Kim, Y. H.; Tae, G., Composite System of PLCL Scaffold and Heparin-Based Hydrogel for Regeneration of Partial-Thickness Cartilage Defects. *Biomacromolecules* **2012,** *13* (8), 2287-2298.

7. Mohanty, S.; Alm, M.; Hemmingsen, M.; Dolatshahi-Pirouz, A.; Trifol, J.; Thomsen, P.; Dufva, M.; Wolff, A.; Emnéus, J., 3D Printed Silicone–Hydrogel Scaffold with Enhanced Physicochemical Properties. *Biomacromolecules* **2016,** *17* (4), 1321-1329.

8. Yan, H.; Saiani, A.; Gough, J. E.; Miller, A. F., Thermoreversible Protein Hydrogel as Cell Scaffold. *Biomacromolecules* **2006,** *7* (10), 2776-2782.

9. Ovsianikov, A.; Deiwick, A.; Van Vlierberghe, S.; Dubruel, P.; Möller, L.; Dräger, G.; Chichkov, B., Laser fabrication of three-dimensional CAD scaffolds from photosensitive gelatin for applications in tissue engineering. *Biomacromolecules* **2011,** *12* (4), 851-858.

10. Gupta, P.; Vermani, K.; Garg, S., Hydrogels: from controlled release to pH-responsive drug delivery. *Drug discovery today* **2002,** *7* (10), 569-579.

11. Van Vlierberghe, S.; Vanderleyden, E.; Dubruel, P.; De Vos, F.; Schacht, E., Affinity study of novel gelatin cell carriers for fibronectin. *Macromolecular bioscience* **2009,** *9* (11), 1105-1115.

12. Anderson, J. M.; Rodriguez, A.; Chang, D. T. In *Foreign body reaction to biomaterials*, Seminars in immunology, Elsevier: 2008; pp 86-100.

13. Hollister, S. J., Porous scaffold design for tissue engineering. *Nature materials* **2005,** *4* (7), 518.

14. Peltola, S. M.; Melchels, F. P.; Grijpma, D. W.; Kellomäki, M., A review of rapid prototyping techniques for tissue engineering purposes. *Annals of medicine* **2008,** *40* (4), 268-280.

15. Yeong, W.-Y.; Chua, C.-K.; Leong, K.-F.; Chandrasekaran, M., Rapid prototyping in tissue engineering: challenges and potential. *TRENDS in Biotechnology* **2004,** *22* (12), 643-652.

16. Sornkamnerd, S.; Okajima, M. K.; Kaneko, T., Tough and Porous Hydrogels Prepared by Simple Lyophilization of LC Gels. *ACS Omega* **2017,** *2* (8), 5304-5314.

17. Okajima, M. K.; Kaneko, D.; Mitsumata, T.; Kaneko, T.; Watanabe, J., Cyanobacteria That Produce Megamolecules with Efficient Self-Orientations. *Macromolecules* **2009,** *42* (8), 3057-3062.

18. Okajima, M. K.; le Nguyen, Q. T.; Tateyama, S.; Masuyama, H.; Tanaka, T.; Mitsumata, T.; Kaneko, T., Photoshrinkage in polysaccharide gels with trivalent metal ions. *Biomacromolecules* **2012,** *13* (12), 4158-63.

19. Chi, L.; Wolff, J. J.; Laremore, T. N.; Restaino, O. F.; Xie, J.; Schiraldi, C.; Toida, T.; Amster, I. J.; Linhardt, R. J., Structural Analysis of Bikunin Glycosaminoglycan. *Journal of the American Chemical Society* **2008,** *130* (8), 2617-2625.

20. Deepthi, S.; Jeevitha, K.; Nivedhitha Sundaram, M.; Chennazhi, K. P.; Jayakumar, R., Chitosan–hyaluronic acid hydrogel coated poly(caprolactone) multiscale bilayer scaffold for ligament regeneration. *Chemical Engineering Journal* **2015,** *260*, 478-485.

21. Yang, A.; Huang, Z.; Yin, G.; Pu, X., Fabrication of aligned, porous and conductive fibers and their effects on cell adhesion and guidance. *Colloids and Surfaces B: Biointerfaces* **2015,** *134*, 469-474.

22. Zhao, Y.; Tan, K.; Zhou, Y.; Ye, Z.; Tan, W.-S., A combinatorial variation in surface chemistry and pore size of three-dimensional porous poly(ε-caprolactone) scaffolds modulates the behaviors of mesenchymal stem cells. *Materials Science and Engineering: C* **2016,** *59*, 193-202.

23. Okajima, M. K.; Mishima, R.; Amornwachirabodee, K.; Mitsumata, T.; Okeyoshi, K.; Kaneko, T., Anisotropic swelling in hydrogels formed by cooperatively aligned megamolecules. *RSC Adv.* **2015,** *5* (105), 86723-86729.

24. Song, W.; Mano, J. F., Interactions between cells or proteins and surfaces exhibiting extreme wettabilities. *Soft Matter* **2013,** *9* (11), 2985-2999.

25. Lee, J. H.; Lee, J. W.; Khang, G.; Lee, H. B., Interaction of cells on chargeable functional group gradient surfaces. *Biomaterials* **1997,** *18* (4), 351-358.

26. Spori, D. M.; Drobek, T.; Zürcher, S.; Ochsner, M.; Sprecher, C.; Mühlebach, A.; Spencer, N. D., Beyond the Lotus Effect: Roughness Influences on Wetting over a Wide Surface-Energy Range. *Langmuir* **2008,** *24* (10), 5411-5417.

27. Kim, H.-W.; Kim, H.-E.; Salih, V., Stimulation of osteoblast responses to biomimetic nanocomposites of gelatin–hydroxyapatite for tissue engineering scaffolds. *Biomaterials* **2005,** *26* (25), 5221-5230.

28. Jin, J.; Jiang, W.; Yin, J.; Ji, X.; Stagnaro, P., Plasma proteins adsorption mechanism on polyethylene-grafted poly (ethylene glycol) surface by quartz crystal microbalance with dissipation. *Langmuir* **2013,** *29* (22), 6624-6633.

29. Peter, M.; Ganesh, N.; Selvamurugan, N.; Nair, S. V.; Furuike, T.; Tamura, H.; Jayakumar, R., Preparation and characterization of chitosan–gelatin/nanohydroxyapatite composite scaffolds for tissue engineering applications. *Carbohydrate Polymers* **2010,** *80* (3), 687-694.

Chapter IV: Preparation of sacran hydrogels with micro-patterned on the surface

1. Introduction

Scaffolds are three-dimension materials for cell growth in new tissue formation and regeneration. To mimic the native tissue, scaffolds need basic requirement such as biocompatible, biodegradable, porosity, and cellular alignment controlled capacity.

Cellular alignment of native tissue is the special property in many biological functions. Native tissues have an innate design with an orientation feature, under which biological function is facilitated in the living body. Most of the tissues have an anisotropic oriented longitudinal with their longitudinal direction, giving asymmetric to their mechanical properties, which is the most important for the living cell. The ability to control cell shape and to engineer tissues with precisely controlled morphology holds great potential in many biomedical applications including regenerative medicine, tissue regeneration and repair, drug screening, development of biosensors, and elucidation of cell−cell and cell−matrix interactions[1]. Thus the orientation controlled in tissues cultivated in vitro is necessary for tissue engineering.

Several of the techniques have been developed to address this function. For example, electrospinning technique[2-7] is the simple way for filament fabrication. However rheological behavior of the polymer solution e.g. viscosity, electricity, plays a crucial role in the electrospinnability for any given sample[2, 8]. Surface topography has been introduced as cell patterned controllable tool. The specific layout can be created by photo crosslinking[9-10], chemical introducing[11-12] or patterned surface[1, 13]. In the above mention cells are oriented in alongside the pattern but, conversely, our micro-pattern hydrogel showed in difference orientated aspect. Because of uni-direction swelling of sacran liquid crystalline polymer impact on that orientation.

Sacran is a newly discovered megamolecular polysaccharide extracted from cyanobacteria, *Aphanothece sacrum*. The chemical structure of sacran is linear polysaccharide chains contains various sugar residues, including Glc, Gal, Man, Xyl, Rha, Fuc, and acidic sugars such as uronic acids and muramic acids, where the chains are sulfated to a degree of 10-20 mol% of sugar residues. The sacran chain has a very high molecular weight over 2.0×10^7 g/mol (molecular length over 30 μm) and shows self-assembly with increasing the solution concentration to be a rigid-rod structure. As a result, the LC properties exhibiting on sacran solution. More than anything else, sacran constitute of amino function like glycosaminoglycan. The glycosaminoglycan is presented on the cell surface or in the extra cellular matrix and involved in cell adhesion, cell-to-cell communication, cell signaling, differentiation, and regulation of other biochemical pathways. Because of their unique properties, thus we selected sacran as raw materials for preparing the scaffolds with the micro pattern on the surface.

The sacran film with micro-patterned on the surface will be created by casted the sacran solution on the polystyrene mold with micro structure size between 200-400 μm. The objective of this study was to demonstrate that this technique can create the micro-patterned scaffolds with well orientation controlled. Furthermore, the orientation scaffolds were perfectly guided the cell alignment, which is the outstanding characteristic of scaffolds.

2. Materials and methods

2.1 Materials.

Sacran was dedicated from Green Science Material Inc. (Kumamoto, Japan) and used as received. Polystyrene mold was provided by Mutoh Industries Limited, Ikejiri, Setagaya Tokyo, 154-8560 Japan.

2.2 Micro-patterned hydrogels fabrication

Sacran hydrogels with micro-patterned on the surface used here were prepared by the procedure shown in Figure 1. First, 5 ml of 0.5 w/v % sacran LC solution was casted on polystyrene mold with micro-patterned on surface and dried in an oven at 60 °C for 24 h to

form translucent films with micro structure on the surface. The LC films were punched into disk-like samples with a diameter of 5 mm and were thermally treated at 120 °C, in order to cross-link the sacran chains in a dry film state. Scanning electron microscopy (SEM, JEOL, JCM-6000PLUS) was used to investigate the surface patterned and layered structure. The samples were mounted onto metal stubs using carbon tape. The stubs were then coated with gold using a sputter coater machine. Then the films were immersed in deionized water at room temperature and kept for 24 h, the translucent self-standing of LC hydrogels were of an almost constant diameter, whereas the thickness was increased. The swelling behavior, LC domains orientation, and mechanical properties of these were evaluated.

To apply these LC hydrogels for scaffolds, porous structure was requested. The precursor LC hydrogels were frozen by keeping in liquid nitrogen for about 10 min and then drying in a freeze-drying apparatus (EYELA, FDU-1200) for 72 hrs. We were able to confirm their complete drying because the samples spontaneously attached to the glass wall by electrostatic force. As a result of freeze-drying, spongy materials were formed. When the sponges were immersed in deionized water, self-standing hydrogels were recovered.

2.3 Orientation observe.

Crossed-polarizing microscopy was used to observe the structure formation of sacran LC polymer. Microscopic observations were made by a microscope (BX51, Olympus) equipped with CCD camera (DP80, Olympus). A specimen of samples was cut to size for microscopic observation (ca. 5 mm × 0.5 mm) and put on the glass plates at room temperature. A first order retardation plate (530 nm) was inserted onto the light path to identify the orientations direction.

2.4 Swelling behavior

The degrees of swelling were measured by monitoring the shape changing. The size ratio of swollen to dry samples were measured by the following method. Firstly, the pattern-size of dry films measured before hydrogel formation by SEM images. After equilibrium swollen by immersed in de-ionize water for 24 h, the optical microscope was used to measure size of

pattern hydrogels. The degree of swelling, Q, was evaluated by the ratio of the swollen size, L_s, to the dry one, L_d:

$$Q=L_s/L_d \quad (1)$$

The swelling in thickness dimension was also calculated same as size swelling method.

The values of 5 specimens were averaged.

2.5 Mechanical properties of the hydrogels. [14-16]

The mechanical properties of the micro-patterned hydrogels were investigated in an elongation test. The elongation probe was set up on an Instron 3365 machine using a 5 kN load cell with a crosshead speed of 1.0 mm/min. Elastic modulus (*E*) of each sample was calculated using the following neo-Hookean equation applied to unidirectional elongation measurements:

$$\tau = \frac{F}{A} = E(\lambda - \lambda^{-2}) \quad (2)$$

where τ is the stress, F is the applied force, A is the original cross-sectional area of the hydrogels, and E is the elastic modulus. $\lambda = h/h_0$, where h is the hydrogel length under strain and h_0 is the hydrogel length before elongation. Plotting F/A versus $(\lambda - \lambda^{-2})$ resulted in a straight line with a slope of E, which is the modulus of elasticity of the swelling hydrogel. The strain energy density was measured by curve area under stress-strain function.

2.6 Cell Culture

A mouse fibroblast-like cell line (L929) was selected for all biological assays in order to evaluate the effect of the micro-patterned surface on cell adhesion. The L929 fibroblast cell line was obtained from the American Type Culture collection (Manassas, VA). The cells were cultured in Dulbecco's Modified Eagle's Medium (DMEM, Sigma, USA) supplemented with 10% heat-inactivated fetal bovine serum (FBS, Biochrom AG, Germany) incubated at 37 °C in a humidified atmosphere with 5% CO_2.

2.7 Cell Adhesion

Prior to biological assays, all scaffolds were sterilized under UV radiation overnight[17], then immersed in ethanol 70% (v/v) for 3 days. Subsequently, the 1 ml of 2.0×10^5 cells·ml^{-1} cell

suspension was seed on each scaffolds and cultured for 24, 48 and 72 h at 37 °C. A bare well plate was used as the control. After each incubation period, the samples were rinsed with a buffer saline (PBS, Sigma-Aldrich, USA). The number of cells adhering to the scaffold was then counted.

2.8 Live/ Dead assay [18-19]

Cell viability on scaffolds was evaluated using live/dead assay. Constructs were harvested, gently rinsed twice with PBS and then incubated with calcein AM and ethidium homodimer-1 (EthD-1) for 15 min to strain live (green) and dead (red), respectively, for 15 min at 37 °C and 5% CO_2 humidified incubator. Samples were viewed viewed using fluorescence microscope (BZ-X700, KEYENCE)

2.9 CCK-8 assay [18]

Cell Counting Kit-8 (CCK-8, dojinb, Japan) was applied to evaluate cell number according to the manufacturer's instruction. Each sample (scaffolds with cells adhered), after rinse with PBS, was incubated in 0.1 ml of growth medium supplemented with 10 µl of CCK-8 stock solution for 3 h at 37 °C in a humidified atmosphere of 5% CO_2, in air. The absorbance at 450 nm was measured. The assay was performed in triplicated.

2.10 Cell morphology

The morphology of the cultured L929 ($2.5x10^5$ cell/scaffold) was observed by SEM images. After 72 h of cultured, the cells were fixed by 10% formalin neutral buffer solution (Wako, Japan) for 24 hours. Dehydration process was performed on each specimen in ethanol (60%, 70%, 80%, 90%, 100% and 100%) and 2 time of *t*-Butanol, each for 1 h then dry at room temperature. After that they were sputter-coated with gold and viewed by SEM.

3. Results and discussion

3.1 Morphology

Hydrogels with orientation property are always modulated by electrospinning method or applying of stretch force on bulk hydrogels[20]. Otherwise this report we prepared hydrogels with orientated structure by the simple method, casting on the micro-patterned mold. The micro-patterned surface hydrogels were made by sacran LC polymer. The chemical structure of sacran. In Figure 1 presented the preparation process of micro-pattered surface hydrogels. At first, 0.5 % wt/v of sacran LC solution was casted on polystyrene mold at 60 °C for 24 h to form the micro-patterned film. Then that films were thermal cross-linked using annealing method at 120 °C for 6 h. To control the LC domain orientation, micro-patterned surface films with different bar-bar distance were fabricated at 200, 250 and 300 μm name as M200, M250, and M300, respectively whereas the bar size was fixed at 400 μm for all of them. SEM images in Figure 2 revealed sacran LC films had micro-patterned that exhibited a semicircular shape in cross-section, which was inherited from the polystyrene mold. We called film deposited on the bar as valley and it was called the mountain for the film deposited on the area between bars. The mountains size increased by increasing the bar-bar distance, and M200 revealed the sharpest shape. Three of films showed the same size of the surface curve due to bar size was fixed. In addition, sacran LC solution was cast on flat polystyrene for controlled. The previous report we showed sacran films with the layered structure[21]. The layered film was generated by the polymer with LC property, which is the basic property requests for orientation control[22]. The layered micro-patterned films were presented in Figure 2. The films revealed curly shape like polystyrene mold instead of the smooth plate. Preparation of the sacran LC film with micro-patterned surface and layered characteristic that faithfully produced is one of the most effective materials in successful patterned controllable of scaffolds.

3.2 Swelling

Water adsorption behavior was main factor for hydrogels in tissue engineering application because the native tissues composed of high water content. The micro-patterned on the surface of films were monitored by soaking in deionized water. For making the equilibrium hydrogels 24 h of soaking was used, the swelling behavior was measured by the ratio of swollen hydrogel to dry film.

Figure 3a showed the expansion of patterns. Curved magnitude expanded the highest for M300, on the other hand, M200 was the lowest expansion. This value indicated that LC domains in M300 almost straight oriented while M200 might be bent structure. The swelling in height was shown in Figure 3b. M200 showed the highest swelling because of bending morphology. And M300 was lowest swelling thanks to the straight alignment. Additionally, swelling degree at mountain zone was higher than valley zone.

Since these films composed of the layered structure, we speculated that the layers established in-plane for river zone whereas that layers established out-of-plane for mountain zone. Thus the mountain zone revealed higher swelling than valley zone. In addition, sacran has a unique property in one-direction swelling, because of layered structure[21]. Considering patterned hydrogels with the different swelling degree, M300 revealed the lowest of the height swelling due to embedded polymer chains in valley zone. Oppositely, the other micro-patterned hydrogels with small mountain zone experienced the height swelling higher. The ratio of height swelling to planar swelling was showed in term of anisotropic swelling (Figure 3c). Figure 3c supported with above mention M200 prefer to swell in thickness, probably it had curly alignment. M300 prefer to expand on the surface due to the straight LC domains. And the LC domains were favored to orient perpendicular to the micro-patterned structure (or mountain) due to their swelling behavior[23].

3.3 Orientation

Sacran appeared LC property at c*~0.2 %wt/v[24]. The sacran films with micro-patterned on the surface showed strong and uniform birefringence under a polarizing optical microscope (POM, Figure 5). The orientation of sacran LC domains was uni-direction, observed by POM. Sacran films with micro-patterned on the surface showed almost homogeneous strong color while sacran film without micro-patterned (flat surface) showed no orientation color on top of samples (Figure 5). From POM pattern, we identified that sacran aligns perpendicular to the micro-patterned structure. However, sacran film with a flat surface was randomly aligned. The 0.5 % wt/v of sacran are LC solution, they gradually deposited across the polystyrene mold during cast, therefore micro-patterned surface films were occurred with highly oriented.

The highly oriented property of sacran was maintained. Swollen micro-patterned hydrogels also revealed strong birefringence color and flat hydrogels was not showed orientation (Figure 6). When observed from the cross-section of hydrogels, the left-hand side and the right-hand side of mountain revealed the contrast orientation direction. Thanks to the LC packing on mountain zone were inhibited by peak, the orientation was presented in two patterns. On the left-hand side was northwest orientation and right-hand side was southwest orientation.

However, the valley zones revealed a slant oriented, due to their terminal were extended by highly swelling of mountain zones. This result correlated with previously discussed, mountain zones showed higher swelling ability than the valley zones. Then the margin on valley zones was drawn by mountain zones, thus aslant oriented patterned was revealed. Many literatures report that; the drawing technique is always used for producing of oriented materials. From our viewpoint, micro-mold played like a drawing machine when the casting process. Because the oriented films were revealed after casting. For a flat surface, which was showed

homogeneously oriented of the layered only in-plane orientation of sacran due to there was no stimulating position on the mold surface.

Otherwise, we prepared the films with the micro-pattern surface using 0.5% xanthan gum as a polymer (Figure 7). Xanthan gum is a natural extracellular, high molecular weight polysaccharide (300-8000 kDa) produced by *Xanthomonas campestris* bacteria. It was reported the biocompatibility and has been widely used in food, cosmetics, and pharmaceutical industries[25]. In contrast, by POM characterization, films with the micro-pattern surface of xanthan gum showed no uniform of orientation. It was indicated that orientation controlled using micro-pattern was a unique property of sacran LC polymer. Owning to sacran is megamolecular polymer 1.6×10^7 g/mol and low c* only ~0.2 % wt/v.

3.4 Mechanical properties

Physically cross-linked hydrogels were mechanically weak. However, scaffolds material need appropriated mechanical properties. Oriented polymer chains are one effective approach to overcome that problem. Tensile properties of micro-pattern surface hydrogels were measured in directions both longitudinal and perpendicular to the pattern structure. The stress−strain curves were presented in Figure 8 and the data were summarized in Table 1.

The flat surface hydrogel showed mechanical isotropy as elastic modulus (E) and tensile strength (σ) in both of longitudinal and perpendicular directions are nearly identical. However, the hydrogels with micro-patterned surface structure exhibited anisotropic mechanical properties (Table 1.). The elastic modulus was increased by increasing the bar-bar distance and micro-patterned surface hydrogels revealed higher elastic modulus than flat surface hydrogel. The elastic modulus increased from 223 to 318 and 414 kPa for M200, M250, and M300 for perpendicular direction, respectively whereas flat hydrogel showed only 173 kPa. For longitudinal direction, the value was 199, 203, 329 and 164 for M200, M250, M300 and flat hydrogels, respectively. The data in longitudinal direction were lower than perpendicular

direction, which coincided well with POM observation in Figure 5 and 6, confirming that polymer chains were oriented across the micro-patterned structure. This is important evidence to support that, sacran LC is oriented perpendicular to micro-patterned and the mechanical strength was improved by orientation control. Hydrogels with micro-pattern on the surface revealed higher modulus than flat surface hydrogel because flat hydrogel did not have orientation pattern. The elastic modulus was significantly increasing as bar-bar space, indicated that wide space was high orientation. M300 revealed the highest value, we believe that polymer chains were almost completely oriented. On the other hand, the narrow space between bars inhibited the polymer chains orientation, may be they showed a little bending shape. Thus they showed small value and a little different between longitudinal and perpendicular values.

The tensile strength (σ) come together accidentally with elastic modulus. Otherwise, the elongation at break (ε) was opposite, the data in longitudinal direction showed higher than perpendicular. These results mean, hydrogels showed elastic property in longitudinal direction higher than perpendicular direction. Finally, the mechanical property as (kJ/m^3) was slightly different.

3.5 In situ cell culture

Above reported, micro-patterned hydrogels were obviously proved the orientation property. To apply for cell supporting materials scaffolds in tissue engineering porous property is also requested for them because of the diffusion of oxygen and nutrients and waste exchange[26]. The inter-connected pores were produced through these micro-patterned hydrogels using the freeze-drying technique. The equilibrium swollen hydrogel was submitted to the freeze-drying machine, the resultant products were like a sponge. During free-drying process, firstly water molecule inside hydrogels became ice crystals. Then the ice crystals were sublimated and instated by pores. By this methods, they showed 45% porosity and pore size

was 18.63 μm. Especially, pores were aligned and duplicate to the layered structure of hydrogels.

The proliferation behaviors of fibroblast L929 cells on hydrogels were showed in figure 9. Figure 9 showed good biocompatibility of sacran hydrogels. After 72 h of culture, the viability and distribution of L929 cells on micro-patterned scaffolds were observed using the fluorescent microscope, and images were showed in Figure 10.

It is clear to see that L929 attached and grew well on all micro-patterned scaffolds and flat surface scaffold. The cell culture dish polystyrene was used as controlled. L929 cells anisotropically attached on micro-patterned scaffolds and replicate to those patterned. Whereas flat scaffold and cell culture dish were showed isotropic attachment.

SEM images in Figure 8 showed virgin scaffolds and cell culture scaffolds. These sponge scaffolds showed micro-patterned structure like films, that means micro-pattern structure was transferred from films to spongy scaffolds. Most importantly, the oriented property was kept in scaffolds. They showed micro-patterned structure on the surface and wrinkle in valley zones however flat scaffold showed only wrinkle. The wrinkle occurred during water sublimation because the water content was changed however volume not changed.

Figure 11 (a3-e3) showed cell attached on scaffolds surfaces. These images showed the surfaces of scaffolds were well-spread by L929 cells after 72 h of incubation. They were showed extended spindle shape on the micro-pattern and flat surface, also on a polystyrene dish.

Cell orientation was clearly influenced by surface patterned of scaffolds. On the micro-patterned surface scaffolds, cells were extended in one direction over the surface. On the other hand, on flat scaffold and polystyrene dish cells were extended in the random direction.

The direction of cell extension on micro-pattern scaffolds was perpendicular with micro-pattern structure, which correlated to polymer chains orientation.

To qualify the orientation of cells attachment in response to the micro-patterned surface of substrates, we measured the angle between the extension direction of L929 cells and the patterning direction of the substrates (Figure 10 and 11, a4-e4). The ImageJ software was used to measure the relative location of cells to scaffolds.

Results were showed in the range -90 to 90°. The angle of 0° represents the extension of cell perpendicular to surface patterned direction. On the other hand, the angle of ±90° represents the cell, which extended in longitudinal with surface patterned direction. The histogram in Figure 11 a4 showed 78% frequency of cells extended at angle ranging from -50 to 50° for M200 scaffold. For M250 and M300 scaffolds showed 90% of cells extended between the angle -10 to +40 and -30 to +30, respectively. Otherwise, flat surface scaffolds and polystyrene dish were not showed any orientation pattern.

Considering the micro-pattern size scaffolds, M200 was the lowest orientation of L929 extension. While M250 and M300 showed the great orientation. However, the flat scaffolds could not guide the orientation of L929 cells, showing that the cell extension angle was strongly influenced by the surface topology of scaffolds.

As discussed previously, polymer chains were oriented perpendicular to micro-pattern thus cells attached in perpendicular direction. From shape change in expansion mode, mechanical properties, and cells orientation angle, these data could summarize that the orientation degree of polymer chains was increased by increasing of bar-bar space. However large space like a flat surface could not show any orientation. The swelling behavior of mountains zone plays an important role in orientation. Since during the scaffolds fabrication, the huge of mountain fraction showed strong force to entangle and draw polymer chains. Therefore, micro-pattern surface scaffolds revealed highly orientation and M300 was highest. Specifically, this is a unique property of sacran, because the xanthan gum polysaccharide micro-patterned surface film could not show the orientation property (Figure 7).

In this present study, not only successful in cells orientation control but also polymer chains. The numerous reports, they showed cell orientation control on surface patterning scaffolds. Otherwise, the cells were longitudinal to the patterned direction, and they could not control the single alignment. All of them examined the bundle of cells.

Shangwu Chen et al made collagen scaffolds with microgroved on the surface, the groove size was 120 to 380 μm. The scaffold at 200 and 380 μm of groove revealed very well orientation of cell bundles in longitudinal to microgroved direction[13]. As can be seen, 380 μm slightly different from our report, however orientation direction was absolutely converse.

The group of Aleesha M. McCormick [10] and Yuhang Hu [1], they made scaffolds with micro-patterned on the surface. The pattern was created using photo lithography technique, which was fine structure around 10 μm. Moreover, cells attachment was highly oriented in longitudinal to micro-patterned direction. The common technique for cell orientation controlled is electrospinning, even though specific device was incorporated. They were showed completely longitudinal of cells with fiber fabricated[5-6, 17, 27].

4. Conclusion

In summary, we successfully prepared micro-patterned surface scaffolds of LC sacran by cast on polystyrene mold. They showed anisotropic swelling on mountain and valley zones, the mountain zone was higher. The LC domains were highly oriented perpendicular to micro-patterned structure on the surface. Such well-oriented scaffolds that were controlled by micro-patterned structure, could increase the mechanical properties as well. By culturing the fibroblast L929 cells, perfectly oriented in duplicate to LC domains orientation. Scaffold without micro-patterned surface was prepared as controlled, it could not reveal any orientation for LC domains of L929 cells. These results suggested that the micro-patterned surface scaffolds, which could effectively control the LC oriented, mechanical properties, and cell attachment might be great materials in tissue engineering application.

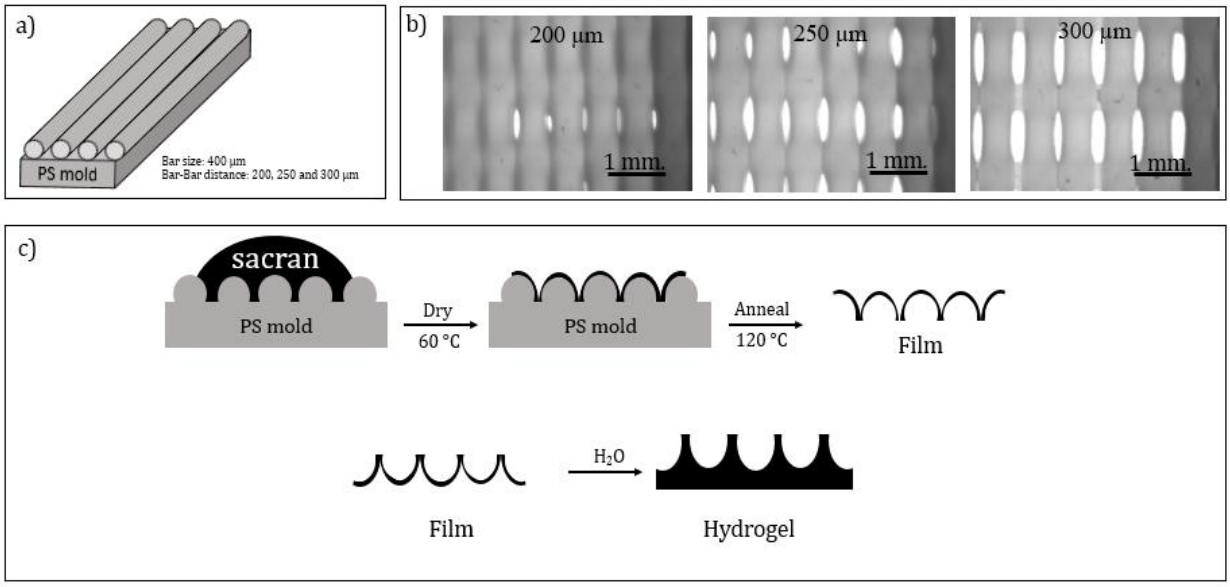

Figure 1. Preparation of sacran hydrogel with micro-pattern surface. Polystyrene (PS) mold has bar size 400 μm and the space between bars is 200, 250 and 300 μm. (b) Images of PS molds has space between bars is 200, 250 and 300 μm, respectively. (c) A schematic showed film preparation process. Sacran liquid crystalline (LC) solution with a concentration of 0.5 w/v % was casted on PS mold at 60 ^{o}C and annealed at 120 ^{o}C for 6 h. The hydrogel was successive water-immersion of film.

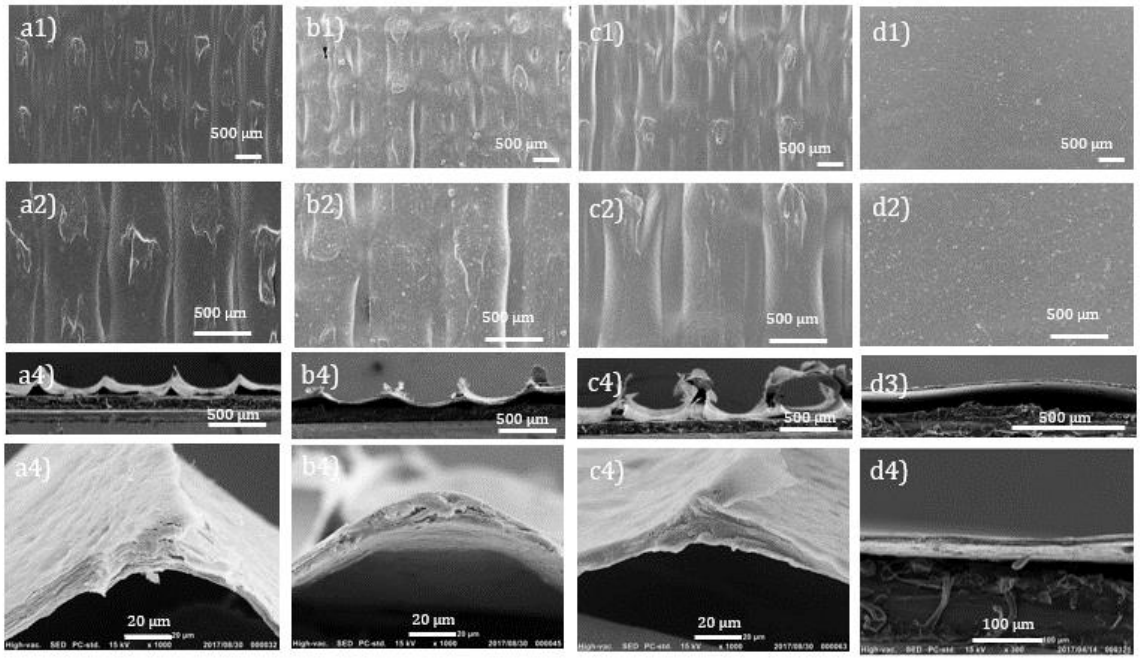

Figure 2. SEM images of sacran film with micro-patterned surface. The difference patterned sized 200, 250, 300 µm and flat surface for controlled were showed in a, b, c and d, respectively. The high magnification of top and side films were showed in a2-d2, and a4-d4, respectively. The layered structure was revealed on a)4-d)4.

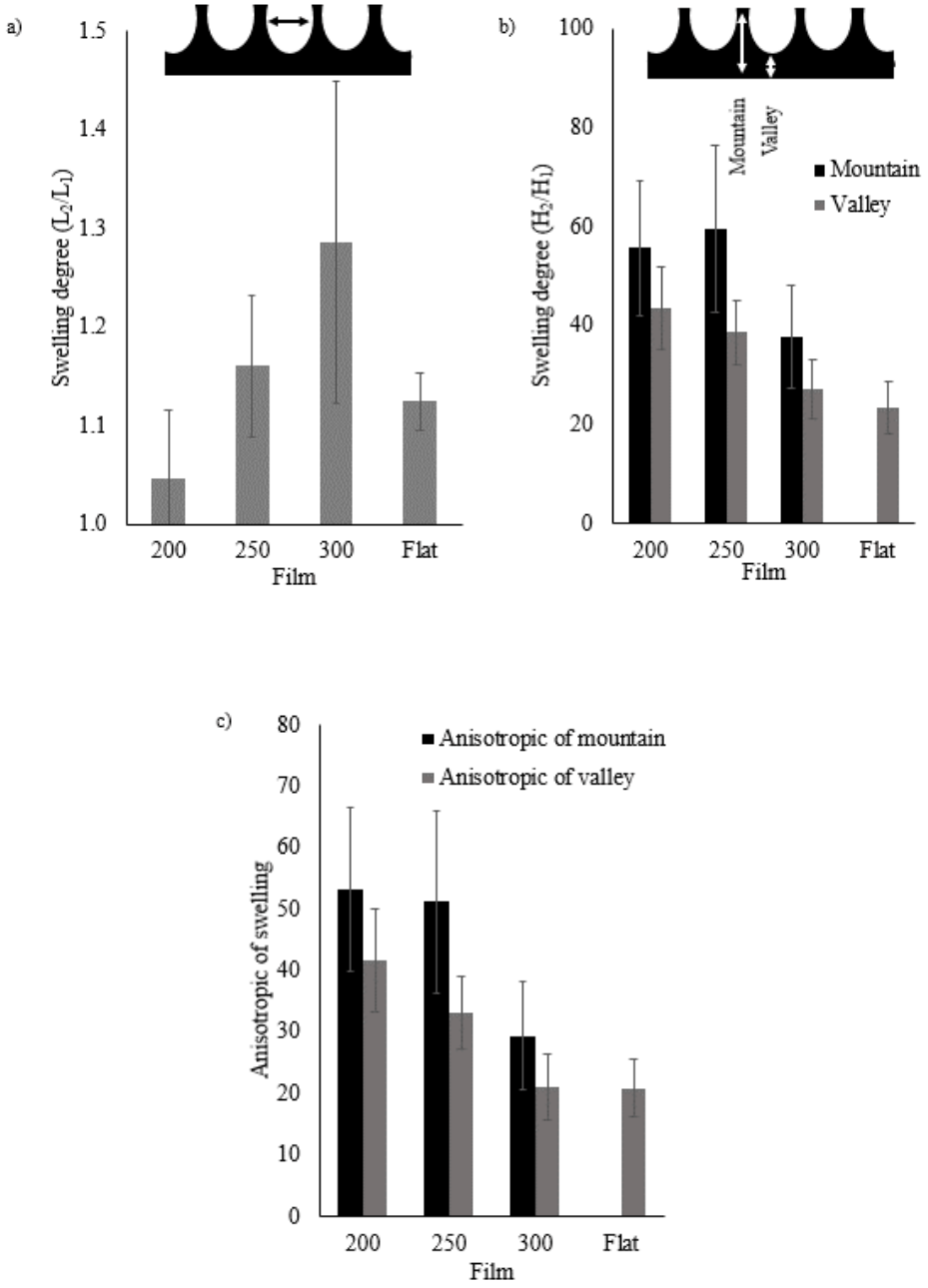

Figure 3. Equilibrium swelling ratio of hydrogels with micro-patterned surface. Patterned expansion increasing with bas space increased. (b) In spite of high swelling decreasing while bar space increased additionally mountain showed higher swelling than village area. (c) Anisotropic swelling revealed ration of high swelling to pattern expansion. The 200 μm bar space preferred to swell in high whereas 300 μm preferred to swell in surface.

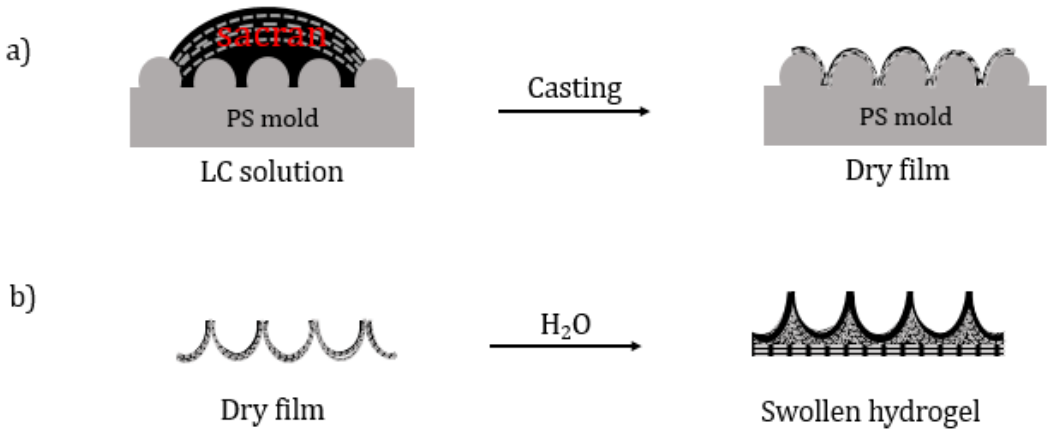

Figure 4. Schematic showed sacran LC domains. a) sacran films were produced by orientation of LC domains. b) Swollen state of LC sacran showed anisotropic swelling. The mountain zones were highly swelling due to out-of-plane of LC oriented, while valley zones with in-plane orientation were lower swelling efficiency.

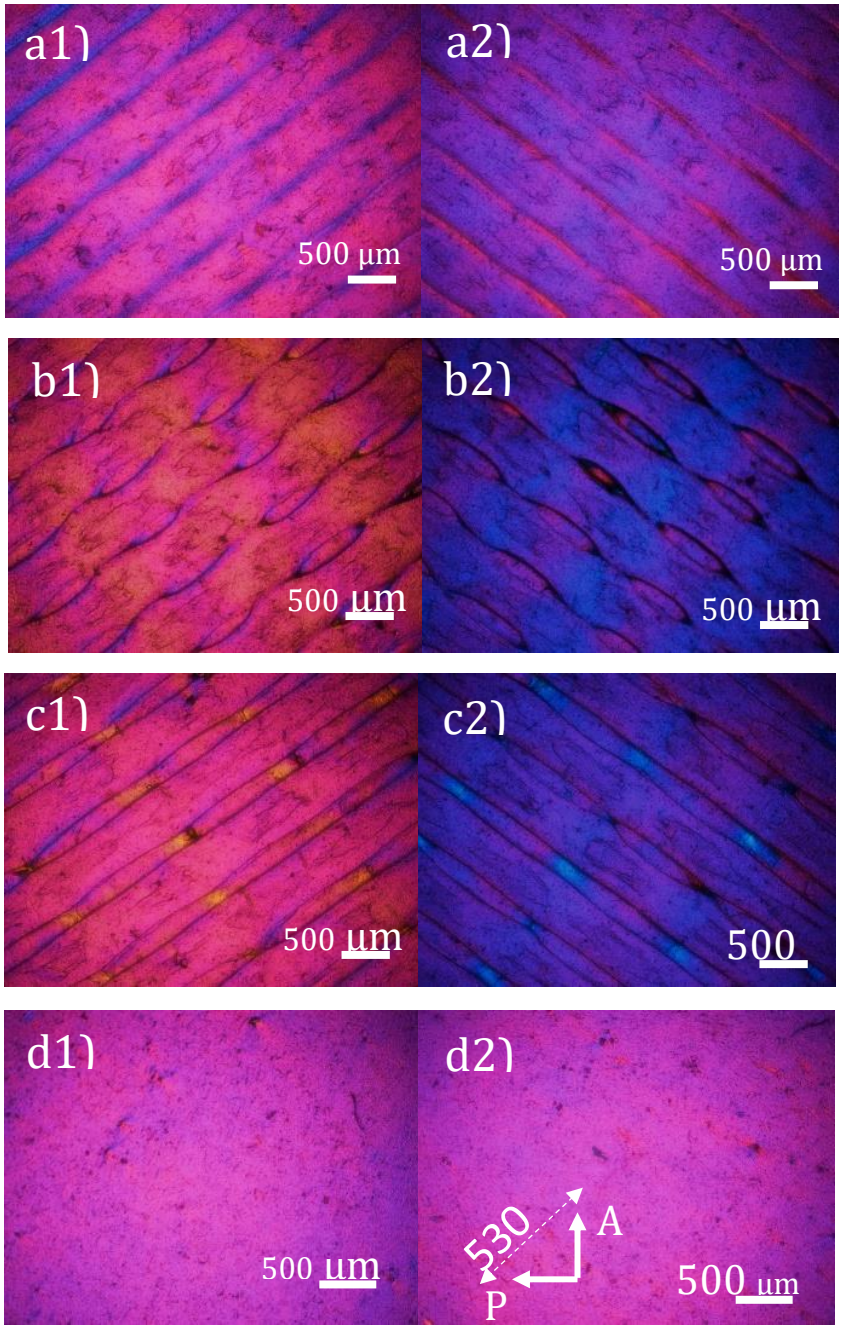

Figure 5. Crossed polarizing microscopic (POM) images under first-order retardation plate (530 nm) of sacran LC films with micro-patterned surface. The difference patterned sized 200, 250, 300 μm and flat surface for controlled were showed in a, b, c and d, respectively.

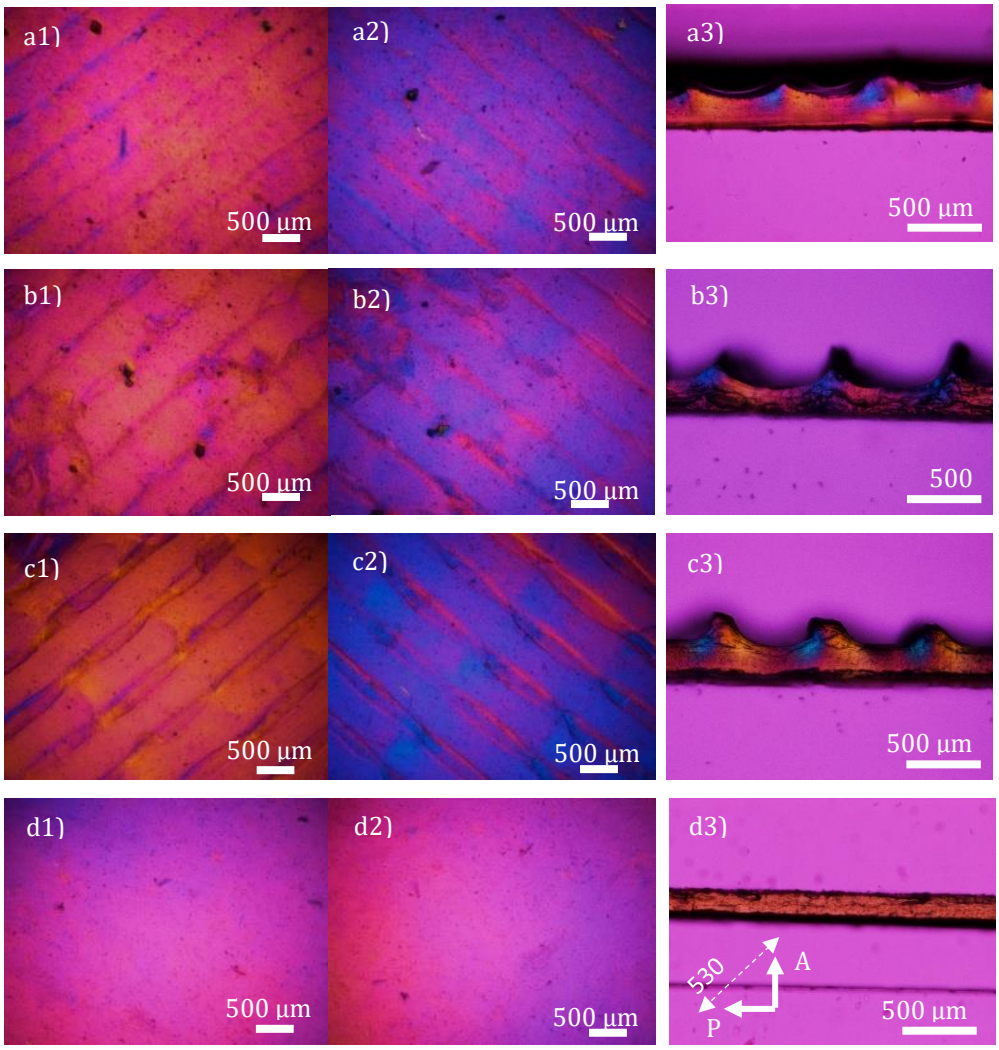

Figure 6. Crossed polarizing microscopic (POM) images under first-order retardation plate (530 nm) of sacran LC hydrogels with micro-patterned surface. The difference patterned sized 200, 250, 300 µm and flat surface for controlled were showed in a, b, c and d, respectively. a1) - d2) showed top view. a3)-c3) revealed side of swollen hydrogels.

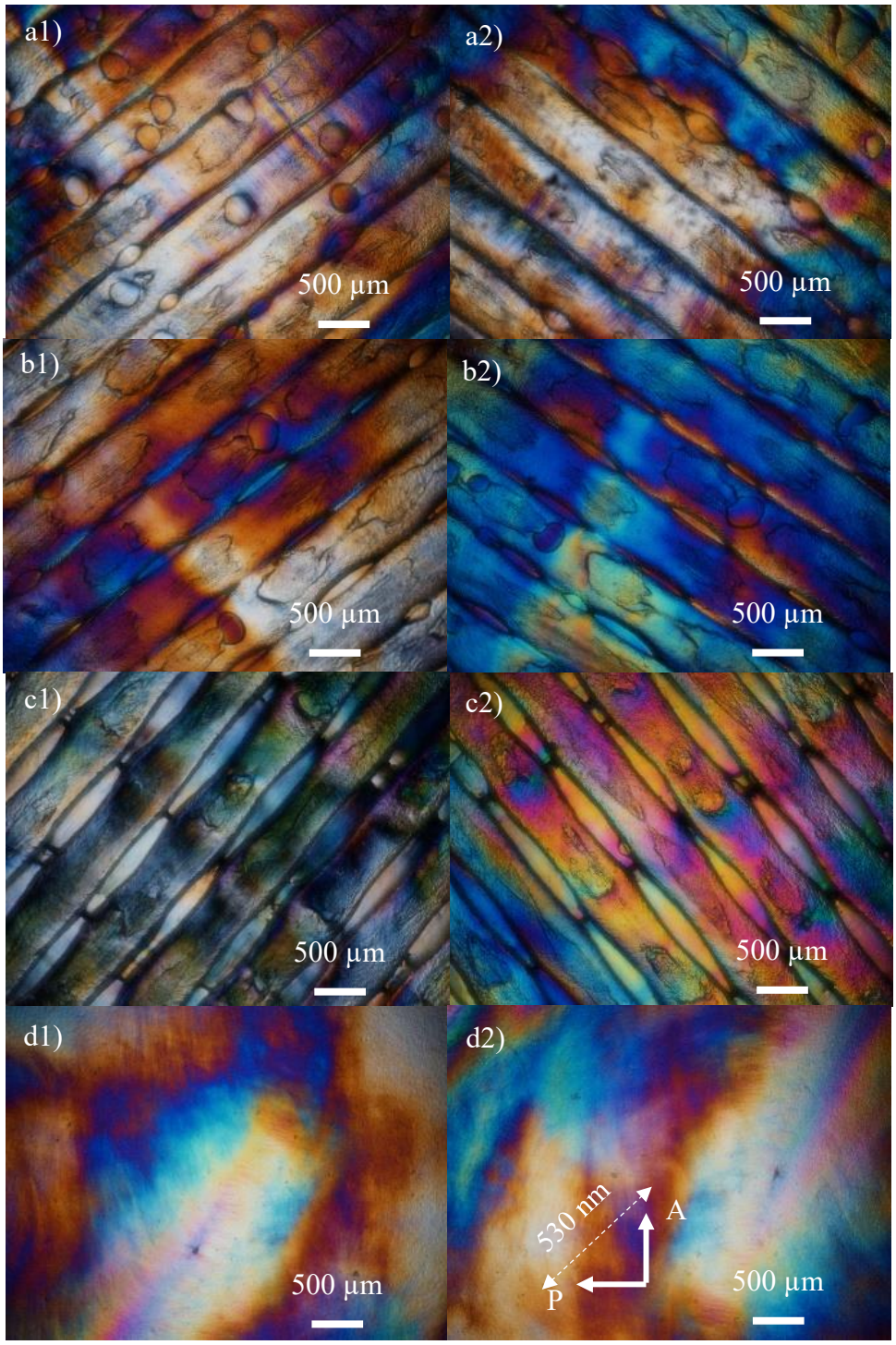

Figure 7. Crossed polarizing microscopic (POM) images under first-order retardation plate (530 nm) of xanthan gum film with micro-patterned surface. The difference patterned sized 200, 250, 300 µm and flat surface for controlled were showed in a, b, c and d, respectively.

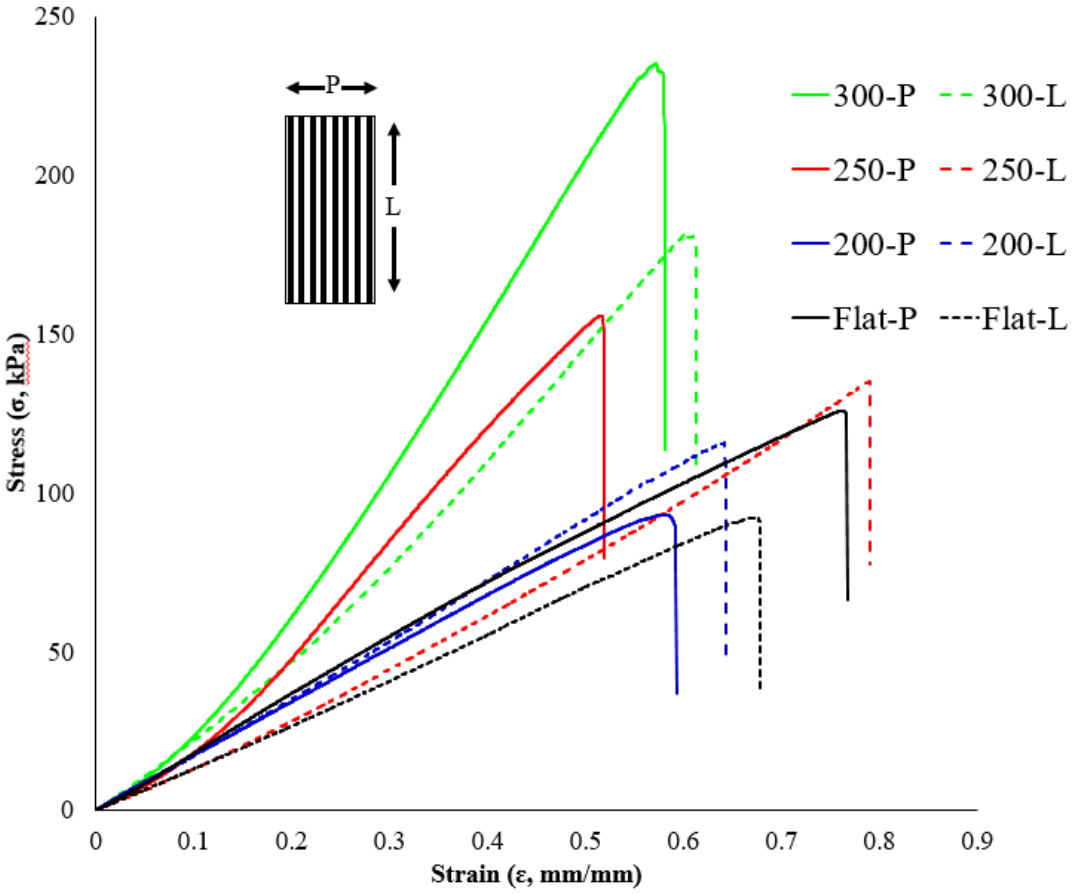

Figure 8. Stress-strain curve of micro-patterned hydrogels in direction perpendicular (P) and longitudinal (L) to the pattern direction.

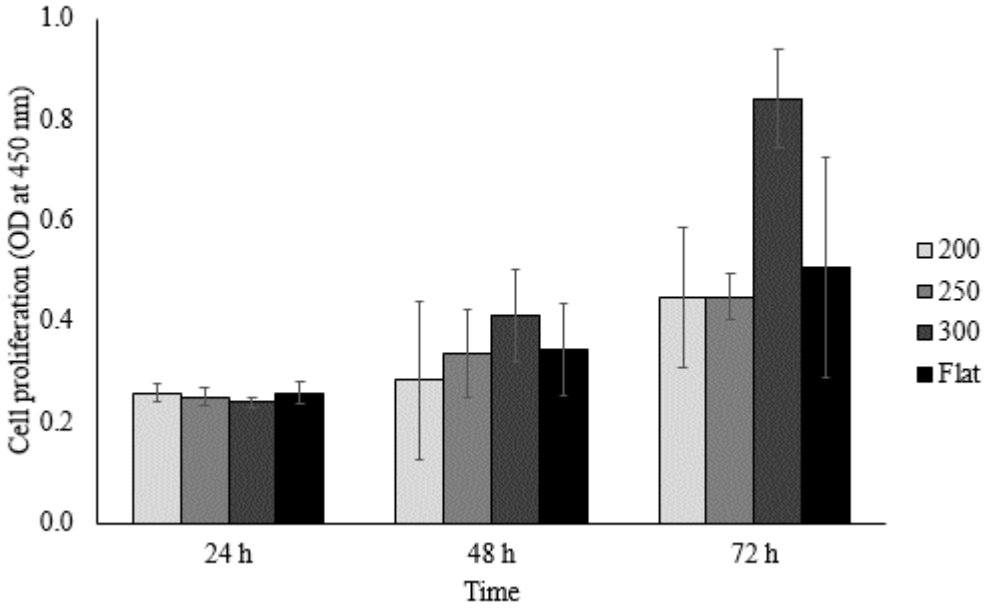

Figure 9. Viability of L929 cells cultured on sacran with micro-patterned surface scaffolds for 24, 48 and 72 h measured via CCK-8 assay. Data are presented as mean ± S.D. with n=5.

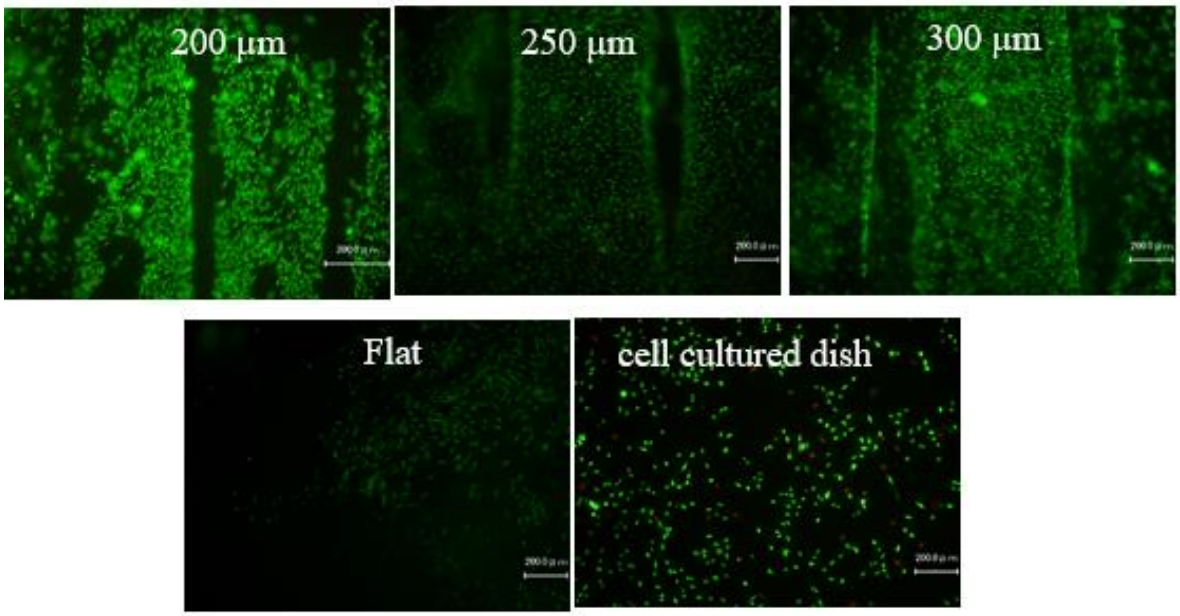

Figure 10. Cell viability on sacran with micro-patterned surface scaffolds. Live/dead assay was performed on L929 cell-seeded after 3 days. Live cells are showed in green (celcein AM) while dead cells are showed in red (edthidium homodimer).

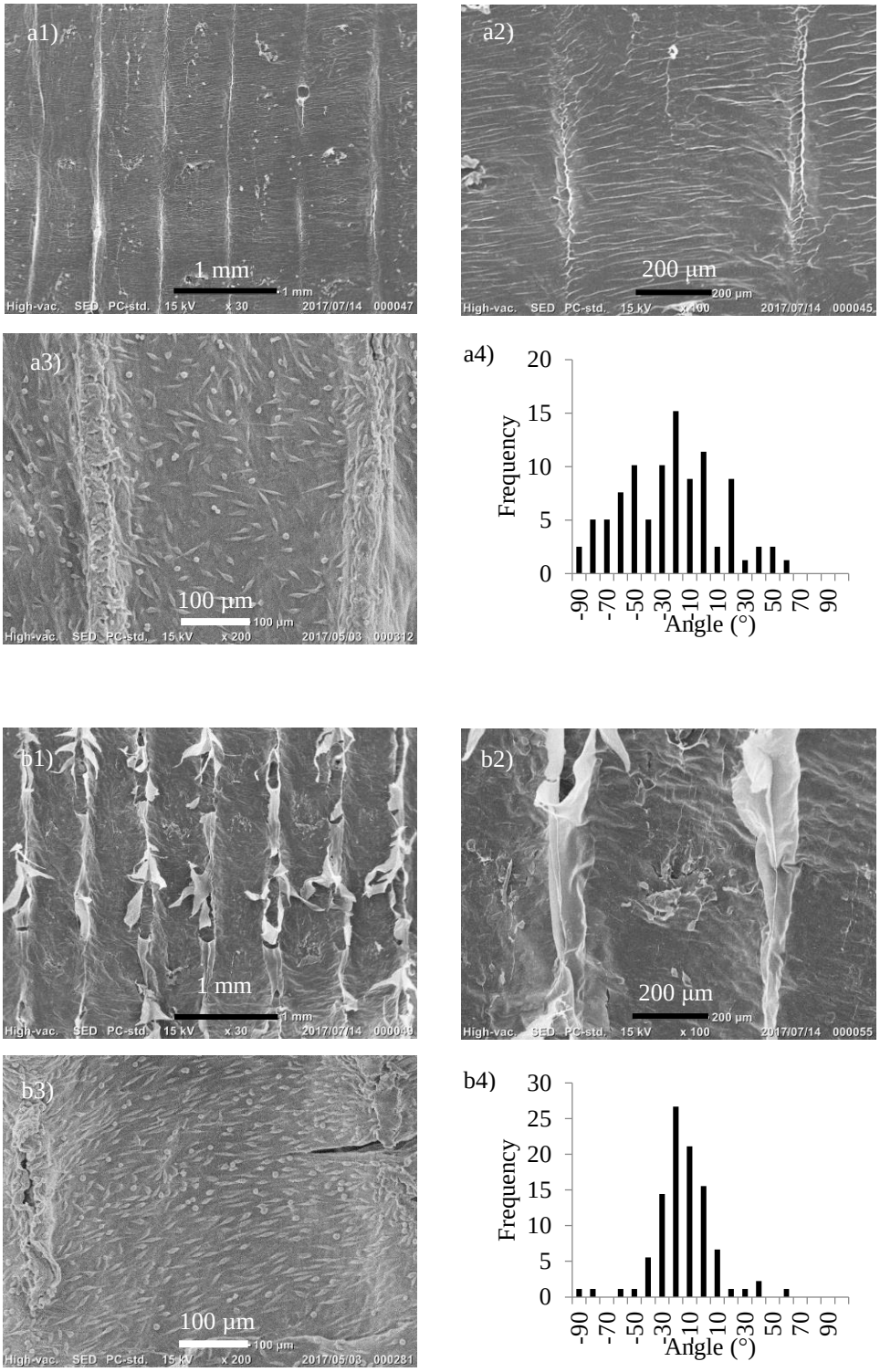
a1)
1 mm
a2)
200 µm
a3)
100 µm
a4)
Frequency
Angle (°)
b1)
1 mm
b2)
200 µm
b3)
100 µm
b4)
Frequency
Angle (°)

Figure 11.

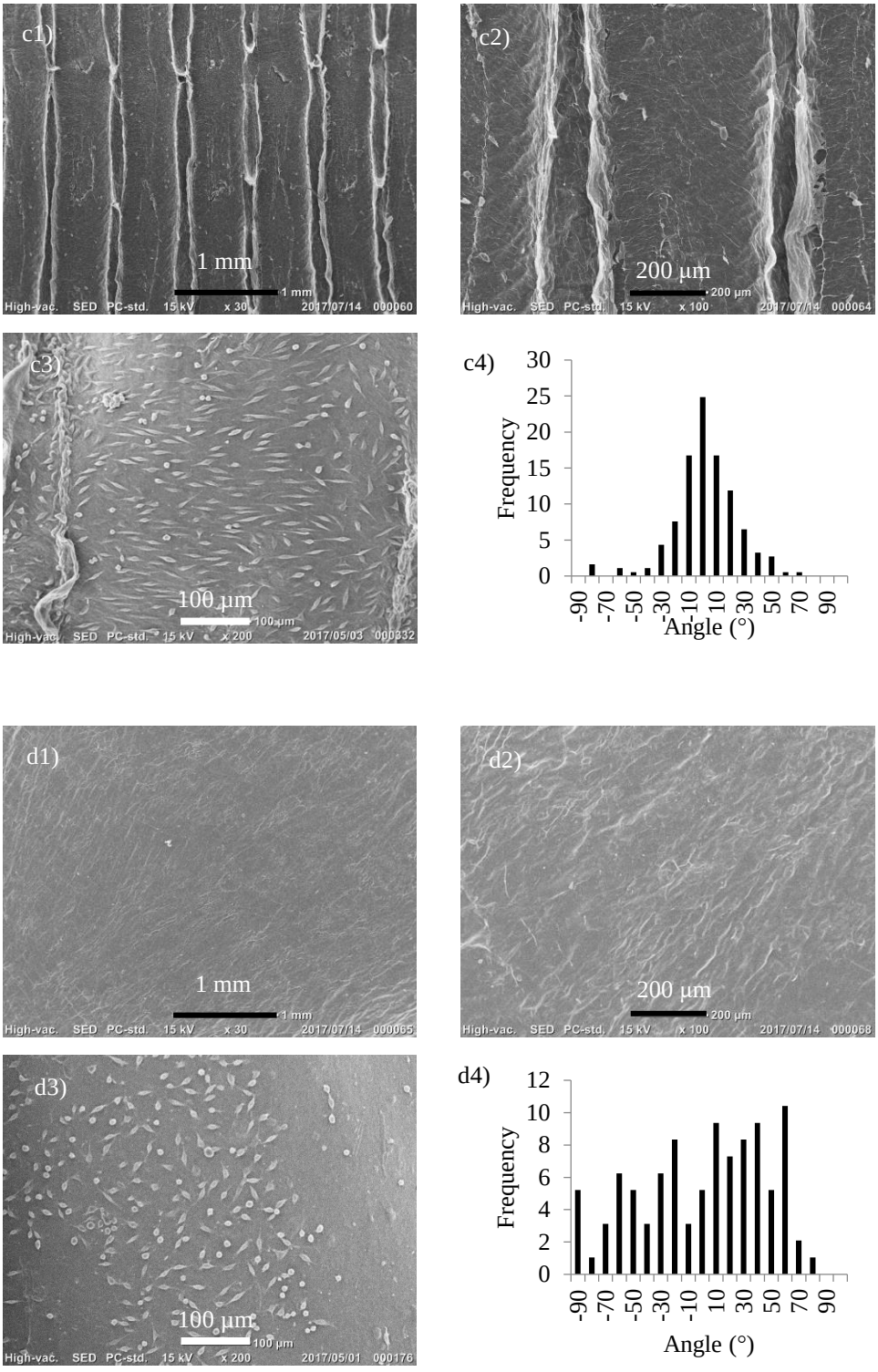
c1)
1 mm
High-vac. SED PC-std. 15 kV x 30 2017/07/14 000060
c2)
200 µm
High-vac. SED PC-std. 15 kV x 100 2017/07/14 000064
c3)
100 µm
High-vac. SED PC-std. 15 kV x 200 2017/05/03 000032
c4)
Frequency
Angle (°)
d1)
1 mm
High-vac. SED PC-std. 15 kV x 30 2017/07/14 000065
d2)
200 µm
High-vac. SED PC-std. 15 kV x 100 2017/07/14 000068
d3)
100 µm
High-vac. SED PC-std. 15 kV x 200 2017/05/01 000176
d4)
Frequency
Angle (°)

Figure 11.

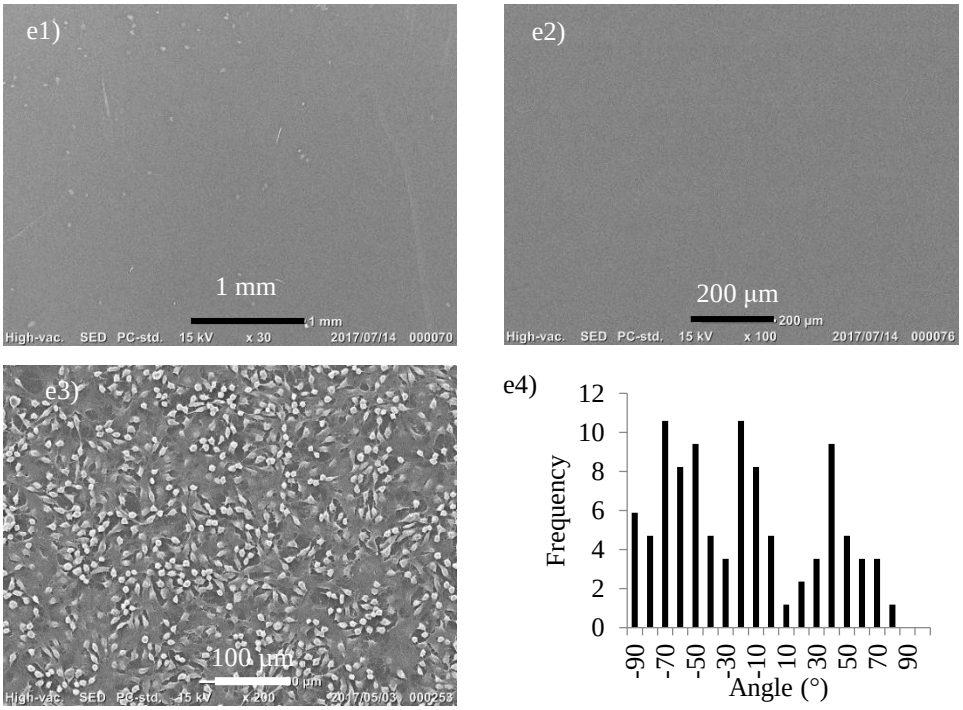

Figure 11. SEM images of freeze-dried sacran with micro-patterned surface scaffolds (a1-e2) and L929 (a3-e3) cells grown on scaffolds for 3 days. Hydrogels were freeze-dried for keeping LC oriented and pore generated. The difference patterned sized 200, 250, 300 μm flat surface and cell culture dish for controlled were showed in a, b, c, d and e, respectively. a3-d3) showed fibroblast L929 cell adhered on hydrogels. a4-e4) Histogram data showed the angle distribution of the longitudinal direction of the extended cell to the pattern direction of the hydrogels.

Table 1. Mechanical properties of porous and freeze-thawed sacran hydrogels[a]

	Longitudinal				Perpendicular			
M[b]	E^c (Kpa)	ε^d (mm/mm)	σ^e (kPa)	strain energy density[f] (kJ/m^3)	E^c (Kpa)	ε^d (mm/mm)	σ^e (kPa)	strain energy density[f] (kJ/m^3)
200	199±63	0.76±0.16	105±27	30±6	223±32	0.5±0.08	102±25	30±9
250	203±45	0.63±0.13	128±16	38±10	318±85	0.50±0.05	190±36	46±18
300	329±85	0.65±0.11	160±49	49±15	414±72	0.48±0.10	228±76	54±20
Flat	164±17	0.74±0.19	108±37	49±16	173±41	0.67±0.23	116±25	38±24

[a]Mechanical properties were determined from stress-strain curves recorded at room temperature using a tensiometer in an elongation mode. [b]Bar-bar distance value on micro-patterned surface. [c]*E* values refer to elastic modulus. [d]ε values refer to elongation at fracture. [e]σ values refer to tensile strength at fracture. [f]Strain energy density values were estimated from area surrounded by stress-strain curves.

REFERENCES

1. Hu, Y.; You, J.-O.; Aizenberg, J., Micropatterned hydrogel surface with high-aspect-ratio features for cell guidance and tissue growth. *ACS applied materials & interfaces* **2016,** *8* (34), 21939-21945.
2. Kiremitler, N. B.; Pekdemir, S.; Patarroyo, J.; Karabel, S.; Torun, I.; Puntes, V. F.; Onses, M. S., Assembly of Plasmonic Nanoparticles on Nanopatterns of Polymer Brushes Fabricated by Electrospin Nanolithography. *ACS Macro Letters* **2017,** *6* (6), 603-608.
3. Huang, C.; Ouyang, Y.; Niu, H.; He, N.; Ke, Q.; Jin, X.; Li, D.; Fang, J.; Liu, W.; Fan, C.; Lin, T., Nerve Guidance Conduits from Aligned Nanofibers: Improvement of Nerve Regeneration through Longitudinal Nanogrooves on a Fiber Surface. *ACS Applied Materials & Interfaces* **2015,** *7* (13), 7189-7196.
4. He, X.; Xiao, Q.; Lu, C.; Wang, Y.; Zhang, X.; Zhao, J.; Zhang, W.; Zhang, X.; Deng, Y., Uniaxially aligned electrospun all-cellulose nanocomposite nanofibers reinforced with cellulose nanocrystals: scaffold for tissue engineering. *Biomacromolecules* **2014,** *15* (2), 618-27.
5. Guan, J.; Wang, F.; Li, Z.; Chen, J.; Guo, X.; Liao, J.; Moldovan, N. I., The stimulation of the cardiac differentiation of mesenchymal stem cells in tissue constructs that mimic myocardium structure and biomechanics. *Biomaterials* **2011,** *32* (24), 5568-5580.
6. Xu, H.; Li, H.; Ke, Q.; Chang, J., An Anisotropically and Heterogeneously Aligned Patterned Electrospun Scaffold with Tailored Mechanical Property and Improved Bioactivity for Vascular Tissue Engineering. *ACS Applied Materials & Interfaces* **2015,** *7* (16), 8706-8718.
7. He, X.; Xiao, Q.; Lu, C.; Wang, Y.; Zhang, X.; Zhao, J.; Zhang, W.; Zhang, X.; Deng, Y., Uniaxially Aligned Electrospun All-Cellulose Nanocomposite Nanofibers Reinforced with Cellulose Nanocrystals: Scaffold for Tissue Engineering. *Biomacromolecules* **2014,** *15* (2), 618-627.
8. Klossner, R. R.; Queen, H. A.; Coughlin, A. J.; Krause, W. E., Correlation of Chitosan's Rheological Properties and Its Ability to Electrospin. *Biomacromolecules* **2008,** *9* (10), 2947-2953.
9. Zawko, S. A.; Suri, S.; Truong, Q.; Schmidt, C. E., Photopatterned anisotropic swelling of dual-crosslinked hyaluronic acid hydrogels. *Acta Biomaterialia* **2009,** *5* (1), 14-22.
10. McCormick, A. M.; Maddipatla, M. V. S. N.; Shi, S.; Chamsaz, E. A.; Yokoyama, H.; Joy, A.; Leipzig, N. D., Micropatterned Coumarin Polyester Thin Films Direct Neurite Orientation. *ACS Applied Materials & Interfaces* **2014,** *6* (22), 19655-19667.
11. Ku, S. H.; Lee, J. S.; Park, C. B., Spatial Control of Cell Adhesion and Patterning through Mussel-Inspired Surface Modification by Polydopamine. *Langmuir* **2010,** *26* (19), 15104-15108.
12. Wosnick, J. H.; Shoichet, M. S., Three-dimensional Chemical Patterning of Transparent Hydrogels. *Chemistry of Materials* **2008,** *20* (1), 55-60.
13. Chen, S.; Nakamoto, T.; Kawazoe, N.; Chen, G., Engineering multi-layered skeletal muscle tissue by using 3D microgrooved collagen scaffolds. *Biomaterials* **2015,** *73*, 23-31.
14. Zhu, C.; Bettinger, C. J., Photoreconfigurable Physically Cross-Linked Triblock Copolymer Hydrogels: Photodisintegration Kinetics and Structure–Property Relationships. *Macromolecules* **2015,** *48* (5), 1563-1572.
15. Salinas, C. N.; Anseth, K. S., Mixed Mode Thiol−Acrylate Photopolymerizations for the Synthesis of PEG−Peptide Hydrogels. *Macromolecules* **2008,** *41* (16), 6019-6026.
16. Baier Leach, J.; Bivens, K. A.; Patrick Jr, C. W.; Schmidt, C. E., Photocrosslinked hyaluronic acid hydrogels: natural, biodegradable tissue engineering scaffolds. *Biotechnology and bioengineering* **2003,** *82* (5), 578-589.
17. Yang, A.; Huang, Z.; Yin, G.; Pu, X., Fabrication of aligned, porous and conductive fibers and their effects on cell adhesion and guidance. *Colloids and Surfaces B: Biointerfaces* **2015,** *134*, 469-474.

18. Zhao, Y.; Tan, K.; Zhou, Y.; Ye, Z.; Tan, W.-S., A combinatorial variation in surface chemistry and pore size of three-dimensional porous poly(ε-caprolactone) scaffolds modulates the behaviors of mesenchymal stem cells. *Materials Science and Engineering: C* **2016,** *59*, 193-202.
19. Mohanty, S.; Alm, M.; Hemmingsen, M.; Dolatshahi-Pirouz, A.; Trifol, J.; Thomsen, P.; Dufva, M.; Wolff, A.; Emnéus, J., 3D Printed Silicone–Hydrogel Scaffold with Enhanced Physicochemical Properties. *Biomacromolecules* **2016,** *17* (4), 1321-1329.
20. Lu, J.; Zou, X.; Zhao, Z.; Mu, Z.; Zhao, Y.; Gu, Z., Cell Orientation Gradients on an Inverse Opal Substrate. *ACS Applied Materials & Interfaces* **2015,** *7* (19), 10091-10095.
21. Okajima, M. K.; Mishima, R.; Amornwachirabodee, K.; Mitsumata, T.; Okeyoshi, K.; Kaneko, T., Anisotropic swelling in hydrogels formed by cooperatively aligned megamolecules. *RSC Adv.* **2015,** *5* (105), 86723-86729.
22. Kaneko, T.; Tran, H. T.; Matsusaki, M.; Akashi, M., Biodegradable LC oligomers with cranked branching points form highly oriented fibrous scaffold for cytoskeletal orientation. *Chemistry of materials* **2006,** *18* (26), 6220-6226.
23. Takahashi, R.; Wu, Z. L.; Arifuzzaman, M.; Nonoyama, T.; Nakajima, T.; Kurokawa, T.; Gong, J. P., Control superstructure of rigid polyelectrolytes in oppositely charged hydrogels via programmed internal stress. *Nature communications* **2014,** *5*, 4490.
24. Mitsumata, T.; Miura, T.; Takahashi, N.; Kawai, M.; Okajima, M. K.; Kaneko, T., Ionic state and chain conformation for aqueous solutions of supergiant cyanobacterial polysaccharide. *Phys Rev E Stat Nonlin Soft Matter Phys* **2013,** *87* (4), 042607.
25. Mendes, A. C.; Baran, E. T.; Lisboa, P.; Reis, R. L.; Azevedo, H. S., Microfluidic Fabrication of Self-Assembled Peptide-Polysaccharide Microcapsules as 3D Environments for Cell Culture. *Biomacromolecules* **2012,** *13* (12), 4039-4048.
26. Kirdponpattara, S.; Khamkeaw, A.; Sanchavanakit, N.; Pavasant, P.; Phisalaphong, M., Structural modification and characterization of bacterial cellulose–alginate composite scaffolds for tissue engineering. *Carbohydrate Polymers* **2015,** *132*, 146-155.
27. Wang, L.; Wu, Y.; Guo, B.; Ma, P. X., Nanofiber Yarn/Hydrogel Core–Shell Scaffolds Mimicking Native Skeletal Muscle Tissue for Guiding 3D Myoblast Alignment, Elongation, and Differentiation. *ACS Nano* **2015,** *9* (9), 9167-9179.

CHAPTER V: CONCLUSION REMARKS

The research in this thesis focused on the preparation of scaffolds with cell orientation, using sacran polymer. Scaffolds play an essential role in tissue engineering as cell supported materials in the artificial tissue fabricating process. It is outstanding property include the cell orientation control, which can be utilized for making uni-direction of cell alignment to mimic the native tissue. Sacran, polysaccharide, is extracted from Aphanothece sacrum cyanobacteria. The polymer contains various kinds of sugar residues such as Glc, Gal, Man, Xyl, Rha, Fuc, Ara, GalN, and Mur. It also consisted of many functional groups such as hydroxyl, carboxylic, sulfate and amide. The amide sugar, acting like glycosaminoglycan, is the main content found in the extra cellular matrix. By this reason, sacran was selected for tissue engineering material. Moreover, liquid crystal behavior was observed in sacran solution. The LC polymer was known for its ability in polymer orientation control. Thus, sacran is one of the most suitable materials for making scaffolds with orientation controllability.

Anisotropic porous hydrogels were prepared by a combination of solvent casting and freeze drying techniques. Firstly, the sacran solution with LC random orientation was casted on polypropylene substrate. The procedure yields the in-plane orientation thin films. The thin films were physical cross-linked at temperature 60, 80, 100, 120 and 140 °C. Then swollen hydrogels with in-plane orientation were created by water immersion of that cross-linked films. Finally, the swollen hydrogels were subjected to freeze dry process. The final products revealed an in-plane porous structure like a tunnel. This is due to the sublimation of water on side surface parallel to the in-plane orientation of sacran polymer chains. In addition, they showed proper mechanical properties in a broad application. At high cross-linking temperature, the anisotropic porous materials showed low porosity, fine size of the pore, and minimal water adsorption. Conversely, the mechanical properties value such as moduli, cross-linking degree and

toughness were very high. For low temperature cross-linking the opposite set of values was observed. The anisotropic porous hydrogels were successfully prepared and precisely controlled for their properties.

There are various applications of porous materials, and tissue engineering scaffold is considered to be one of the most significant. The mouse fibroblast cell L929 was used in cell culture experiment. This material showed favorable cell compatibility property. The morphology of cells attachment was analyzed. The cells orientation on side surfaces is parallel to the in-plane orientation of polymer chains. The scaffolds can be altered to mimic the native tissue that represents uni-direction of the muscle orientation. Moreover, the water contact angle and protein adsorption were studied. In the results, water contact angle, protein adsorption and cell orientation are also related to cross-linking temperature like the above-mention properties. However, the cell attached on top of the surface were randomly oriented. Another method was employed to control the cell orientation on the top surface of the scaffolds.

The scaffolds were casted on polystyrene, with micro-patterned on its surface. The pattern was set in a bar-shape mold with a diameter of 400 μm. The bars were arranged in parallel. The space between bars was fixed at 200, 250 and 300 μm. Sacran scaffolds with surface orientation were prepared with the same procedure to that of anisotropic porous scaffolds except for the mentioned patterned substrate surface. The pattern of the scaffold revealed orientation perpendicular to that of bar molds. During the drying process, LC domains were slightly arranged to form an in-plane orientation like a layer. Looking at the side of bar molds, the top point of each bar has the sacran layer accumulated. The point is called nucleation point of orientation. Then the ends of polymer chains are aligned between bars. Polarization optical microscope technique was used to confirm the orientation of LC domains, and the result showed a clear and complete visible orientation. Consequently, the mouse fibroblast cell L929 was used in cell culture experiment. The distribution of cell orientation degree showed very

well oriented mimic to polymer orientation on the top surface. Finally, the orientation of cell was efficiently controlled on sacran LC polymer.

According to the development of technology for human's bioengineering, the field of tissue engineering scaffolds is growing and progressing continuously. Today, the scaffolds are mainly the work of laboratory and research. However, it has the potential to be utilized, especially to save many lives on this planet, in the future.

ACHIEVEMENTS

Journal publications

1. Sornkamnerd, S.; Okajima, M. K.; Kaneko, T., Tough and Porous Hydrogels Prepared by Simple Lyophilization of LC Gels. *ACS Omega* **2017,** *2* (8), 5304-5314.

2. Okeyoshi, K.; Joshi, G.; Rawat, S.; Sornkamnerd, S.; Amornwachirabodee, K.; Okajima, M. K.; Ito, M.; Kobayashi, S.; Higashimine, K.; Oshima, Y.; Kaneko, T., Drying-Induced Self-Similar Assembly of Megamolecular Polysaccharides through Nano and Submicron Layering. *Langmuir* **2017,** *33* (20), 4954-4959.

3. Okajima, M. K.; Sornkamnerd, S.; Kaneko, T.,Development of Functional Bionanocomposites using Cyanobacterial Polysaccharides. *Submitted*

*Saranyoo Sornkamnerd, Maiko K. Okajima, Kazuaki Matsumura and Tatsuo Kaneko**

4. Sornkamnerd, S.; Okajima, M. K.; Matsumura, K.,;Kaneko, T., Surface-selective control of cell-orientation on liquid crystalline gels. *Submitted*

Conference

1. Saranyoo Sornkamnerd, Kosuke Okeyoshi, Maiko K. Okajima, and Tatsuo Kaneko "Resveratrol-loaded-sacran hydrogel for drug delivery system" 64th Symposium on Macromolecules, Shiroishi-ku, Sapporo, Japan, May 27-29, 2015.
2. Saranyoo Sornkamnerd, Kazuaki Matsumura, Kosuke Okeyoshi, Maiko K. Okajima, and Tatsuo Kaneko "Sacran hydrogels for tissue engineering application" 7th Annual and 1st International Symposium on Sacran, Kyushu Institute of Technology, November 21, 2015.

3. Saranyoo Sornkamnerd, Kazuaki Matsumura, Kosuke Okeyoshi, Maiko K. Okajima, and Tatsuo Kaneko "Sacran complexation with collagen and the performance of cell attachment" 27th polymer gel research, University of Tokyo, Sanjo Conference Hall large conference rooms, January 18-19, 2016.
4. Saranyoo Sornkamnerd, Kosuke Okeyoshi, Maiko K. Okajima, Kazuaki Matsumura, and Tatsuo Kaneko "Sacran-collagen complex for cells culture application" Pure and Applied Chemistry International Conference 2016 (PACCON2016), Bangkok, Thailand, February 9-11.
5. Saranyoo Sornkamnerd, Kazuaki Matsumura, Kosuke Okeyoshi, Maiko K. Okajima, and Tatsuo Kaneko "Layered sacran hydrogels with anisotropic pore structures prepared by simple freeze-drying" 65th Symposium on Macromolecules, Yokohama, Japan, September 14-16, 2016.
6. Saranyoo Sornkamnerd, Hojoon Shin, Shinji Ando, and Tatsuo Kaneko "Evaluation of Molecular Orientation on Biopolyimide Film Using Polarized ATR/FT-IR" The 24th Japan Polyimide & Aromatic Polymer Conference 8th, Ishikawa High-tech Exchange Center, Nomi, Ishikawa, Japan December 8, 2015.
7. Saranyoo Sornkamnerd, Kazuaki Matsumura, Kosuke Okeyoshi, Maiko K. Okajima, and Tatsuo Kaneko "Layered sacran hydrogels with anisotropic pore structures prepared by simple freeze-drying and their tissue engineering application" The 11th SPSJ International Polymer Conference (IPC 2016), Fukuoka, December 13 -16, 2016.
8. Saranyoo Sornkamnerd, Hojoon Shin, Shinji Ando, and Tatsuo Kaneko "Evaluation of three-dimension molecular orientation in biopolyimide film using polarized ATR/FT-IR" JAIST Japan-India Symposium on Materials Science 2017, Ishikawa High-Tech Center, Ishikawa, Japan, March 6-7, 2017.

9. Saranyoo Sornkamnerd, Maiko K. Okajima, Kazuaki Matsumura, Kosuke Okeyoshi, and Tatsuo Kaneko "Porous sacran scaffolds with micro patterned structures for cell alignment controlled" 6th JACI/GSC Symposium, Tokyo International Forum, Tokyo, Japan, July 2-3, 2017.
10. Saranyoo Sornkamnerd, Maiko K. Okajima, Kazuaki Matsumura, Kosuke Okeyoshi, and Tatsuo Kaneko "Uniaxial cell elongation using LC sacran hydrogel with micro-pattern on surface" Kick-off symposium of JSPS Core-to-Core Program, Okasa University, Osaka, Japan July 31-June 2, 2017.
11. Saranyoo Sornkamnerd, Maiko K. Okajima, Kazuaki Matsumura, Kosuke Okeyoshi, and Tatsuo Kaneko "Controlled cell extension on micro-patterned surface of sacran hydrogels" 66th Symposium on macromolecules, Ehime University, Ehime, Japan, 20-22 September, 2017.
12. Saranyoo Sornkamnerd, Maiko K. Okajima, Kazuaki Matsumura, Kosuke Okeyoshi, and Tatsuo Kaneko "Layered scaffolds for cell alignment controlling" The 6th Asian Symposium on Advanced Materials: Chemistry, Physics & Biomedicine of Functional and Novel Materials, Hanoi, Vietnam, 27-30 September, 2017.
13. Saranyoo Sornkamnerd, Maiko K. Okajima, Kazuaki Matsumura, Kosuke Okeyoshi, and Tatsuo Kaneko "Sacran for cell engineering applications" 9th Symposium on Sacran, Sojo University, Kumamoto, Japan, 21 October 2017.

Award:

Title: Sacran-collagen complex for cells culture application

Best poster presentation: Pure and Applied Chemistry International Conference 2016 (PACCON 2016), Bangkok, Thailand, February 9-11, 2016.

ACKNOWLEDGEMENTS

Firstly, I would like to thank my supervisor, **Prof. Tatsuo Kaneko**, for the patient guidance, encouragement and advice he has provided throughout my time as his student. I have been extremely lucky to have a supervisor who cared so much about my work, and who responded to my questions and queries so promptly. His guidance helped me in all the time of research and writing of this thesis. I could not have imagined having a better advisor and mentor for my Ph.D study.

In particular, I would like to thank **Prof. Kazuaki Matsumura** for the suggestions he made in cell experiment of this work. Additionally, **Mutoh Industries** Limited company for giving me the three-dimension printing polystyrene mold.

Besides my advisor, I would like to thank the rest of my thesis committee: **Prof. Noriyoshi Matsumi**, **Prof. Kazuaki Matsumura**, **Prof. Takumi Yamaguchi** and **Prof. Hidetoshi Arima**, for their insightful comments and encouragement, but also for the question which incented me to widen my research from various perspectives.

My sincere thanks also goes to **Dr. Maiko K. Okajima, Dr. Kosuke Okeyoshi, Dr. Seiji Tateyama, Dr. Kenji Takada and Dr. Hojoon Shin** who provided me an opportunity to join their team as intern, and who gave access to the laboratory and research facilities. Without they precious support it would not be possible to conduct this research.

I thank my fellow l**abmates** in for the stimulating discussions, for the sleepless nights we were working together before deadlines, and for all the fun we have had in the last three years.

Completing this work would have been all the more difficult were it not for the support and friendship provided by them.

Last but not the least, I would like to thank my **family**: my parents and to my sister for supporting me spiritually throughout writing this thesis and my life in general.

Saranyoo Sornkamnerd